A COMPREHENSIVE STUDY ON ELECTRICAL AND MECHANICAL PROPERTIES OF CNT-POLYMER COMPOSITES

By

Yves Ngabonziza

A dissertation submitted to the Graduate Faculty in Mechanical Engineering in partial fulfillment of the requirements for the degree of Doctor of Philosophy, The City University of New York

2009

This manuscript has been read and accepted for the
Graduate Faculty in Engineering in satisfaction of the
dissertation requirement for the degree of Doctor of Philosophy.

Jacqueline Li

Date | Chair of Examining Committee

Mumtaz Kassir

Date | Executive Officer

Feridun Delale

Carol Barry, University of Massachusetts at Lowell

Benjamin Liaw

Ali Sadegh

Supervisory Committee

THE CITY UNIVERSITY OF NEW YORK

ABSTRACT

A Comprehensive Study on Electrical and Mechanical Properties of CNT-Polymer Composites

By

Yves Ngabonziza

Advisor: Professor Jackie Li

The aim of this dissertation is to study electrical and mechanical properties of carbon nanotube (CNT)-polymer composites. Two types of polymers, polypropylene (PP) and polycarbonate (PC) are chosen as polymer matrix materials. Synthesis, characterization and theoretical modeling of CNT composites are conducted.

In the processing of CNT composites, an injection molding method which is a melt mixing method is used to produce CNT-polymer composites. Processing parameters such as injection speed, temperature, pressure and time are optimized to obtain uniform samples. The influence of injection velocity on electrical and mechanical properties of the nanocomposites is studied in characterization.

In the experimental investigation of the produced nanocomposites, three types of testing are carried out: i) the electrical conductivity of the samples is measured. The influence of CNT content and injection velocity on the electrical conductivity is then studied. ii) Tensile tests under different strain rates are conducted. From this mechanical tensile testing, the elastic modulus and stress-strain relation can be obtained. Then these mechanical behaviors can be studied in terms of CNT content, injection velocity and

strain rate loading. iii) Electrical resistance measurement is carried out during the tensile tests for those with higher CNT contents than the percolation threshold. This allows us to study the piezoresistive behavior of CNT-polymer composites for sensing applications.

Finally, theoretical modelings are carried out to study electrical and elastic properties of CNT-polymer nanocomposites parallel to the experimental testing. First, a percolation theory is adopted to study the electric conductivity of the system in terms of CNT contents; the results are compared with our experimental data and the percolation threshold is determined. Second, a micromechanics theory with three different models is applied to study the elastic modulus of the nanocomposites. And last, a statistical approach is developed to investigate the resistance change under tensile loading. All results are compared with the experimental data.

To my wife, Bernadette

To my parents, Agnes and Denis and my brothers, Richard and William.

Your endless love and support made this possible.

ACKNOWLEDGEMENTS

It is under the guidance of the Almighty that I have been able to achieve such a step toward the completion of my doctorate studies.

May I have the pleasure to express my sincere thanks to my advisor, Professor Jackie Li, for the cooperation, advices and encouragement she offered during my graduate study. Her enthusiasm and serenity to develop my research understanding and work ethic is appreciated. It has been an honor to work with her, and I will always be grateful for her help.

I also want to thank my research committee members, Professor Carol Barry, Professor Feridun Delale, Professor Benjamin Liaw, and Professor Ali Sadegh for their time, advices and support.

I would like to thank Professor Carol Barry from the Plastic Engineering Department at the University of Massachusetts at Lowell for her support throughout the years. She helped and advised me in the manufacture of the testing specimens as well as in thesis preparation.

I would like to convey my gratitude to the “Self-Sensing project” group at the City College of New York. Professors Feridun Delale, Jackie Li and Benjamin Liaw helped me shaping the mechanical engineer I am today through their advices and support. I am also grateful to the other group members (Dr. Erickan Sevkat, Dr. Ergun Hale, Regina Kuznetsova, and Claudia Boldrini), for the help, support and technical advices they provided.

I am grateful for my colleagues and friends (also officemates through out my graduate studies), Zhao Ping and Cao Yang, who helped me in different ways. I would like to let them know they are part of my success.

I would also like to thank my friends and colleagues Dave Budhoo and Ali S. Yaghoubi for the good time we spent not only doing research but also exchanging ideas about several issues.

I am especially grateful to CUNY administration, for the financial support through the Robert Gilleece Fellowship, the school of engineering, and the department of Mechanical Engineering for the valuable academic and social help gained from them.

I would like in particular to express my gratitude to my wife, Bernadette, for her unconditional and endless support, to my parents, Agnes and Denis, and my brothers, Richard and William, for the support they always offer.

To you all, I say Thank you.

TABLE OF CONTENTS

LIST OF FIGURES

LIST OF TABLES

1. INTRODUCTION

Since the discovery of carbon nanotubes (CNTs) two decades ago by Ijima [1], a considerable amount of research has been conducted on properties [2-9], processing [10-21], and applications [22] of CNTs. Single-walled carbon nanotubes (SWCNTs) or multi-walled carbon nanotubes (MWCNTs) are single or multiple layers of cylinders rolled up from graphene sheets. It has been found experimentally and theoretically that carbon nanotubes can possess exceptional mechanical properties [2-5]. In addition to their exceptional mechanical properties, CNTs also display superior thermal and electrical properties [22-25, 30-33]. Their thermal conductivity is about twice as high as diamond and their electric current carrying capacity is 1000 times higher than copper wires [26]. The exceptional mechanical and electrical properties of CNTs, combined with their low density, make them an excellent candidate for composite reinforcement [27]. CNTs composites have been studied by researchers and found to improve the aforementioned properties when mixed with polymer materials. Polymers can be changed from being insulator to electrical conductive materials with considerable low contents of CNTs, and their mechanical properties also improved dramatically. In this regard, our choice of polymer materials will be studied as far as electrical and mechanical properties are concerned, as well as strain-rate sensitivity of the composites.

Currently, there are three commonly used methods to introduce CNTs into polymers, i.e. solution processing, in situ polymerization of CNTs-polymer monomer mixture and melt mixing of CNTs with polymers [28-31]. In context with industrial applications of polymer-CNTs systems, melt mixing is the preferred method of composite preparation. Here, an injection molding method which belongs to the melt mixing method

is used to produce our CNT-polymer nanocomposite specimens. The main challenge is how to optimize production parameters such as injection speed, temperature, and pressure, among others, to achieve homogeneous dispersion of CNTs in target polymer base.

Electrical conductivity of CNT-polymer nanocomposite specimens produced by injection molding will be measured through 2-probe method. The transition from an insulator to conductor with respect to the CNT content, also called the percolation threshold, is determined. The percolation theories regard to electrical conductivity of nanocomposite system is applied and compared with our experimental data. For mechanical behaviors of CNT-polymer composites, first, the tensile tests are carried out in the Advanced Material Lab at the City College of New York. Then, a micromechanics modeling is developed to study the elastic properties of the system in terms of CNT content and loading conditions. The results will then be compared between the experimental data and micromechanical modeling.

To the author's knowledge, few researchers have investigated injection molding production parameters, and their effects on electrical and mechanical properties of the CNT-polymer composites. In addition to study electrical and mechanical properties of CNT-polymer composites in terms of weight concentration of CNTs and loading conditions, the effect of injection rate on these properties is investigated.

Finally, the piezoresistivity of CNT-polymer composites is carried out by combining the electrical resistance measurement and mechanical stress-strain measurement under tensile loading. The electrical resistance change in response to the applied load is analyzed.

This thesis is composed in the following orders: In Chapter 2 literature review related to the CNT composites including their processing, characterization and modeling is briefly given. The rest of the dissertation can be classified into three parts: Part I: Processing: it includes Chapter 3 only. Part II: Characterization: this part focuses on experimental investigation of CNT-polymer nanocomposites. It consists of Chapter 4, Chapter 5, and Chapter 6. In Chapter 4, electrical conductivity of the system is measured. Then mechanical behavior under tensile testing is given in Chapter 5. Combination of electrical resistance and mechanical measurements under tensile testing is in chapter 6. Part III: Theoretical modeling. It starts from Chapter 7 to Chapter 9. Finally, the conclusions and remarks are given in Chapter 10.

2. LITTERATURE REVIEW

The uniqueness of electrical and mechanical properties that present in carbon nanotubes (CNT) beyond other available conventional materials has made them attractive for the engineering applications as reinforcing materials. The outstanding properties that possess carbon nanotubes are the result of their structure, which can be pictured as being formed by rolling a graphene sheet into a cylinder. Carbon nanotubes can be classified into three categories: single walled nanotubes (SWNT), multi-walled nanotubes (MWNT), and nanotube bundles or ropes.

SWNT consist of a single layer of carbon atoms wrapped into a cylindrical shape. Typical diameters for SWNT are on the order of 1 nm, while lengths are often on the order of μm. Both the diameter and the length of the SWNT are typically dependent on the particular technique used to create the nanotubes.

MWNT consist of several concentric layers of individual carbon nanotubes that are coupled to each other through van der Waals forces. The diameter and number of shells comprising a MWNT is again dependent on the fabrication process, although diameters on the order of 30 nm may be considered as an estimate [62, 63].

Typically, nanotubes tend to form bundles [64, 65] consisting of several to hundreds of SWNT or MWNT arranged in a closest-packed two-dimensional lattice. Within these bundles the nanotubes normally display a monodisperse range of diameters, with adjacent tubes weakly coupled via van der Waals interactions.

Even though we are interested in mechanical and electrical properties of CNT-polymer composite, let us look at some literature review about the mechanical properties

of CNT. Much of the initial work on the mechanical properties of nanotubes consisted of computational methods such as molecular dynamics models [68-71]. They have found nominal values for the axial Young's modulus on the order of 1TPa with values for the Poisson ratio approximately 0.20 to 0.30.

In his paper, Lu [72] used an empirical force-constant method. Elastic moduli of approximately 1TPa were calculated for SWNT and MWNT, while values for SWNT bundles were between 0.4 and 0.8TPa and found to be very dependent on the diameter of the individual tubes.

Incorporating carbon nanotubes with polymer, metal, and ceramic materials to improve their properties or to develop advanced engineering composites have also become an interesting area of research now a days. Many researchers have studied deferent ways of successfully incorporating CNTs into different composite materials. In regards to polymer materials, three methods namely solution processing, in situ polymerization and melt mixing have been studied [10-21, 28-31].

In the context with industrial applications of CNT-polymer systems, melt mixing is the preferred method of production for bulk nanocomposites. Researchers [10-15] have examined the melt mixing of polymers with nanoscale fillers, primarily nanoclays, and found that mixing depends on the interaction between the filler and polymer, the deformation (shear) rates and residence time in the mixing process. Recent work [42] with polyethylene terephthalate and nanoalumina (Al_2O_3) has shown that dispersion of nanoparticulate fillers into a polymer melt depends on the melt viscosity, shear rate in the process, and strength of the filler agglomerates; this dispersion was consistent with models developed by Manas-Zloczower, Nir, and Tadmor [43, 44] for mixing of rubber

and carbon black in batch mixers. Little work, however, has examined dispersion in the injection molding process. For the PP nanocomposites used in this study, melt-mixed CNT-PP concentrate was diluted with neat PP in the injection molding process. This letdown of pelletized masterbatches is a very common practice for handling fine particles during injection molding. The main challenge was how to optimize processing parameters, including temperatures, pressures, and injection velocities (flow rates) to retain homogeneous dispersion of CNTs in the targeted polymer base. CNTs have shown a tendency to form bundles due to van der Waals forces (interatomic forces) [45, 46]. The melting (plastication) of polymers in the injection unit of an injection molding machine has three stages: screw rotation, soak (i.e., the delay between the end of screw rotation and the start of injection), and injection. During screw rotation, higher screw speeds increase shear, but reduce shearing time. They also permit addition conductive melting of the polymer during soak; this melting, in turn, decreases shearing (and can adversely affect feeding of the polymer pellets). While greater back pressures increase shearing time, and thus mixing, during screw rotation, excessive back pressure does not provide a stable injection molding cycle. Therefore, the plastication conditions of barrel temperature, screw speed, and back pressure can only be optimized to limit the length of the soak time, provide a stable molding cycle, and allow the best mixing within this injection unit.

The injection stage produces very little change in melt temperature, but does cause the polymer chains to align (orient) in the direction of flow. Fountain flow during mold filling creates a highly-aligned layer of melt (i.e., the frozen layer) along the cavity walls. In the center of the mold cavity, slower cooling of the polymer melt permits relaxation of

the oriented the polymer chains. The result is a core-skin structure within injection molded parts. Typically, oriented polymer chains facilitate the alignment of fillers within the polymer melt. These fillers, however, cannot easily become randomized, and so, restrict relaxation of the polymer chains. For example, in unfilled acetal, the mold shrinkage, which is a measure of relaxation, is 2.0 and 1.5% in the flow and cross-flow directions, respectively; addition of 10 wt% glass fibers reduces the flow-direction shrinkage to 1.1%, but has little effect on cross-flow shrinkage [47]. Orientation increases with injection velocity.

One issue of practical importance for nanotube reinforced polymers is the separation and dispersion of the nanotubes within the matrix, which is critical as the nanotubes tend to assemble into bundles due to van der Waals interactions between the individual tubes. While some researchers have been able to separate individual nanotubes from the bundles via ultrasound and polar solvents, maintaining separated nanotubes during the processing is still the subject of ongoing work. Some results suggest that the use of a surfactant as a coupling agent may overcome van der Waals attractive force and allow good dispersion of the nanotubes within the polymer [44]. However, it is unclear whether such processing agents can enhance nanotube dispersion without compromising the nanotube-polymer interface.

In their research, Pujari et al. [73] prepared samples using Solid State Pulverization (SSSP) technique. This technique showed a degree of dispersion slightly better than the one achieved in melt-mixing but other properties such as low electrical conductivity indicated the SSSP technique is less effective in forming percolated nanotube networks.

As well known, most polymers are naturally insulators; combined with CNTs, they become more conductive and make them even more attractive due to this additional property they acquire on top of their other interesting properties (light weight, machinability, optical, to mention few). Different studies have been conducted on electrical conductivity of CNTs composites. To analyze the electrical behavior of CNT composites, different models have been proposed.

Kirkpatrick [32] proposed a percolation model. The concepts of percolation theory have a wide application in many disciplines of sciences. In general, percolation theory deals with the number and properties of clusters on virtual two, three or higher dimensional lattices. His model can be also extended to predict the electrical behavior of CNT-polymer composites.

McLachlan et al [33] also proposed a model to interpret both AC and DC conductivity results of carbon nanotubes and the scaling of these results. In addition to that, they also discussed and compared results obtained in the previous works on CNT-polymer composites and other percolation systems; the modeling of those results was also discussed.

Ahmad et al. [23] studied alumina/multiwalled carbon nanotube composites with different MWNT contents. The dc electrical conductivity and dielectric properties of the composites were investigated and found the composite had a percolation threshold below 1%. In their study, So et al. [25] investigated electrical conductivity of MWCNTs reinforced polyimide nanocomposites synthesized by in situ polymerization using 4, 4’-oxydianilline, MWCNTs, and pyromellitic dianhydride followed by casting, evaporation and thermal imidization. The resultant polyimide/MWCNTs nanocomposites

were electrically conductive with significant conductivity enhancement at 3 weight% MWCNTs.

Chang et al. [22] analyzed annealed polystyrene (PS) composites with varying concentrations of SWCNTs. The composite showed higher electrical conductivity and a lower percolation threshold (less than 1 wt %).

Several researchers have been interested in the use of piezoresistivity and electrical conductivity for sensing purposes [52-54]. Most of those studies were carried out on carbon fiber composites and proved to be efficient. However, little work has examined the effect of mechanical loading on electrical conductivity of polymer composites. Pham et al. [55] developed carbon nanotube polymer composite films that can be used as strain sensors with tailored sensitivity. The films were fabricated by either melt processing or solution casting of poly (methyl methacrylate) (PMMA) with MWNT.

A number of researchers have looked at the mechanical properties of CNT-polymer composite and realized an increase in mechanical properties with the introduction of CNT within the polymer materials. Schadler et al. [66] mixed 5 wt% MWNTs with epoxy and formed macroscale samples; the tensile moduli measured in the mechanical testing were about 3.1GPa for the epoxy and 3.71GPa for the polymer composite.

Researchers at the University of Kentucky [67] have published experimental work measuring the tensile moduli and strength of 1 wt% MWNTs in polystyrene. A homogeneous distribution (on the μm scale) of MWNTs was achieved by an ultrasound-assisted solution-evaporation method. They found a 25% increase in the tensile strength and an approximately 40% increase in the tensile modulus, with both

values being relatively independent of nanotube length.

To study elastic properties of CNT composites, several different approaches have been proposed. In their research, Odegard and Gates [34] have modeled CNT composites using the equivalent continuum method in conjunction with the Mori-Tanaka micromechanics method to obtain the effective elastic constants for both aligned and misaligned CNTs and found effective elastic moduli to be several times that of the matrix for aligned CNTs and almost one and half times the matrix value for misaligned CNTs at a volume fraction of 1% CNTs. Experimentally obtained values for effective Young's modulus were found to be substantially lower.

Li and Shen [35] proposed a uniform replacement method (URM) to study the effect of an inhomogeneous interphase with varying elastic properties in the radial direction on the effective elastic moduli of composites reinforced by fibers/spheres. Between the matrix and the fiber, an interphase region is formed which makes the composites a three-phase composite. The interphase is defined as a region between a homogeneous core and the homogeneous matrix in composites. The elastic properties of the interphase are uniformly described by a general function that varies in the radial direction. The central idea of this model is to convert a three-phase composite into a two-phase composite.

Other theoretical models have also been proposed. At the molecular level, Liao and Li [36] studied the interfacial characteristics of a CNT-polystyrene (PS) composite system through molecular mechanics simulations and elasticity calculations. At the continuum level, Wagner [37] proposed to use the modified classical Kelly-Tyson model, which is applicable to the interfacial strength of traditional micro-fiber reinforced

composites, to calculate the interfacial shear strength of nanotube-polymer composites. Fisher and Brinson [17] presented a continuum model that accounts for the mobility change of so-called non-bulk polymer behavior at the interphase.

In regards to strain-rate sensitivity of CNT composites, Ingram et al. [48] studied the effect of strain rate on tensile behavior of CNT-polymer composite produced by extrusion. The results showed that both the polymer and the polymer composites were strain rate strengthening materials. Li and Weng [49, 50] studied the strain-rate sensitivity and complex moduli of viscoelastic composites with different inclusion shapes and alignments. They found that stress-strain curves strongly depend on applied strain rate and inclusion shape.

A number of researchers have looked at the use of piezoresistivity and electrical conductivity for sensing purposes in case of carbon fiber reinforced composites [52-54, 74-76]. The same analysis in case of CNT-polymer composites is recently being a subject of attention to the researchers. Numerous researchers have recently started to look into a way to use the electrical properties of CNT-polymer composites for Electromagnetic Interference (EMI) shielding [77-92].

It has also been reported that nanotubes embedded in a polymer matrix can be used as strain sensors at a nanoscale level by observing the Raman band shift, as the load is transferred from the matrix to the nanotubes [93]. However, this method is not practical in field applications due to the difficulties associated with the implementation of the measuring equipment.

Park et al. [94] noted an increase in electrical resistance when MWCNT-epoxy films were subjected to tensile stresses. In another research, Pham et al. [95] measured

the electrical resistance of PMMA/ MWNT composite films subjected to tensile strains was measured, and the surface resistivity of the films was observed to increase with increasing tensile strain.

We can realize that a number of models have been proposed to estimate the electrical and mechanical properties of CNT-polymer composites. However, none of the above study is specific as far as the production parameters as well as the injection molding process are concerned; for the above reasons, both the experimental and theoretical studies will be carried out on CNT-polymer composites produced by injection molding.

PART I: PROCESSING

3. FABRICATION OF CNT-POLYMER COMPOSITES USING INJECTION MOLDING

The CNT composite specimens were produced using a 55-ton reciprocating screw injection molding machine (Cincinnati Milacron-Fanuc, Model: Robo 55R-22) shown in Figure 3.1, at the University of Massachusetts, Department of Plastics Engineering, Lowell.

Figure 3.1: Robo 55R-22 reciprocating screw injection molding machine

The injection system mainly consists of a hopper, a reciprocating screw and barrel assembly, and an injection nozzle. The reciprocating screw is used to compress, melt, and convey the material. The flights on the reciprocating screw compress the material against the inside diameter of the barrel, which creates viscous (shear) heat. This shear heat is mainly responsible for melting the material. The heater bands outside the barrel help maintain the material in the molten state. Typically, a molding machine can have three or more heater bands or zones with different temperature settings. In our case, our screw injection molding machine has four heating zones (3 barrel zones and one nozzle zone).

Two thermoplastic materials: polypropylene (PP) and polycarbonate (PC) were chosen as polymer matrix materials. The choice of the polymer matrix materials was based on the fact both PP and PC are homopolymers and widely used in the plastic industry. The PP is used in food packaging, ropes, textiles, plastic parts and reusable containers of various types, thermal pants and shirts made for the military, laboratory equipment, loudspeakers, automotive components, and polymer banknotes to mention a few. In regards to PC, it is used in lighting lenses, sunglass/ eyeglass lenses, safety glasses, automotive headlamp lenses, compact discs, DVDs, lab equipment, research animal enclosures, drinking bottles, advertisement (signs, displays, poster protection), construction (domelights, flat or curved glazing, sound walls), in computers, etc.

Even though both PP and PC were not originally designed for structural applications, simple processing and low cost make them ideal candidates for many other applications such as EMI/RFI shielding, coatings for enclosures, gaskets, electrostatic dissipation (ESD), antistatic materials and conductive coatings, and radar-absorbing for low-observable application, military and aerospace.

3.1. Fabrication of MWCNT-PP composites

The PP virgin material grade is Acclear @8449. The multiwalled carbon nanotubes (MWCNTs) were purchased from Hyperion. Material grade of Hyperion PP masterbache is MB 3020-01 with 20 weight percentage of MWCNTs in PP.

According to the standard procedure of injection molding for the PP, the heating zone temperatures are 410^{o}F-410^{o}F-400^{o}F-380^{o}F. The above heating zone temperatures are set based on the melting temperature of the materials to be molded.

In order to study the effect of injection velocity on structures and properties of MWCNT-PP composites, three different injection speeds were adopted as low (1in/s), medium (4in/s) and high (7in/s). Pure PP polymers as well as MWCNT-PP composite specimens were produced. The mixture of PP masterbache with virgin PP was used to get the ratio of 2%, 3.5%, 4.5%, 5%, 7%, 10% and 12% weight percentage of CNT.

Apart from the molding parameters mentioned above, a number of additional parameters have to be controlled to make a good sample. Those parameters include the short size, decomposition distance, decomposition velocity, cooling time, mold temperature, position transfer, packing pressure and the extrusion pressure. Their numerical values for different injection velocities are given below in Table 3.1.

Table 3.1: Processing parameters for PP with three different injection velocities

Parameters	**Injection velocity (in/s)**		
	1	**4**	**7**
Short size (in)	1.650 in	1.650 in	1.650 in
Decompression distance (in)	0.1in	0.1in	0.1in
Decompression velocity (in/s)	2 in/s	2 in/s	2 in/s
Cooling time (s)	20sec	20sec	20sec
Mold temperature (^{o}F)	90^{o}F	90^{o}F	90^{o}F
Transfer position	0.4 in	0.5 in	0.6 in
Packing pressure (2 steps)	4000psi for 1sec and 1000psi for 5sec	4000psi for 1sec and 2000psi for 5sec	4000psi for 1sec and 2000psi for 5sec
Plastication pressure	500psi at the speed of 150 rpm	500psi at the speed of 150 rpm	500psi at the speed of 150 rpm

Transmission Electron Microscope (TEM) images were used to visualize and analyze the polymers as well as their MWCNTs composites. The images also show the dispersion of the MWCNT within the polymer matrice. Figure 3.2 (a) to (c) show the TEM images for PP and MWCNT-PP composites at different injection speed and weight percentages of CNTs.

Figure 3.2 (a) shows the TEM image of the virgin PP material. Figure 3.2 (b) shows the TEM image of the MWCNT-PP composite with 2% CNT produced with low injection speed of 1in/s where as figure 3.2. (c) shows the same composite but produced with higher injection of 7in/s.

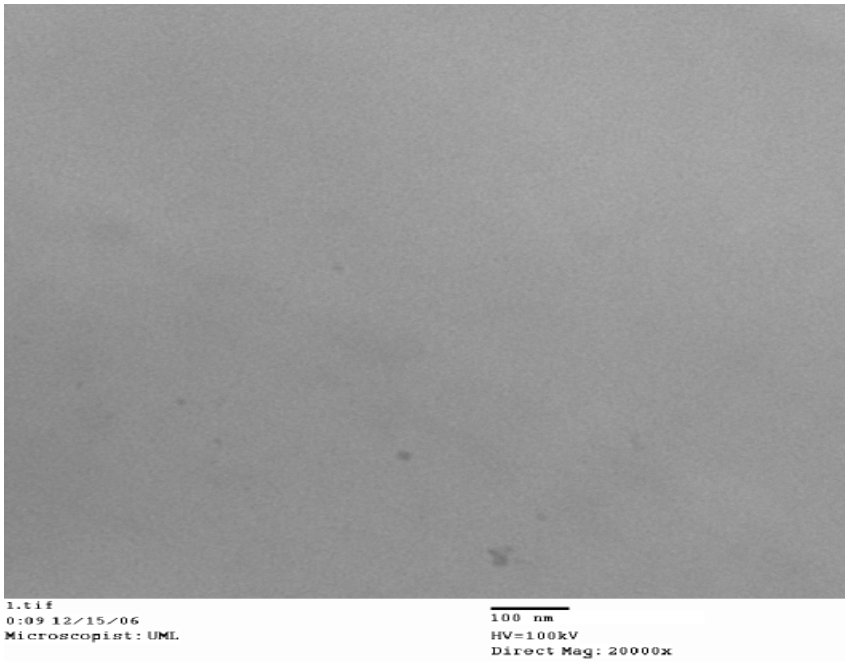

(a) Pure PP

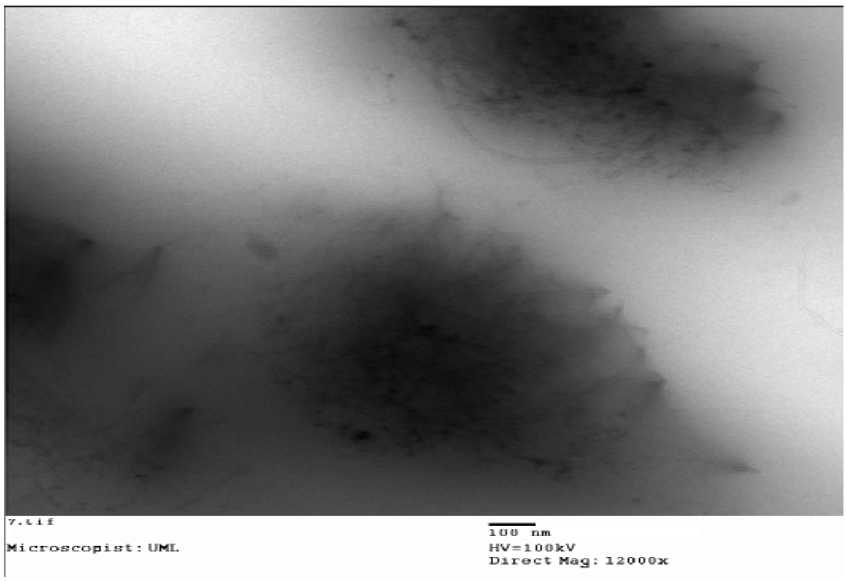

(b)

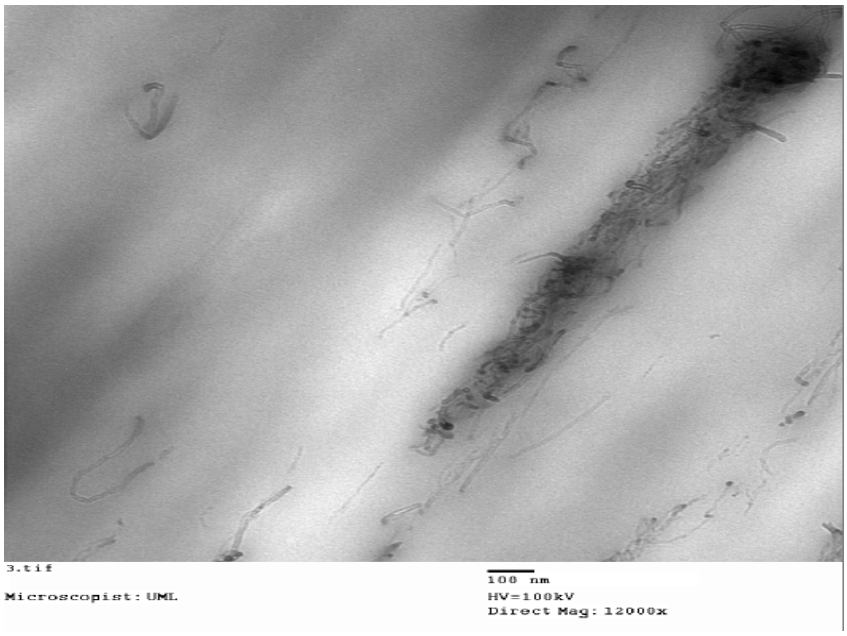

(c)

Figure 3.2: TEM images for (a) virgin PP material, (b) MWCNT-PP composite with 2%CNTs produced at the injection speed of 1in/s, and (c) MWCNT-PP composite with 2%CNTs produced at the injection speed of 7in/s.

From the above images, one clear conclusion can be drawn. For the composites produced at a low injection velocity (refer to Figure 3.2 (b)), the CNT within the polymer are agglomerated in bundles. A different outcome could be observed for the same composites but produced at a higher injection velocity (refer to Figure 3.2.c); the CNT are not longer agglomerated in bundles, rather they are forming fiber-like structure along the direction of injection.

3.2. Fabrication of MWCNT-PC composites

The PC virgin material grade is Lexan 121. The multiwalled carbon nanotubes (MWCNTs) were also purchased from Hyperion. Material grade of Hyperion PC masterbache is MB 6015-00 with 15 weight percentage of MWCNTs in PC. Comparing to CNT-PP composites, the major differences are the processing parameters.

In regards to PC specimens' production parameters, the temperatures of the heating zones are 550^{o}F-550^{o}F-530^{o}F-510^{o}F. Three different injection speeds were also adopted as low (1in/s), medium (4in/s) and high (7in/s). Pure PC polymers as well as MWCNT-PC composite specimens were produced. The mixture of PC masterbache with virgin PC was used to get weight percentage of CNT from 1%, 1.5%, 1.6%, 1.7%, 1.8%, 1.9%, 2%, 3%, 4%, 5% up to 7% respectively. The other production parameters are given below in Table 3.2.

Table 3.2: Processing parameters for PC with three different injection velocities

Parameters	**Injection velocity (in/s)**		
	1	**4**	**7**
Short size (in)	1.8 in	1.8 in	1.8 in
Decompression distance (in)	0.1in	0.1in	0.1in
Decompression velocity (in/s)	2 in/s	2 in/s	2 in/s
Cooling time (s)	20sec	20sec	20sec
Mold temperature (^oF)	90^oF	90^oF	90^oF
Transfer position	0.5 in	0.6 in	0.7 in
Packing pressure (2 steps)	5000psi for 1sec and 1500psi for 5sec	5000psi for 1sec and 1500psi for 5sec	5000psi for 1sec and 1500psi for 5sec
Plastication pressure	500psi at the speed of 150 rpm	500psi at the speed of 150 rpm	500psi at the speed of 150 rpm

TEM images were also taken for PC material and MWCNT-PC composites. Figure 3.3 (a) shows the TEM image of the virgin PC material. Figure 3.3 (b) shows the TEM image of the MWCNT-PC composite with 2% CNT produced with low injection speed of 1in/s where as Figure 3.3 (c) shows the MWCNT-PC composite with 2% CNT produced with higher injection of 7in/s.

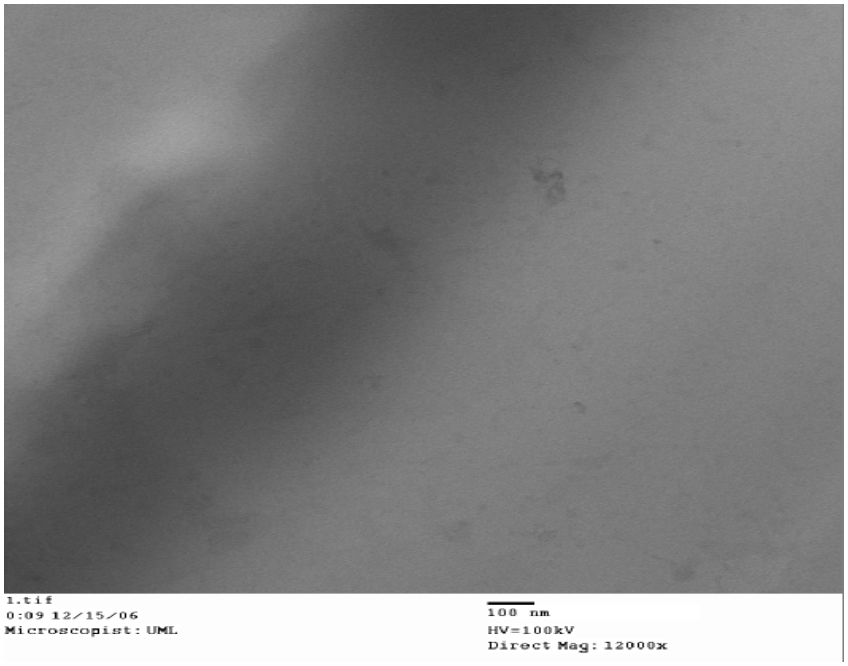
1.tif
0:09 12/15/06
Microscopist: UML
100 nm
HV=100kV
Direct Mag: 12000x

(a) Pure PC

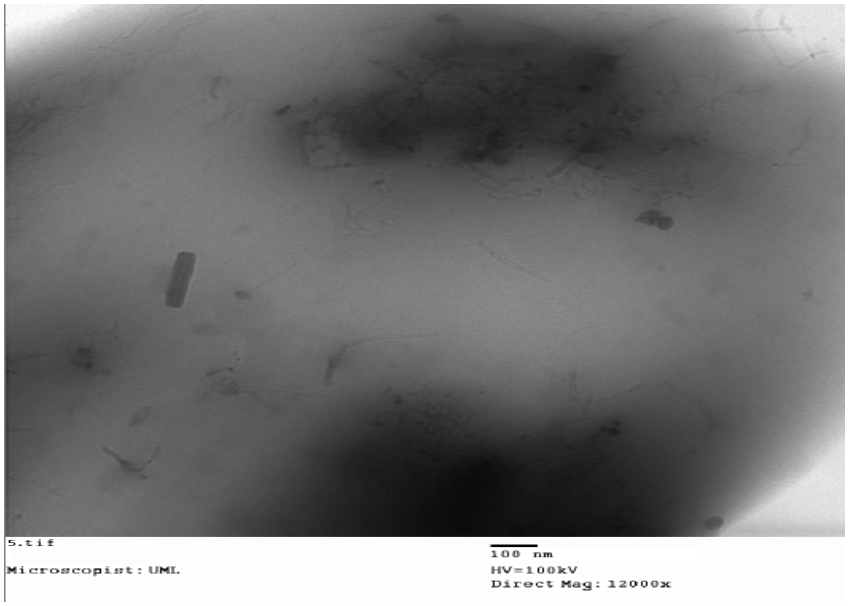
5.tif
Microscopist: UML
100 nm
HV=100kV
Direct Mag: 12000x

(b)

(c)

Figure 3.3: TEM images for (a) virgin PC material, (b) MWCNT-PC composite with2%CNTs produced at the injection speed of 1in/s, and (c) MWCNT-PC composite with 2%CNTs produced at the injection speed of 7in/s.

Again from Figure 3.3, one can visualize that CNTs inside the polymer matrice are agglomerated into bundles at low injection velocity, and aligned to fibers at high injection velocity.

PART II: CHARACTERIZATION

4. ELECTRICAL CONDUCTIVITY OF CNT-POLYMER COMPOSITES

The uniqueness of physical properties that present in CNTs beyond other available conventional materials has made them attractive for the engineering applications as reinforcing materials. Incorporating carbon nanotubes with polymer materials to improve their properties make them more attractive as they become conductive, and at the same time keep their interesting properties. In this study, first, these nanocomposites were characterized for their electrical conductivity using 2-Probe measurement.

From the previous chapter, we realized that micrographs from the TEM images show different structure appearance with the change in injection speed. In this chapter, we will also try to analyze if there is an effect of the injection speed on electrical conductivity of polymer composites.

Referring to the literature review, different researchers have looked into the percolation of different CNTs composite systems. We will compare our findings about the percolation value with theirs to see if our choice of polymer materials and MWCNTs are comparable to the existing literature results.

4.1. Experimental Set-Up

To study electrical conductivity of MWCNTs-Polymer nanocomposites, a 2-Probe electrical resistance measurement is used; both ends of the rectangular section samples were painted with the silver paint as electrodes. Then, the volume resistance can be measured, and the corresponding conductivity can be calculated. Figure 4.1 below shows the experimental set-up. The rectangular specimens tested for electrical resistance measurements have dimensions of 60.0mm (L) x 12.5mm (W) x 2.95mm (T).

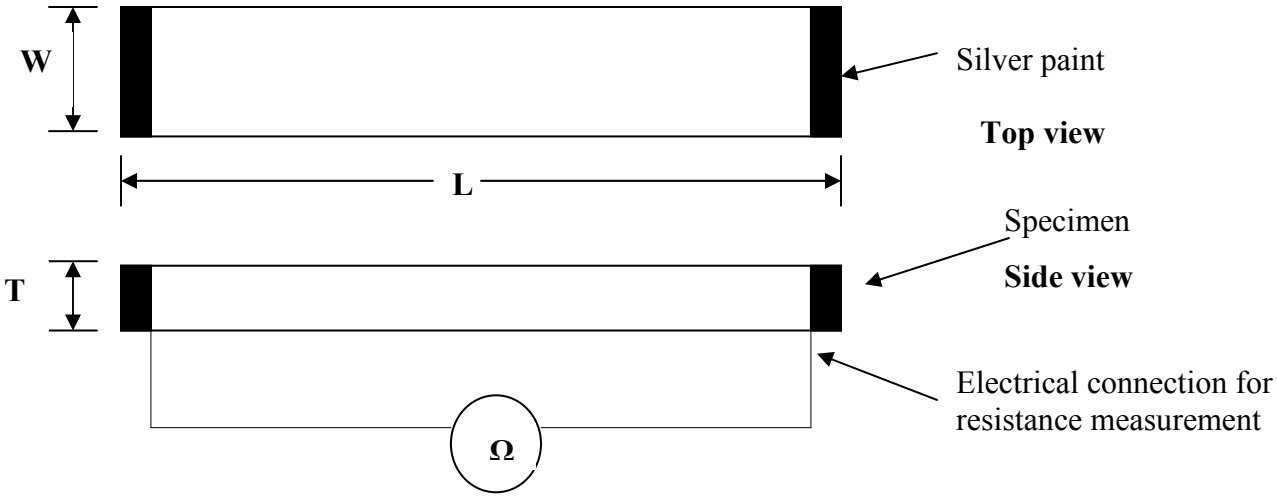

Figure 4.1: Experimental set-up for resistance measurement.

Keithley (model # 2002) electrometer was used to measure the electrical resistance. For the same type of materials, five identical specimens were tested for consistency. The average value with standard derivation error bar was used for the final data points.

Once the electrical resistance is obtained, the corresponding resistivity ρ was calculated through the equation given below:

$$\rho = \frac{R \times A}{l} \qquad (1)$$

where R is the electrical resistance, A the cross section area of the specimen, and l the distance between the two electrodes.

Then the electrical conductivity σ can also be calculated as the inverse of the electrical resistivity i.e.

$$\sigma = \frac{1}{\rho}. \qquad (2)$$

4.2. Experimental Results

4.2.1. MWCNT-PP composites

The electrical conductivity of MWCNT-PP nanocomposites in terms of weight percentage of CNT content at three different injection velocities is shown in Figures 4.2. There is a significant shift in electrical conductivity (or the percolation threshold) between 2wt% and 5wt% CNT contents. When the CNT weight percentage increases to 7%, the conductivity of CNT composite increases more than seven orders of magnitude comparing to the pure polypropylene. This indicates that the polypropylene can be turned from an insulator to a more conductive material by adding a small amount of CNTs. From Figure 4.2, the approximate percolation threshold is about 4 wt% of CNT.

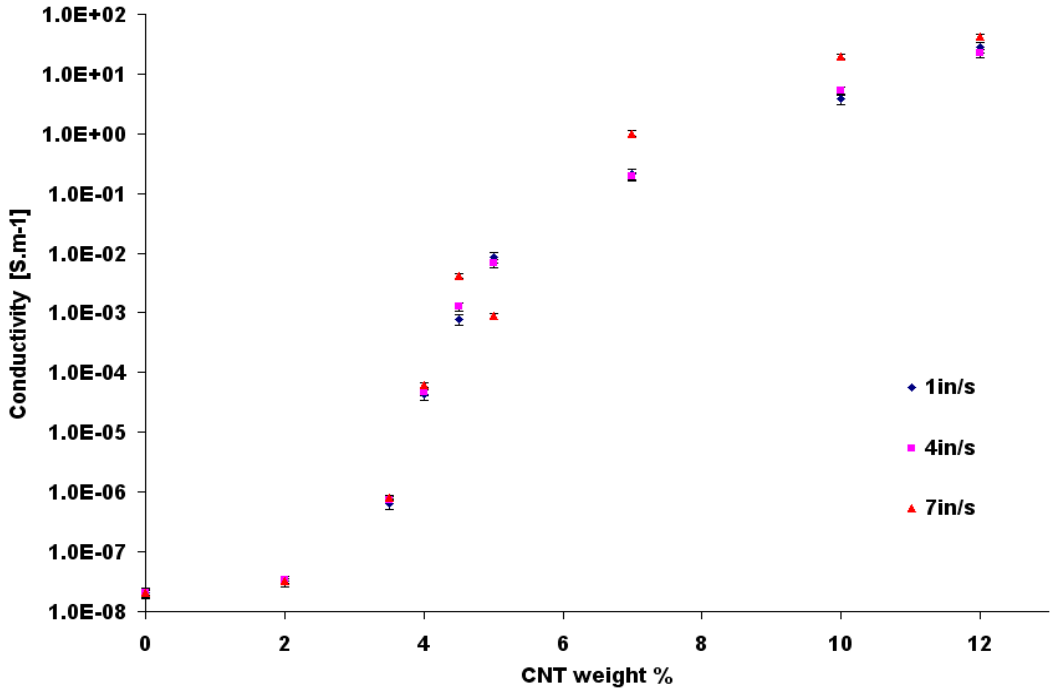

Figure 4.2: Electrical conductivity of MWCNT-PP composites in terms of CNT content on a logarithmic scale.

Figure 4.3 shows the influence of injection velocity on normalized electrical conductivity of the CNT-PP system with various CNT content. The normalized conductivity is the ratio between the conductivity at any given injection rate and the conductivity at the low injection rate (1in/s). When the CNT content was well above the percolation threshold (i.e., 7, 10, and 12 wt %), injection velocity has significant effect on the normalized electrical conductivity. For CNT content near the percolation threshold (i.e.5 wt %), electrical conductivity decreased as injection velocity increases. At very low carbon nanotube concentrations (i.e., 2 and 3.5 wt %), however, the electrical conductivity was independent of injection velocity.

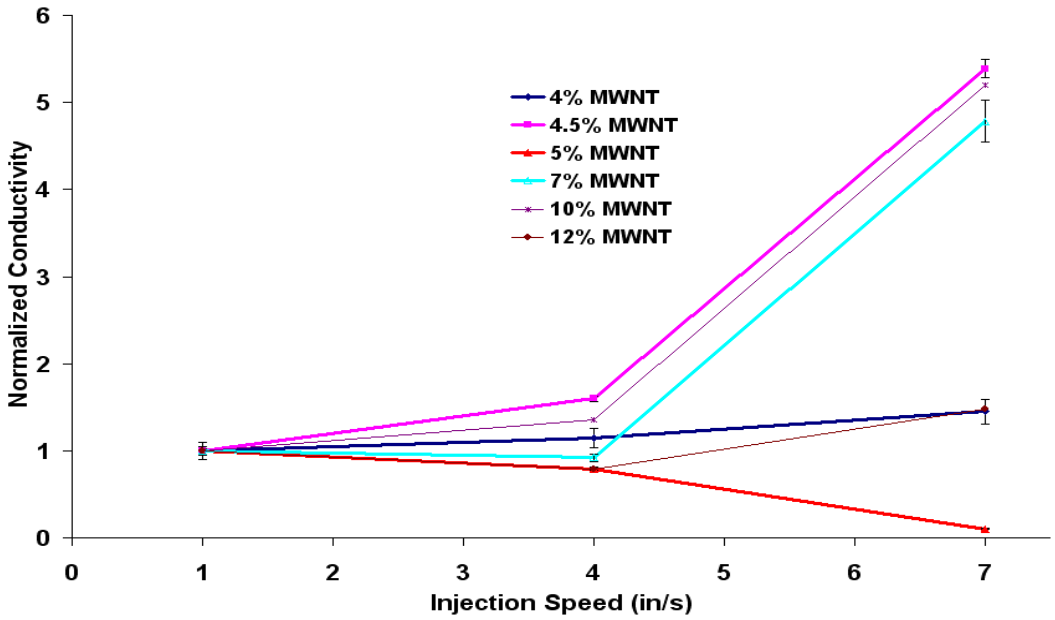

Figure 4.3: Effect of Injection velocity on normalized electrical conductivity of CNT-PP nanocomposites.

This performance is mainly due to the distribution of MWNTs within the nanocomposite. As illustrated in Figure 4.4, the MWNTs appeared as "clumps" in TEM images. These MWNT clumps were randomly distributed in all nanocomposite specimens, but as the injection velocity is increased they exhibited a preferred orientation pattern in the direction of melt flow. Thus, the carbon nanotubes aligned themselves from random bundles (at low injection speed) to aligned fibers (at high injection speed). With a MWNT load of 2 wt%, the aligned clumps still did not connect, and so, the electrical conductivity was low. At a content of 5 wt%, contact of aligned clumps provided a significant increase in electrical conductivity; whereas at loadings of 7, 10, and 12 wt% even the randomly aligned clumps were in contact with each other. Overall, this behavior was consistent with poor mixing of the MWNT masterbatch with the neat polypropylene diluent. It is a clear indication that even though the MWNTs are randomly distributed in

the composite, they have a preferred orientation pattern when the injection speed is higher.

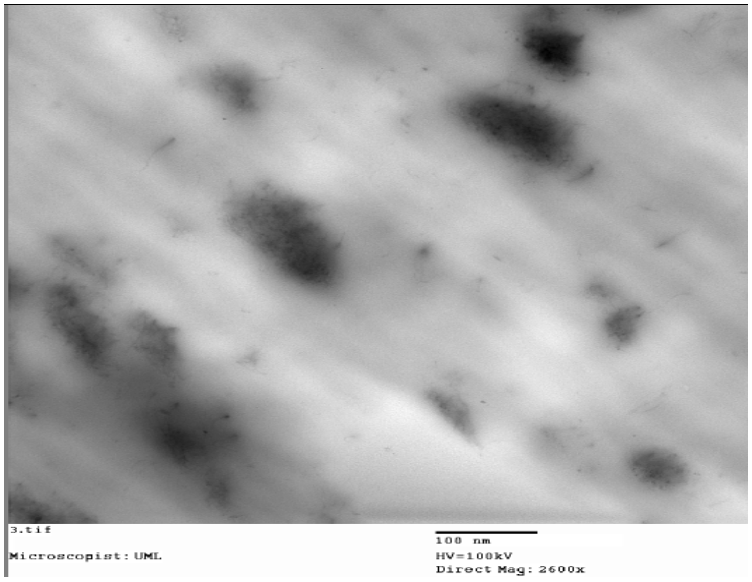

(a) 1in/s

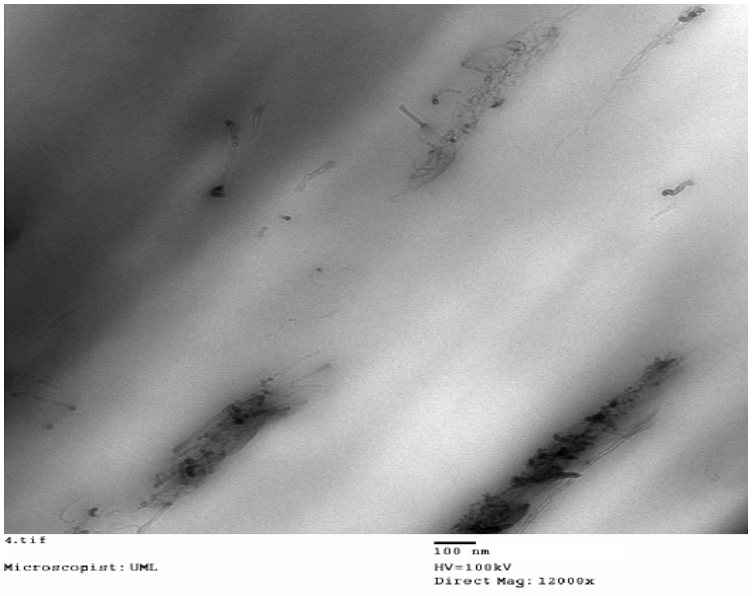

(b) 7in/s

Figure 4.4: TEM images for MWNT-PP nanocomposite with 2wt%CNT with the injection speed of (a) 1in/s and (b) 7in/s.

4.2.2. MWCNT-PC composites

Figure 4.5 shows the experimental results for electrical conductivity of MWCNT-PC nanocomposites in terms of different contents of CNTs at three injection velocities. It clearly indicates a significant increase (more than 5 orders of magnitude higher) of electrical conductivity at 2wt% of CNTs comparing to pure PC polymers. The percolation of conductivity occurs well below 2 wt % of CNTs. According to the PC datasheet form Hyperion catalysis, the percolation threshold of conductivity for MWCNT-PC composites should be around 2% which falls in our experimental results; another research paper [11] in the literature showed the percolation threshold for MWCNT-PC system produced by melt processing to be around 5 wt%.

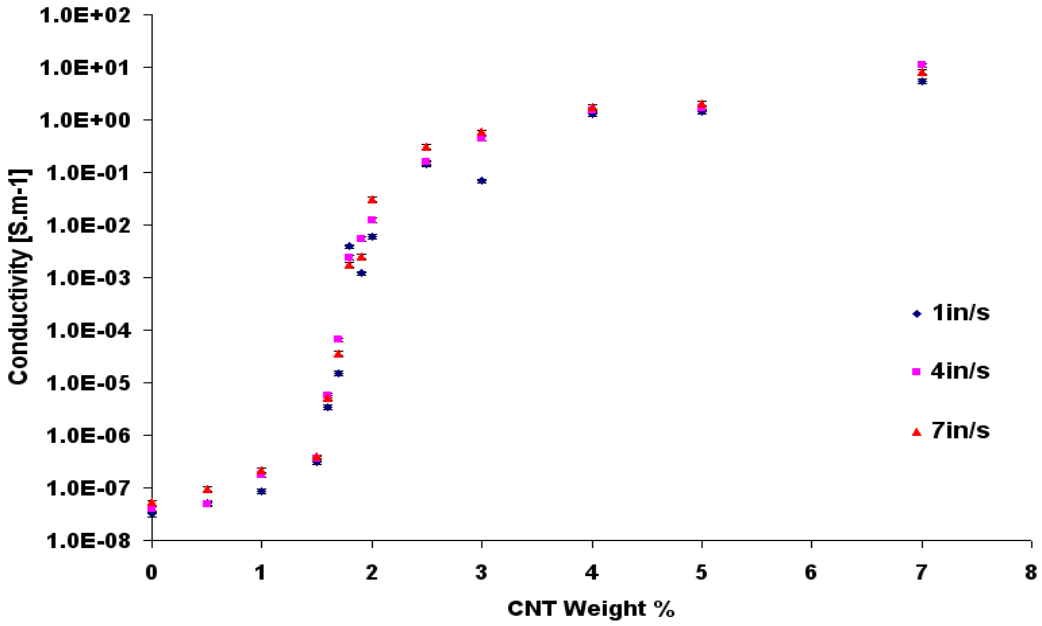

Figure 4.5: MWCNT-PC composites electrical conductivity in terms of CNT content on a logarithmic scale.

Figure 4.6 shows the normalized conductivity of MWCNT-PC nanocomposites in terms of injection speed at various CNT contents. All different contents of CNT show tendency of conductivity increase with increasing injection speed.

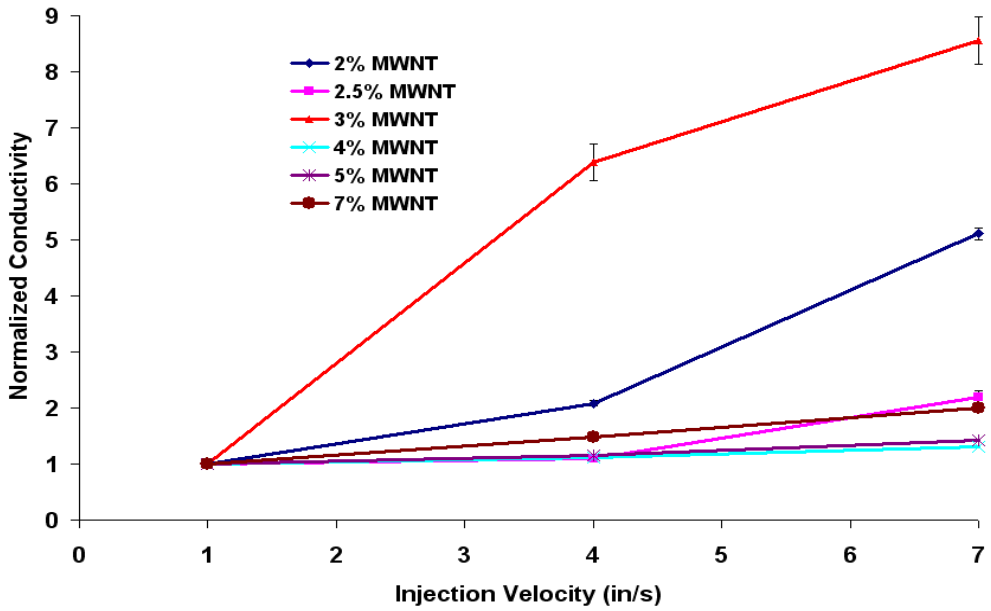

Figure 4.6: Effect of Injection velocity on PC-MWCNT composites electrical conductivity.

5. EXPERIMENTAL INVESTIGATIONS ON MECHANICAL BEHAVIORS OF CNT COMPOSITES

It has been found experimentally and theoretically that carbon nanotubes can possess exceptional mechanical properties. For example, their axial Young's modulus can be higher than 1 TPa (the elastic modulus of diamond is 1.2 TPa), their tensile strength may approach 100 GPa, which is about 10-100 times higher than the strongest steel at a fraction of the weight.

Due to exceptional mechanical properties of CNTs, they have attracted much attention as one of the ideal reinforcement materials in composites. With less than 10wt% CNT in polymer matrix composites, the strength of the system can reach up to comparable or even higher level than the ones of commercial available carbon fiber reinforced polymer composites with more than 60% of carbon fibers in the same polymer base materials. However, the experimental results were still off from the theoretical predictions. The main concerns come from processing of CNT composite, which include dispersion of CNTs, processing parameters control such as temperatures, pressures, among others. Here we systematically study the mechanical behaviors of CNT-polymer composites produced by injection molding. The CNT contents, injection velocity and strain-rate controlled loading are our main focus.

This chapter deals with the experimental investigations on mechanical behavior of MWCNT-polymer composites. Tensile tests are carried out under different strain rates loading. The elastic modulus of CNT-polymer nanocomposites is obtained from tensile tests and studied in terms of CNT contents. Also, the influence of injection velocity and

strain-rate loading conditions on elastic properties and stress-strain relations of the system are analyzed.

5.1. Experimental Set-Up and Material Preparation

Mechanical tensile tests were conducted using INSTON 5882 universal testing machine with Blue Hill software. Strain and extension were recorded using the video extensometer. The set-up is shown in Figure 5.1.

According to ASTM Standard D3039 (Reapproved ‘06) for the test procedures of polymer composites, the standard strain rate is set to be 0.01/min for static loading. Then the elastic modulus of the specimens can be obtained and the stress-strain curves can be generated. In order to study the strain-rate sensitivity of the nanocomposites, other strain rates may be applied.

Standard tensile test specimens shown in Figure 5.2 were produced by injection molding as described in Chapter 3. The specimens had average dimensions of 97.0mm (Gauge L) x 12.5mm (W) x 2.95mm (T).

Both CNT-PP and CNT-PC nanocomposites were used for tensile testing. For CNT-PP specimens, the selected range of weight percentage of CNT is from 0%, 2%, 5%, 7%, 10% to 12% respectively. For MWCNT-PC composites, the range of weight concentration of CNT is from 0wt%, 1wt%, 3wt%, 5 wt% and 7wt%. Beyond 7wt% of CNT, the composite specimens became too brittle to be obtained through injection molding.

For each different type of nanocomposites, at least three specimens were tested under the same loading condition to secure the repeatability and accuracy of the tests.

The strain was recorded using the video extensometer and the stress was obtained from Instron Blue Hill software.

(a) (b)

Figure 5.1: Tensile test experimental set-up with (a) front view, and (b) back view of the INSTRON universal testing machine.

Figure 5.2: The tensile test dog bone specimen

5.2. Experimental Results

5.2.1. Experimental results for MWCNT-PP composites

5.2.1.1. Elastic Properties of MWCNT-PP Composites

During the tensile tests, the elastic modulus of the system was obtained from the Blue Hill Software. Again for each type of sample, at least three specimens have been tested and compared for consistency. Table 5.1 shows the numerical values for the modulus of elasticity of the MWCNT-PP composites at injection velocities of 1in/s, 4in/s and 7in/s respectively.

Table 5.1: Numerical values of modulus of elasticity of MWCNT-PP composites at a strain-rate of 0.01/min

wt % CNT	Elastic modulus (GPa)				Standard deviation (%)
	Injection velocity (Vinj)			Average	
	1in/s	4in/s	7in/s		
0	0.670	0.674	0.673	0.672	0.001
2	0.710	0.701	0.733	0.715	1.425
5	0.894	0.872	0.902	0.889	4.487
7	1.044	1.016	1.149	1.070	3.734
10	1.313	1.226	1.368	1.302	2.874
12	1.472	1.537	1.415	1.475	2.046

From Table 5.1, we can realize the effect of injection speed on the modulus of elasticity of MWCNT-PP composites is small (standard deviation is below 5%); thus we can use average values of elastic moduli to show the effect of CNT content on MWCNT-PP composites. Even though the influence of the injection velocity is small, a slight

increase in elastic modulus at higher injection speed except for the CNT weight percentage of 12% can be observed. We have not so far identified what might be the reason. Figure 5.3 shows the effect of CNT content on modulus of elasticity of MWCNT-PP composites tested at a standard strain-rate of 0.01/min.

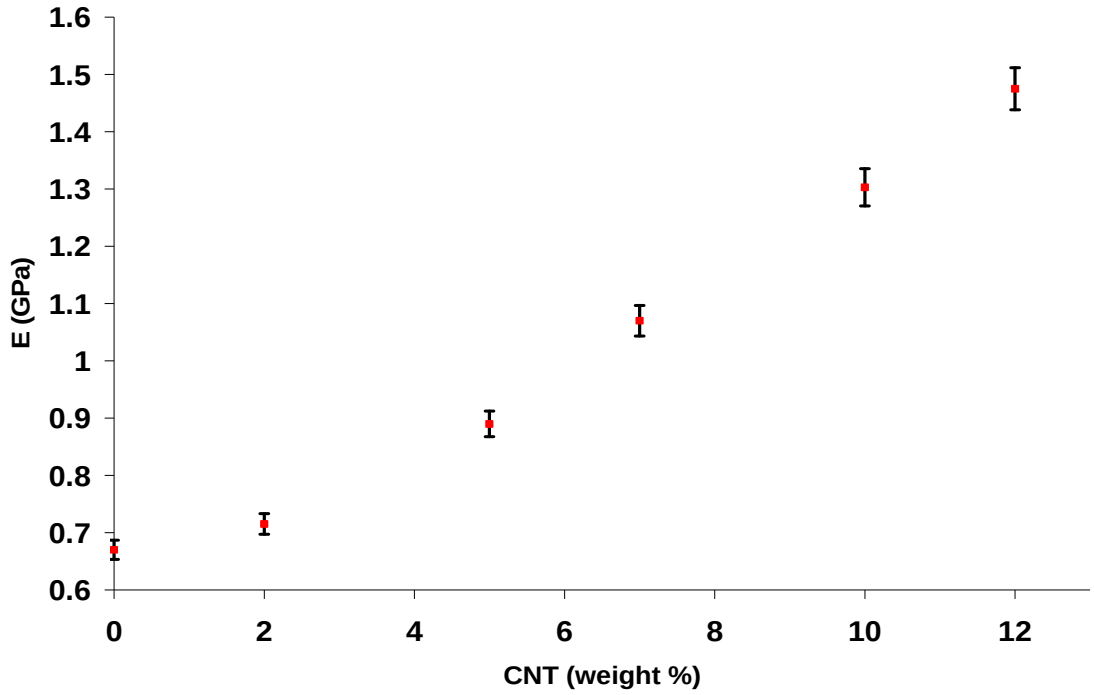

Figure 5.3: Effect of CNT content on elastic modulus for MWCNT-PP composites tested at a standard strain-rate of 0.01/min.

From Figure 5.3, one can conclude that the elastic modulus of the nanocomposite system increases with the increase of CNT content. With 12 wt% CNT, the elastic modulus is more than doubled compared to the pure polypropylene matrix. A micromechanics approach will be applied to verify our results in Chapter 7.

5.2.1.2. Effect of Strain-Rate on Elastic Properties of MWCNT-PP Composites

Most polymer materials exhibit sensitivity in regards to strain rate. In our study, two strain rates were used namely 0.01/min and 0.1/min. Table 5.2 shows the numerical values for the modulus of elasticity of the MWCNT-PP composites tested at a strain-rate of 0.1/min.

Table 5.2: Numerical values of modulus of elasticity of MWCNT-PP composites tested at a strain-rate of 0.1/min.

wt % CNT	Elastic modulus (GPa)				Standard deviation (%)
	Injection velocity (Vinj)			Average	
	1in/s	4in/s	7in/s		
0	0.634	0.659	0.640	0.644	2.817
2	0.703	0.706	0.712	0.707	1.391
5	0.861	0.840	0.846	0.849	2.475
7	0.935	0.954	0.992	0.961	2.120
10	1.132	1.168	1.142	1.147	4.008
12	1.282	1.276	1.298	1.285	3.294

Similarly to the tests at the standard strain-rate of 0.01/min, we can realize the effect of injection speed on the modulus of elasticity of MWCNT-PP composites tested at a strain-rate of 0.1/min is not significant (standard deviation is below 5%); thus we can use average values of elastic moduli to show the effect of CNT content on MWCNT-PP composites tested at a strain-rate of 0.1/min, which is given in Figure 5.4.

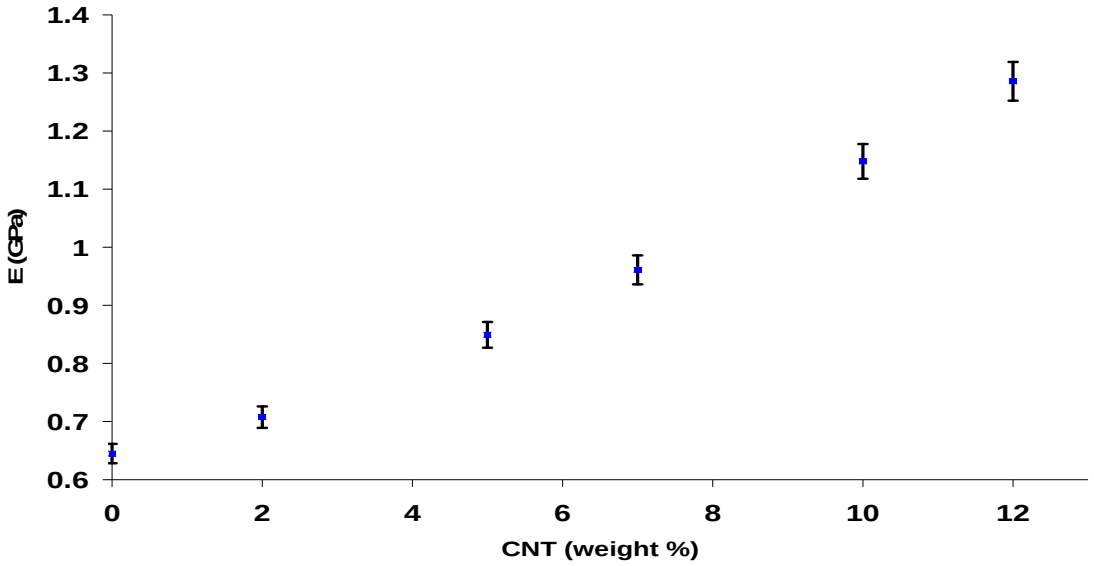

Figure 5.4: Effect of CNT content on elastic modulus for MWCNT-PP composites tested at a standard strain-rate of 0.1/min.

Figure 5.5 combines figures 5.3 and 5.4 to show the effect of strain-rate on modulus of elasticity of MWCNT-PP composites. We realized the increase in strain-rate resulted in decrease in elastic modulus of MWCNT-PP composites.

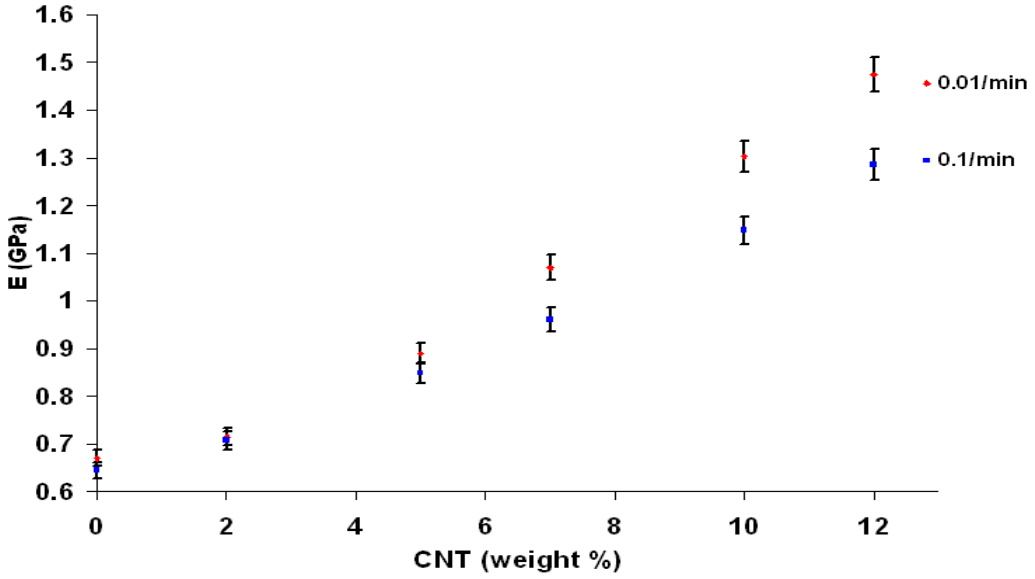

Figure 5.5: Effect of CNT content on elastic modulus for MWCNT-PP composites.

5.2.1.3. Stress-Strain Relations of MWCNT-PP Composites

In order to study the complete mechanical behavior of MWCNT-PP composites under tensile loading, the stress-strain curves have been obtained under two different strain-rate loadings: 0.1/min and 0.01/min.

a. Effect of CNT Content on Stress-Strain curves

The effect of CNT contents on Stress-strain curves of MWCNT-PP composites at a strain rate of 0.01/min at different injection velocities are shown in figures 5.6, 5.7 and 5.8 below. A clear increase in the slope of the stress-strain curves with increase in CNT weight content can be observed. In addition to that, as the CNT content increases, the MWCNT-PP composites become more brittle.

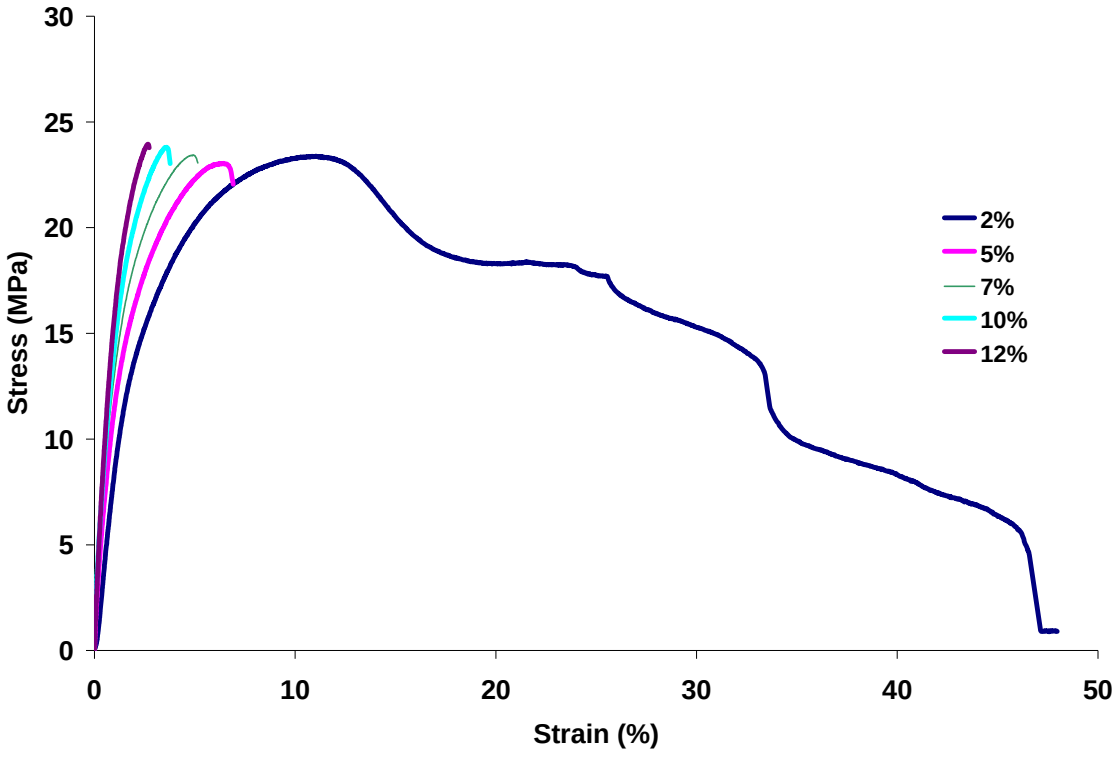

Figure 5.6: Stress-strain curves for the MWCNT-PP composites produced with injection velocity of 1in/s.

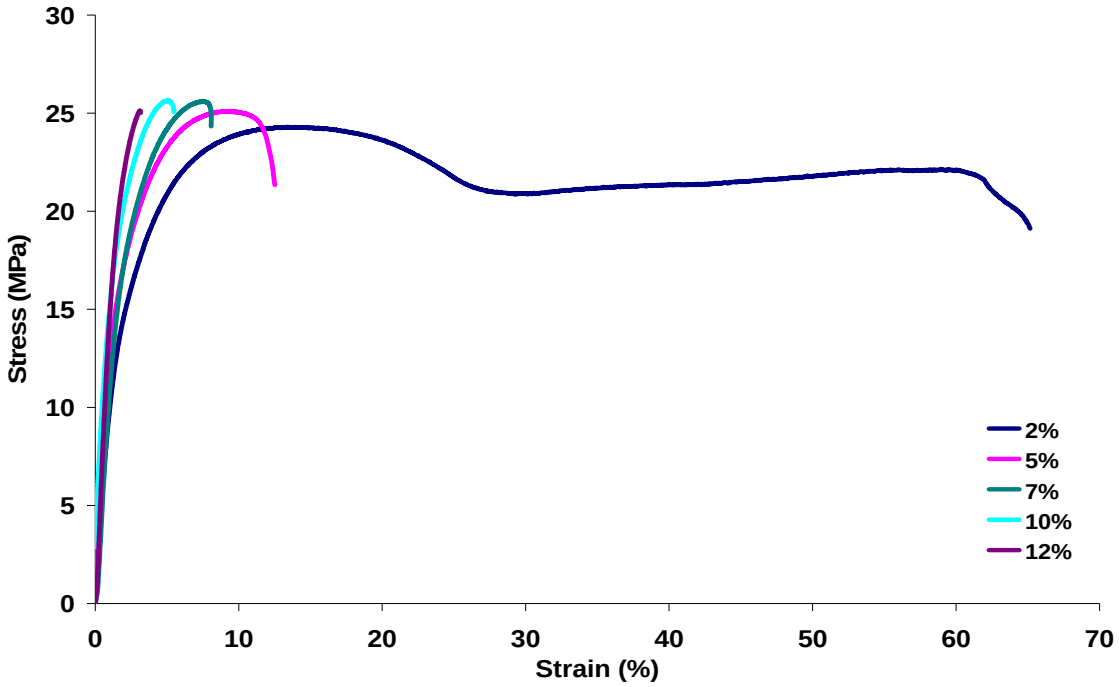

Figure 5.7: Stress-strain curves for the MWCNT-PP composites produced with injection velocity of 4in/s.

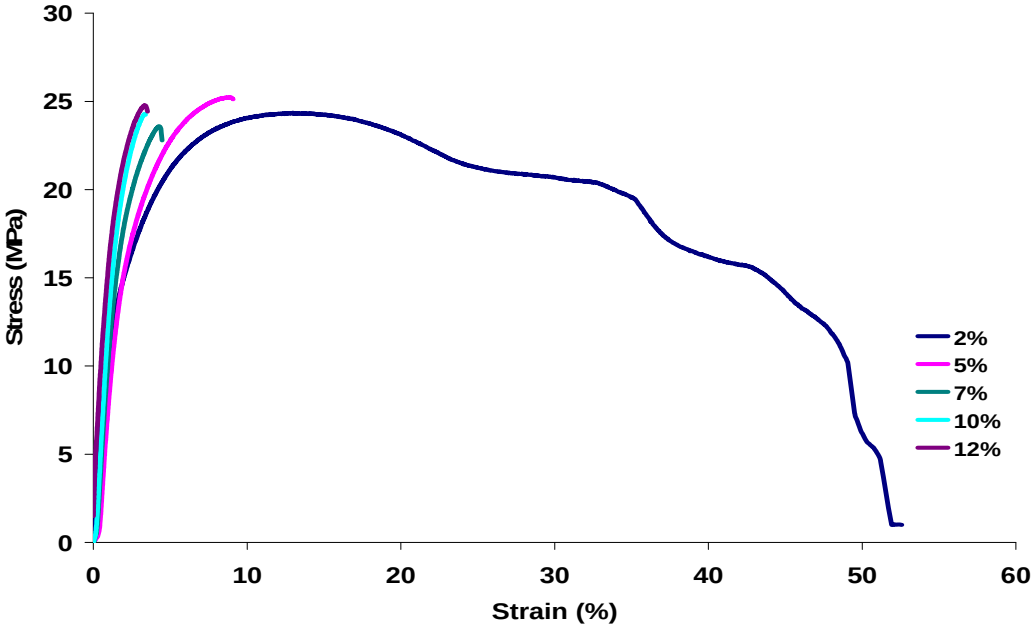

Figure 5.8: Stress-strain curves for the MWCNT-PP composites produced with injection velocity of 7in/s.

b. Effect of injection speed on Stress-Strain curves

Figures 5.9 shows the effect of injection speed on stress-strain curves for MWNT-PP composites tests with 0.01/min strain-rate at different CNT weight contents. From the figures, no unambiguous effect of injection speed on stress-strain curves can be drawn.

c. Effect of strain-rate loading on stress-strain curves

Figures 5.10 shows the effect of strain-rate loading on stress-strain curves for MWNT-PP composites produced with the injection velocities of 1in/s at different CNT weight contents. Unlike most polymers, this PP composite system with CNT reinforcement does not show consistent strain-rate sensitivity such as increased strength with increasing strain-rate loading. To verify the strain-rate effects, more tests are needed.

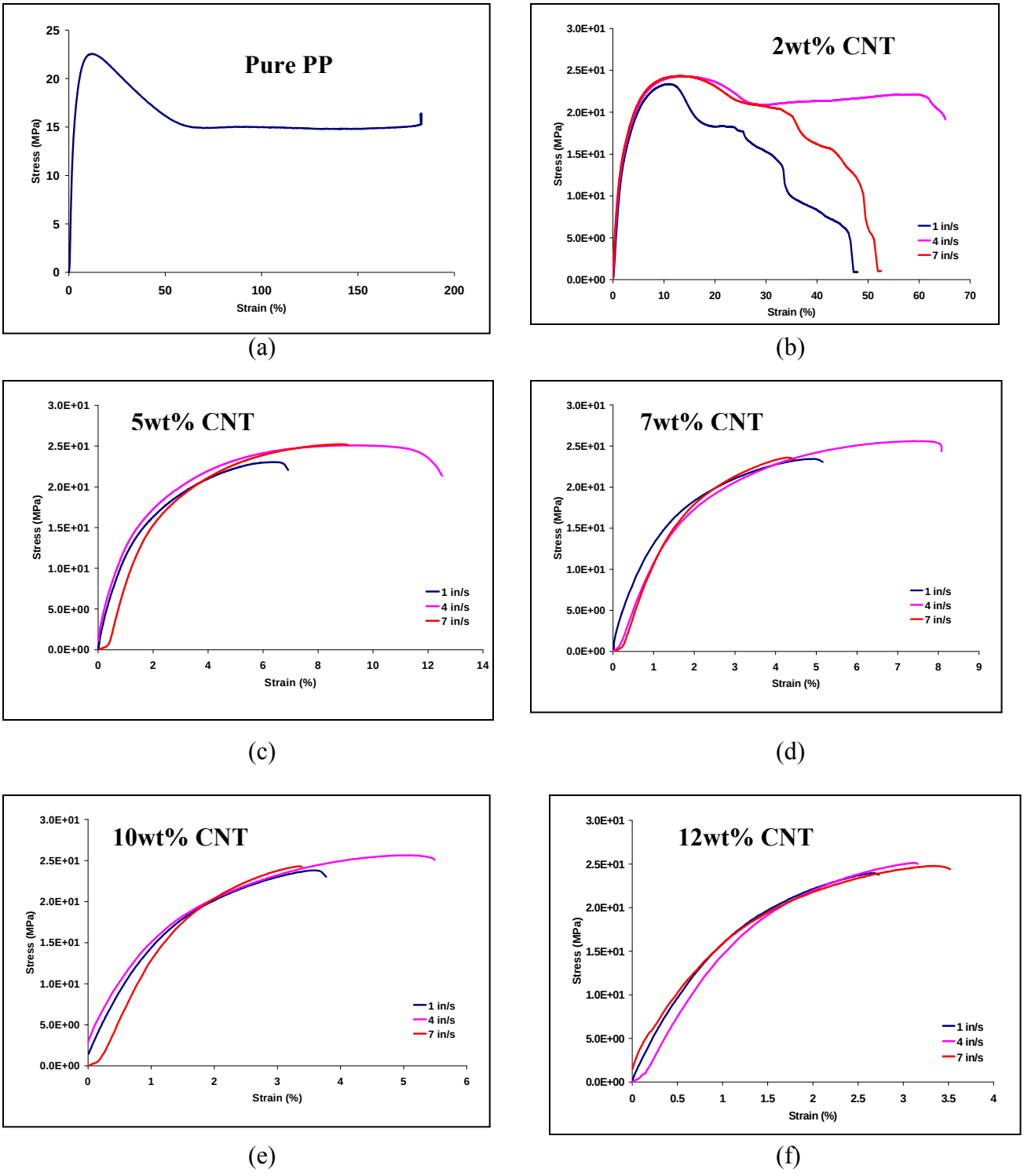

Figure 5.9: Effect of injection speed on stress-strain curves for MWCNT-PP composites at (a) 0wt%, (b) 2wt%, (c) 5wt%, (d) 7wt%, (e) 10wt%, and (f) 12wt% CNTs.

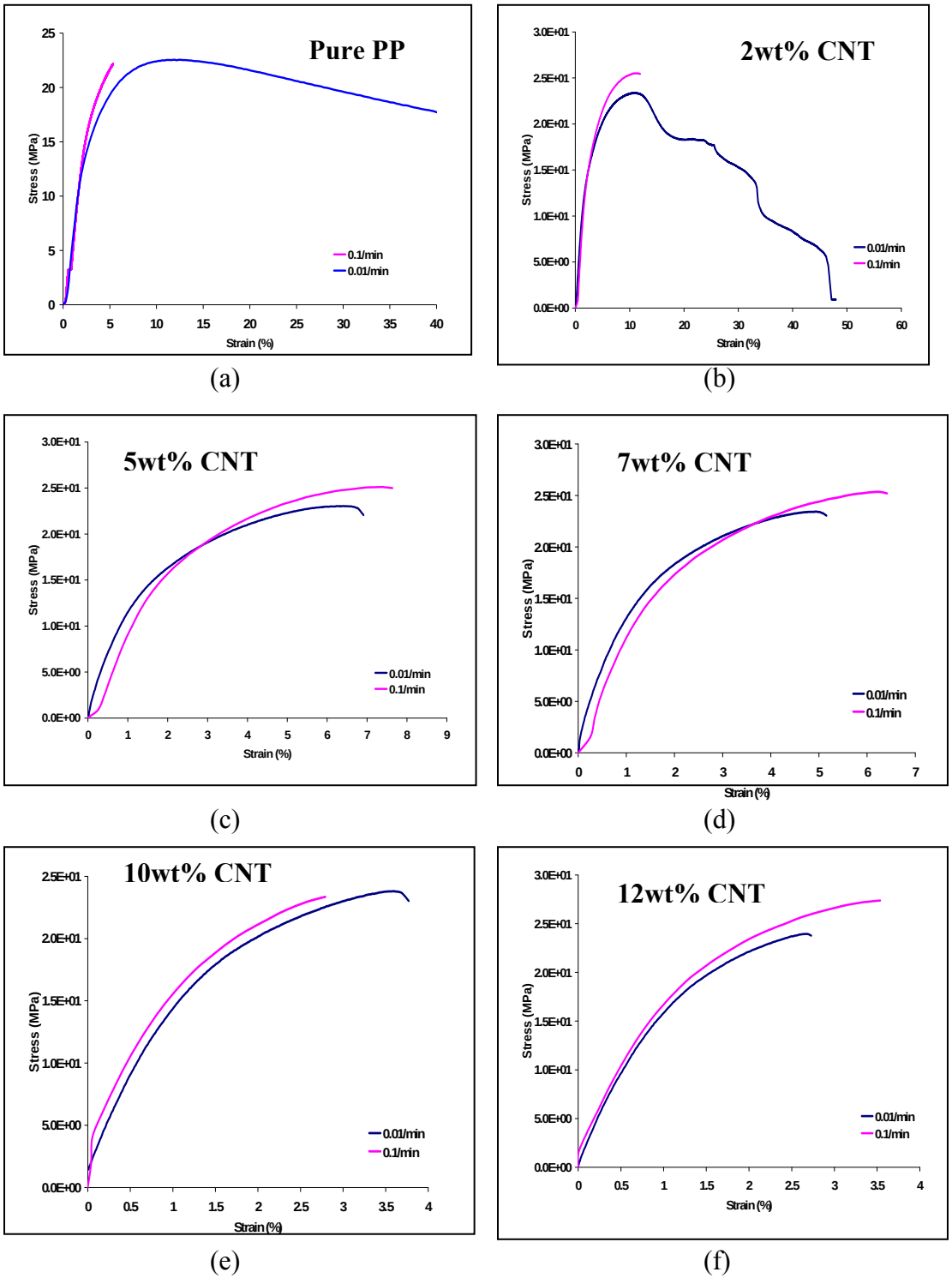

Figure 5.10: Effect of strain-rate loading on stress-strain curves for MWCNT-PP composites at (a) 0wt%, (b) 2wt%, (c) 5wt%, (d) 7wt%, (e) 10wt%, and (f) 12wt% CNTs with Vinj=1in/s.

5.2.2. Experimental results for MWCNT-PC composites

5.2.2.1. Elastic Properties of MWCNT-PC Composites

Similarly, tensile tests were conducted on MWCNT-PC polymer composites. Again for each type of sample, at least three specimens have been tested and compared for consistency. Table 5.3 shows the numerical values for the modulus of elasticity of the MWCNT-PC composites under standard strain-rate loading of 0.01/min at injection velocities of 1in/s, 4in/s and 7in/s respectively.

Table 5.3: Numerical values of modulus of elasticity of MWCNT-PC composites at a strain-rate of 0.01/min

wt % CNT	Elastic modulus (GPa)				Standard deviation (%)
	Injection velocity (Vinj)			Average	
	1in/s	4in/s	7in/s		
0	2.276	2.387	2.375	2.346	3.6
1	2.418	2.600	2.485	2.501	2.9
3	2.512	2.750	2.630	2.630	3.5
5	3.251	3.350	3.537	3.380	3.5
7	3.300	3.650	3.712	3.554	5

From table 5.3, it is clear the effect of injection speed on the modulus of elasticity of MWCNT-PP composites is small (standard deviation is below 5%); thus we can use average values of elastic moduli to show the effect of CNT content on MWCNT-PC composites, which is plotted in Figure 5.11. Again, when the CNT content increases the elastic modulus increases. With 7wt% of CNT, the elastic modulus of composite is more than one and half times higher comparing to the pure polycarbonate matrix.

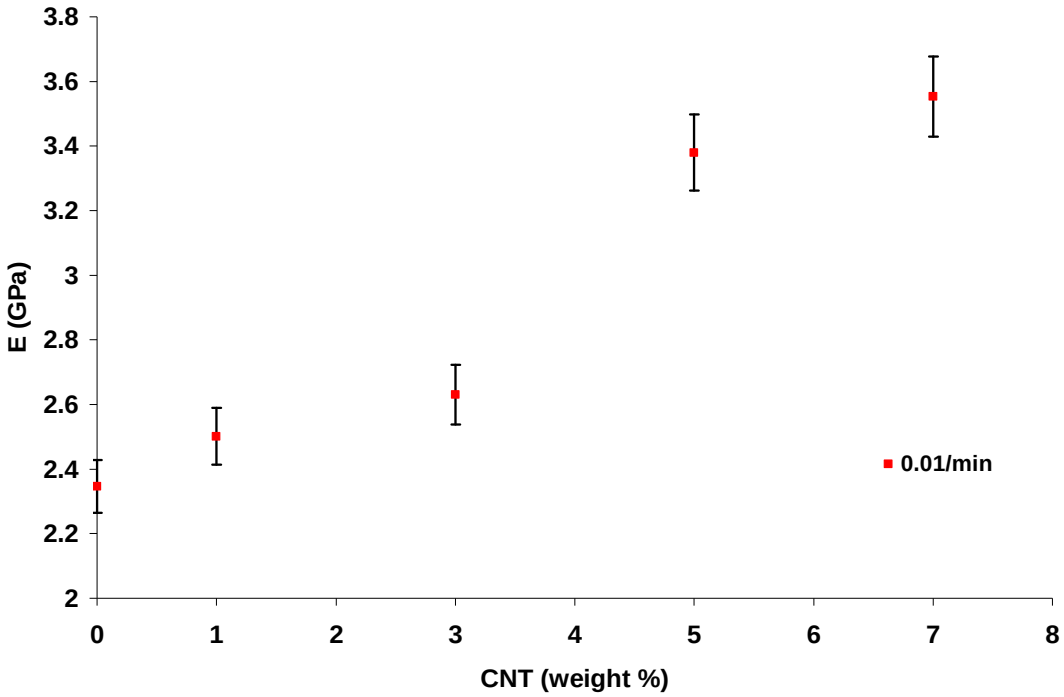

Figure 5.11: Effect of CNT content on elastic modulus for MWCNT-PC composites tested at a standard strain-rate of 0.01/min.

.

5.2.2.2. Effect of Strain-Rate on Elastic Properties of MWCNT-PC Composites

Similar tests on the effect of strain rate were conducted on MWCNT-PC composites. Here we have adopted three different orders of magnitude of strain-rates at 0.1/min, 0.01/min and 0.001/min. Table 5.4 shows the numerical values for the modulus of elasticity of the MWCNT-PC composites tested at a strain-rate of 0.1/min.

Table 5.4: Numerical values of modulus of elasticity of MWCNT-PC composites tested at a strain-rate of 0.1/min.

wt % CNT	Elastic modulus (GPa)				Standard deviation (%)
	Injection velocity (Vinj)			Average	
	1in/s	4in/s	7in/s		
0	2.265	2.236	2.285	2.262	0.9
1	2.532	2.430	2.430	2.464	1.3
3	2.700	2.816	2.69	2.736	2
5	3.375	3.575	3.675	3.521	3.5
7	3.505	3.850	3.830	3.730	4.4

In the same way to numerical values of moduli of elasticity of MWCNT-PC composites tested at the standard strain-rate of 0.01/min, we can realize the effect of injection speed on the modulus of elasticity of MWCNT-PC composites tested at a strain-rate of 0.1/min is also small (standard deviation is below 5%); thus we can use average values of elastic moduli to show the effect of CNT content on MWCNT-PC composites tested at a strain-rate of 0.1/min.

Figure 5.12 shows the effect of CNT content on modulus of elasticity of MWCNT-PC composites tested at the strain-rate of 0.1/min. Similar to Figure 5.11, the elastic modulus increases as CNT content increases.

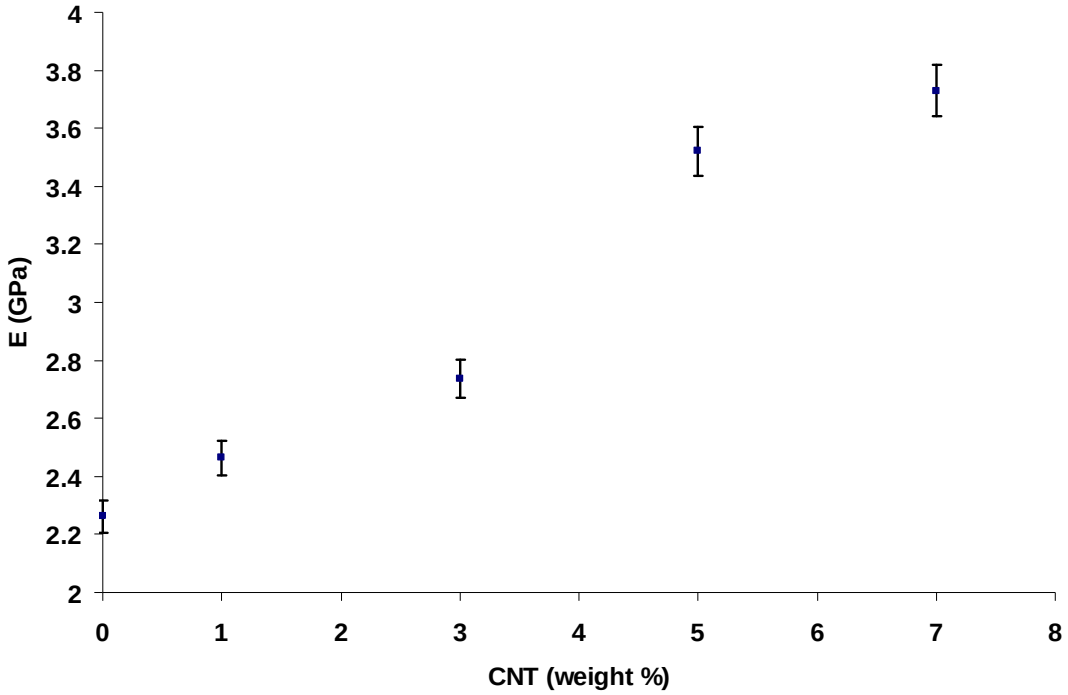

Figure 5.12: Effect of CNT content on elastic modulus for MWCNT-PC composites tested at a standard strain-rate of 0.1/min.

An additional strain rate of 0.001/min was also used to test MWCNT-PC composite. Since the effect of injection speed is insignificant and can be neglected, and also at much low strain-rate, the testing time will be considerably much longer, here we only conducted the tensile tests at this low strain-rate loading for the specimens produced by 4in/s injection velocity. Again, at least three identical specimens for each CNT content have been tested for consistency. Table 5.5 shows the average numerical values of the modulus of elasticity at different CNT weight percentages.

Table 5.5: Numerical values of modulus of elasticity of MWCNT-PC composites tested at a strain-rate of 0.001/min.

wt % CNT	Elastic modulus (GPa)	Standard deviation (%)
	Average	
0	2.325	0.5
1	2.448	1.4
3	2.482	2.4
5	3.165	1.8
7	3.360	2.9

Figure 5.13 shows the effect of CNT content on modulus of elasticity of MWCNT-PC composites tested at the strain-rate of 0.001/min. Again, similar trend to other strain-rate loadings has been observed in Figure 5.13.

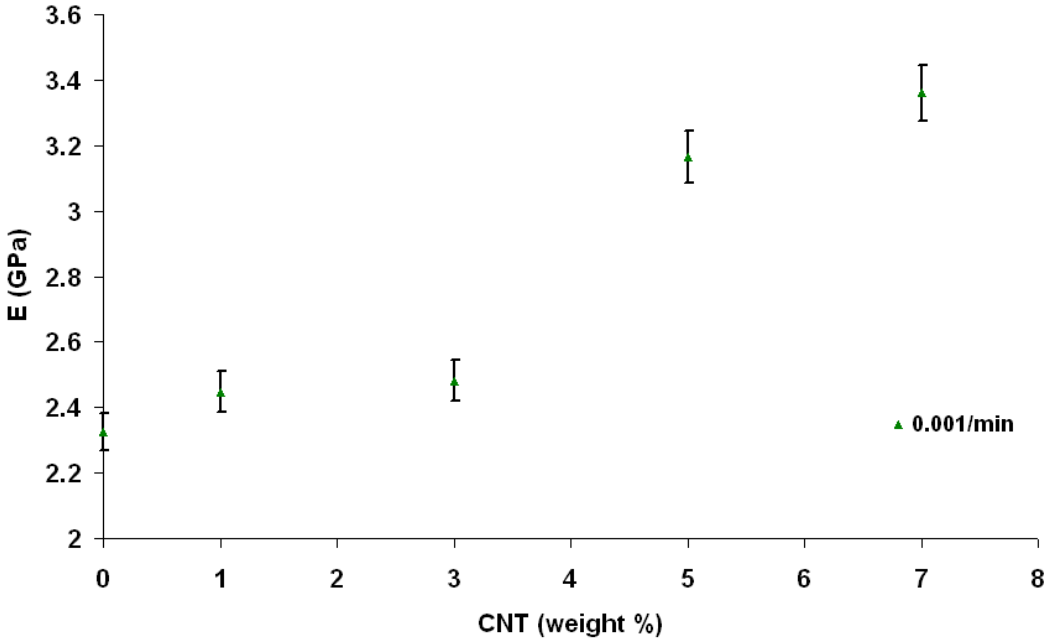

Figure 5.13: Effect of CNT content on elastic modulus for MWCNT-PC composites tested at a standard strain-rate of 0.001/min.

Figure 5.14 combines figures 5.11, 5.12 and 5.13 to show the effect of strain-rate on modulus of elasticity of MWCNT-PC composites. We realized the increase in strain-rate resulted in increase in elastic modulus of MWCNT-PC composites.

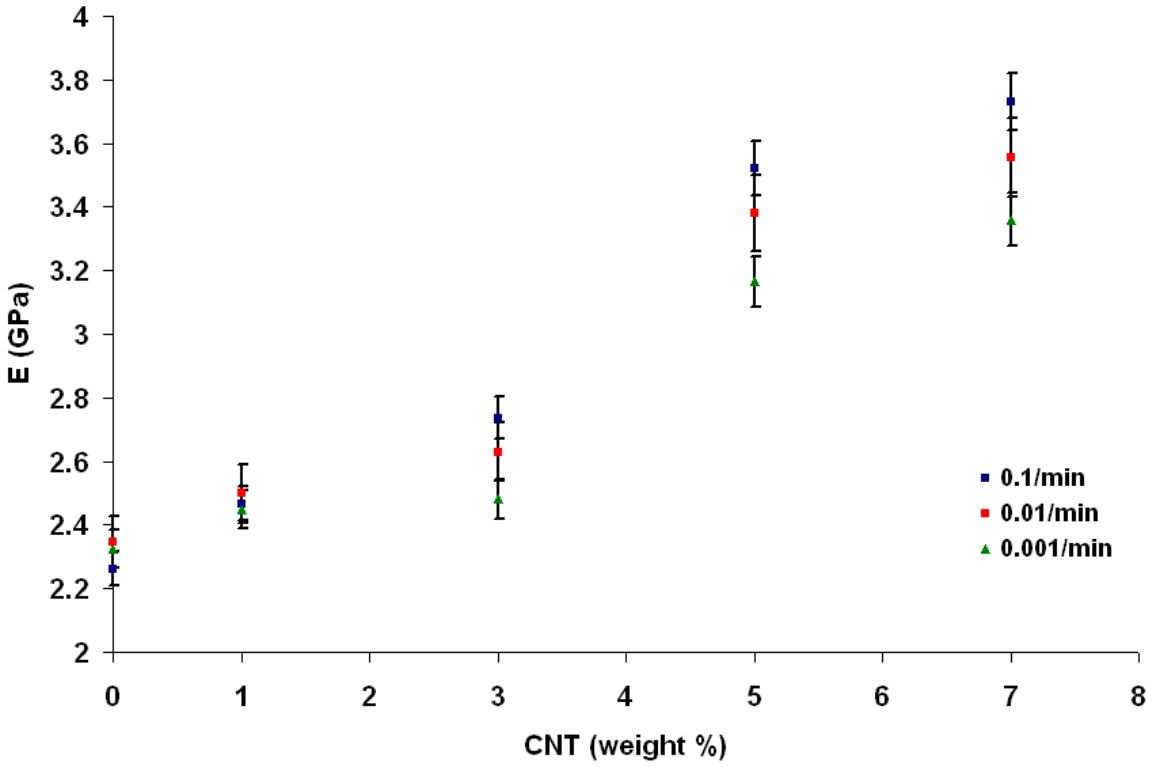

Figure 5.14: Effect of CNT content on elastic modulus for MWCNT-PC composites.

5.2.2.3. Stress-Strain relations of MWCNT-PC Composites

Stress-strain curves, for MWCNT-PC composites, have been obtained under three different strain-rate loadings: 0.1/min, 0.01/min and 0.001/min.

a. Effect of CNT Content on Stress-Strain curves

The effect of CNT contents on Stress-strain curves of MWCNT-PC composites at a strain rate of 0.01/min at different injection velocities are shown in figures 5.15, 5.16 and 5.17 below. A clear increase in the slope of the stress-strain curves with increase in

CNT weight content can be observed. In addition to that, as the CNT content increases, the MWCNT-PC composites become more brittle.

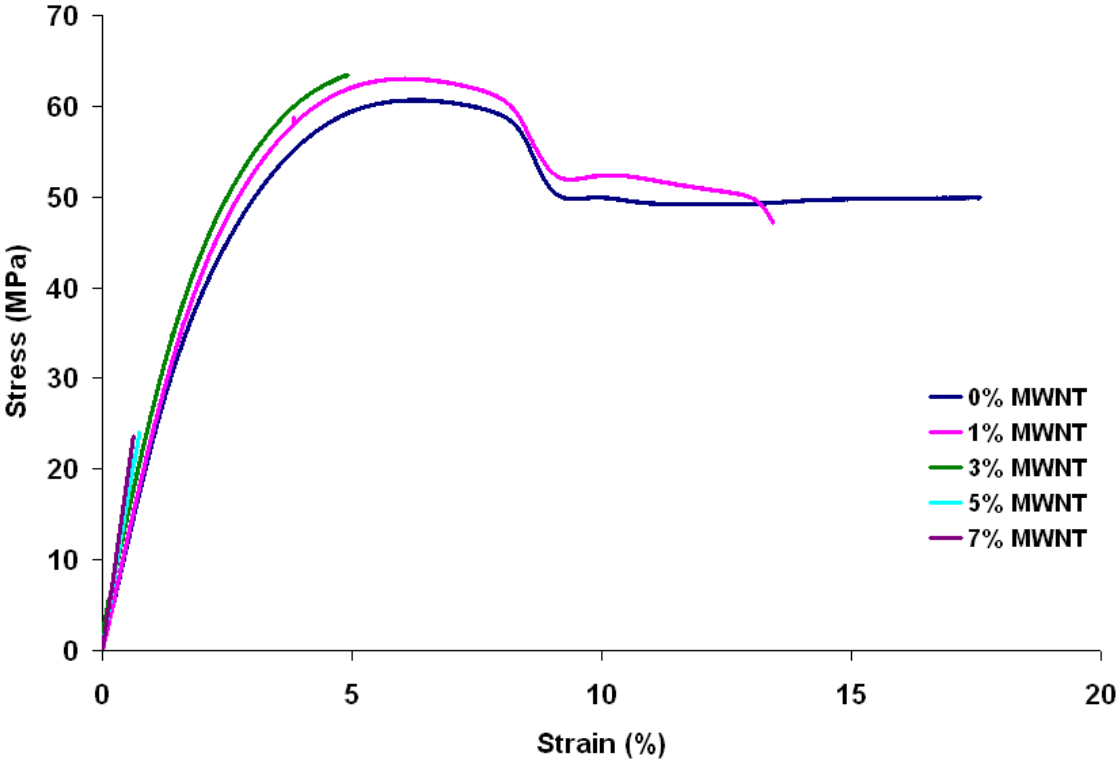

Figure 5.15: Stress-strain curves for the MWCNT-PC composites produced with injection velocity of 1in/s.

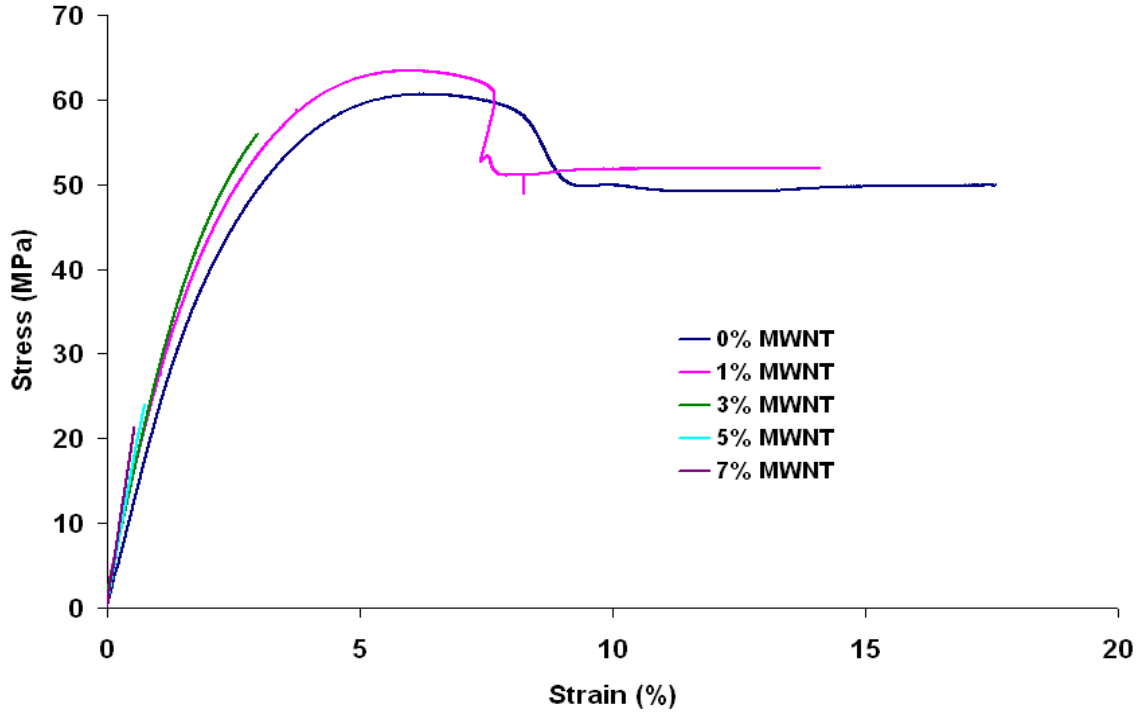

Figure 5.16: Stress-strain curves for the MWCNT-PC composites produced with injection velocity of 4in/s.

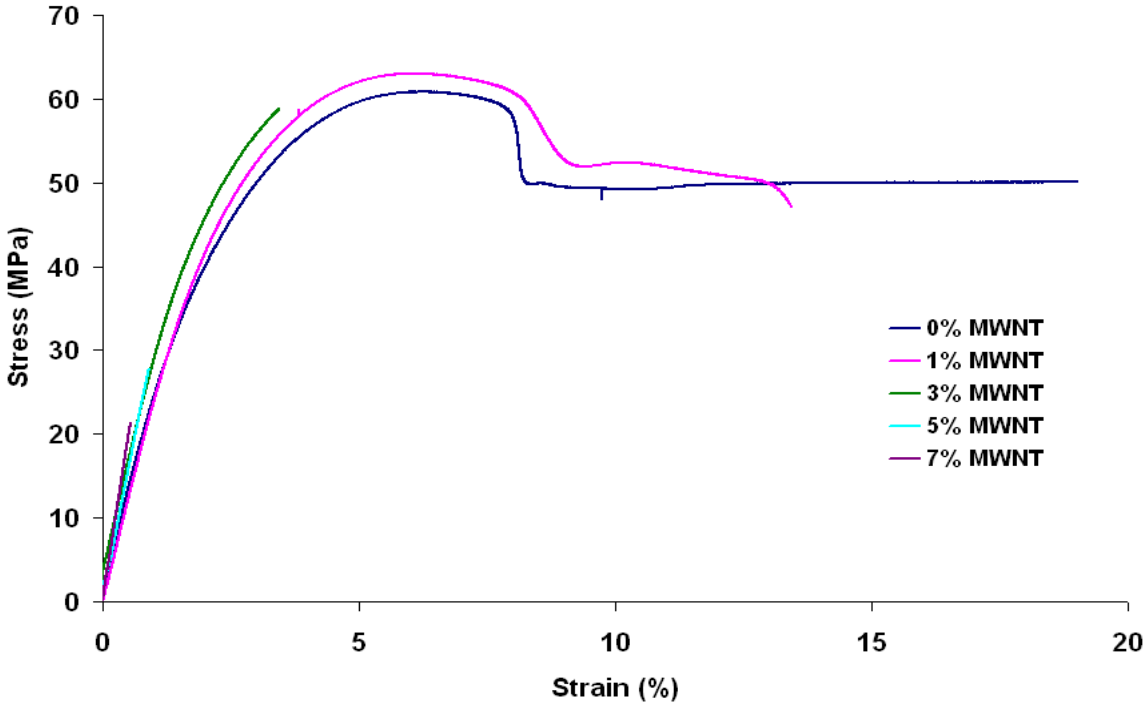

Figure 5.17: Stress-strain curves for the MWCNT-PC composites produced with injection velocity of 7in/s.

b. Effect of injection speed rate on Stress-Strain curves

Figures 5.18 show the effect of injection speed on stress-strain curves for MWNT-PC composites tests with 0.01/min strain-rate at different CNT weight contents. From the figures, no clear effect of injection speed on stress-strain curves can be drawn.

c. Effect of strain-rate loading on stress-strain curves

Figures 5.19 shows the effect of strain-rate loading on stress-strain curves for MWNT-PC composites produced with the injection velocities of 1in/s at different CNT weight contents. The effect of strain rate on MWCNT-PC composites is more pronounced in stress-strain curves compared to MWCNT-PP composites.

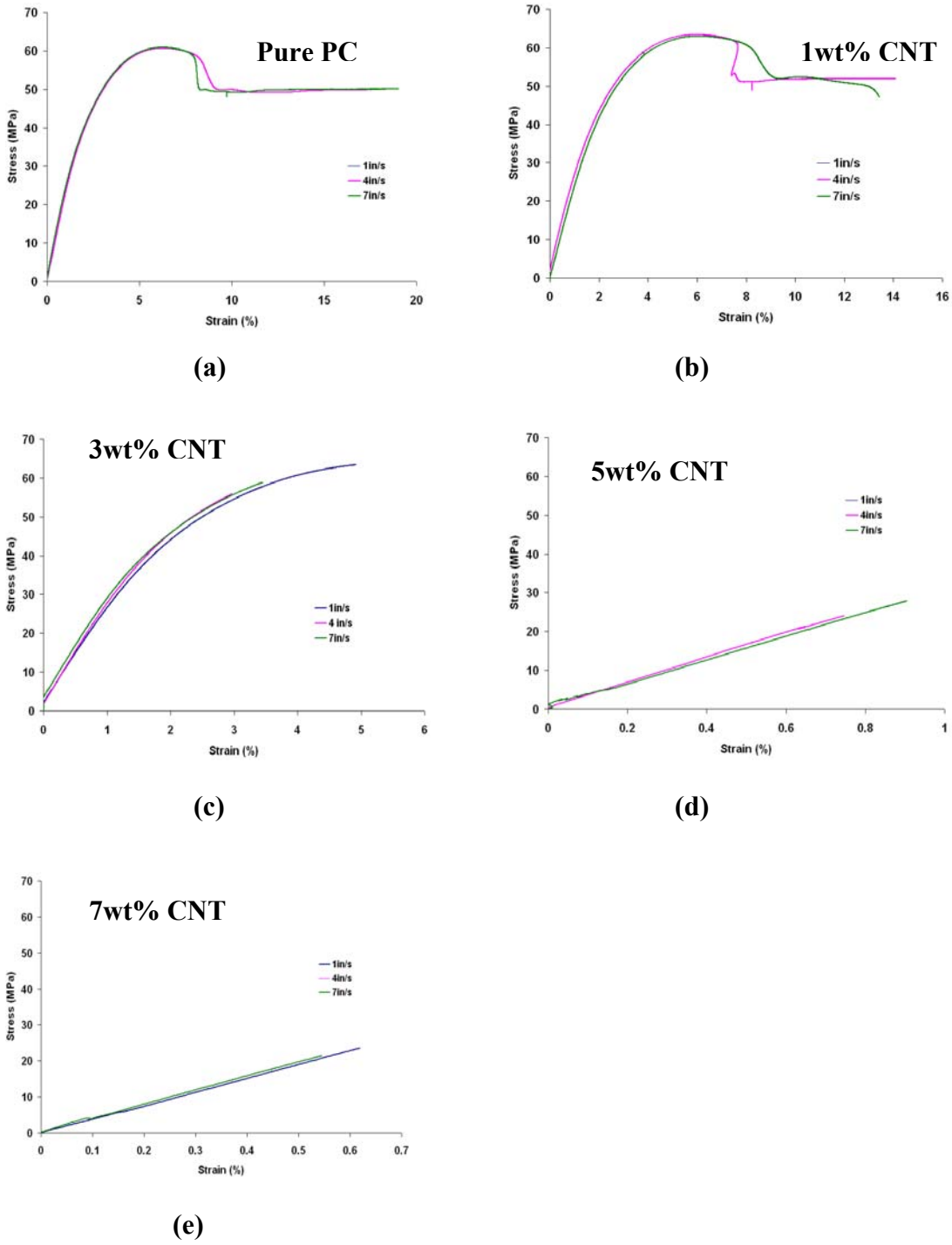

Figure 5.18: Effect of injection speed on stress-strain curves for MWCNT-PC composites at (a) 0wt%, (b) 1wt%, (c) 3wt%, (d) 5wt% and (e) 7wt% CNTs.

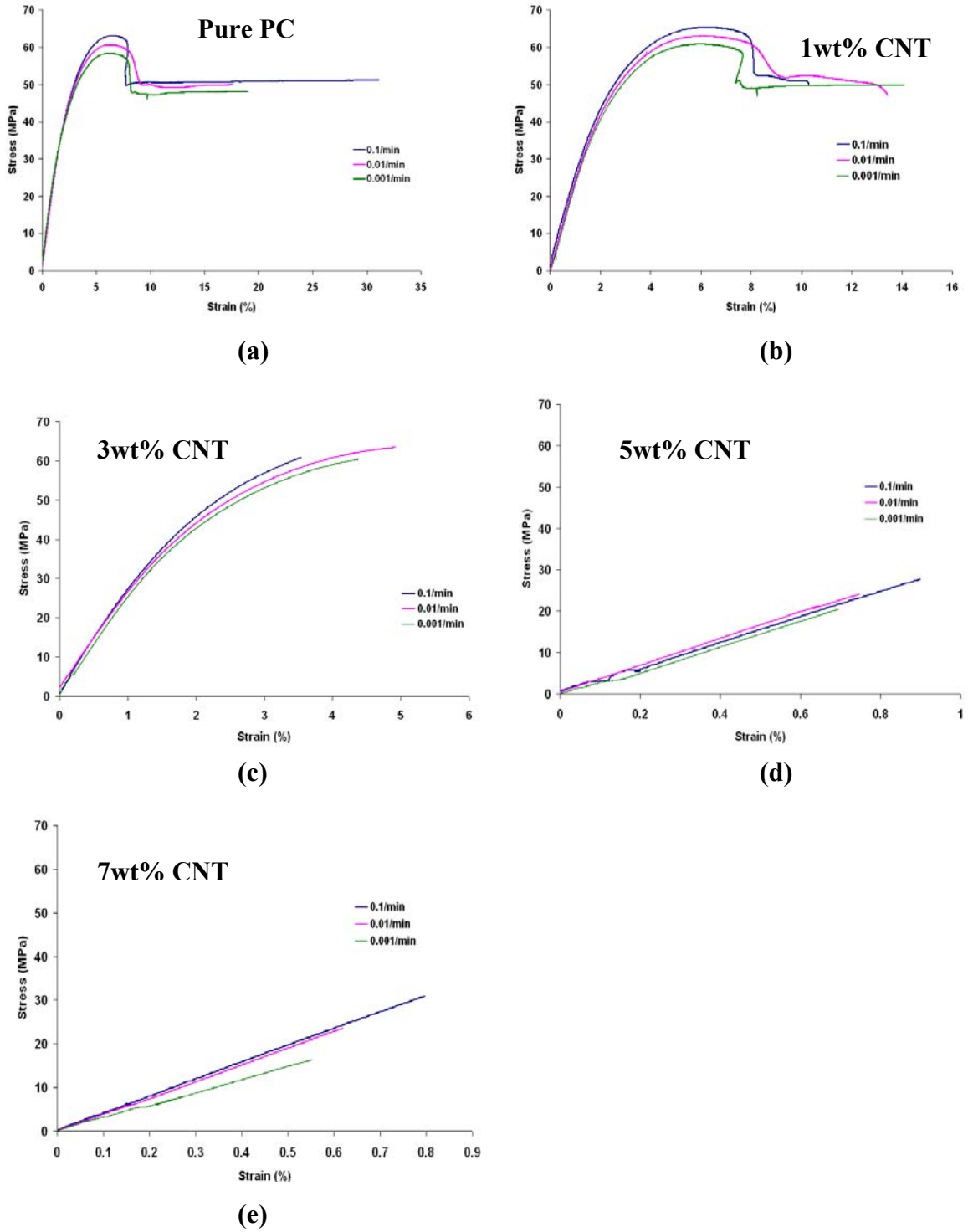

Figure 5.19: Effect of strain-rate loading on stress-strain curves for MWCNT-PC composites at (a) 0wt%, (b) 1wt%, (c) 3wt%, (d) 5wt% and (e) 7wt% CNTs.

6. ELECTROMECHANICAL BEHAVIOR OF MWCNT-POLYMER COMPOSITES UNDER TENSILE LOADING

Several researchers have been interested in the use of piezoresistivity and electrical conductivity for sensing purposes [52-54]. Most of those studies were carried out on carbon fiber composites and proved to be efficient. In this chapter, we will extend the same concept to the MWCNT-Polymer composites.

From the previous chapters on the MWCNT-Polymer nanocomposites, through electrical conductivity tests on our research composites, the percolation threshold of electrical conductivity was found to be around 3.8 wt% of CNT for MWCNT-PP composites and around 1.8 wt% of CNT for MWCNT-PC composites.

Electrical resistance responses of MWCNT-Polymer nanocomposites under mechanical tensile loading are studied in this chapter. A standard tensile test was conducted while the electrical resistance was measured using 2-probe method. The influence of the percolation threshold on the electrical resistance upon mechanical loading will be investigated. The results will be discussed and compared, and some models will be used to model our experimental data in Chapter 9 of Part III.

6.1 Experimental Set-Up and Material Preparation

For mechanical loading, mechanical tensile tests were conducted using an INSTRON model 5882 universal testing machine; strain were recorded using an extensometer. A mechanical load was applied at a standard rate of 0.01/min. Again for each type of sample, three specimens have been tested and compared for consistency. Figure 6.1 shows specimen mounted in the INSTRON machine, with the extensometer and electrical resistance probes connected.

Figure 6. 1: Specimen in the INSTRON machine with the extensometer and the electrical probes.

Standard 2-Probe method was used to measure the electrical resistance of the nanocomposites. Since the percolation threshold has been evaluated to be around 4% weight CNT for MWCNT-PP composites, only specimens with CNT weight percentages higher than the percolation threshold were tested. The tested MWCNT-PP specimens had

the CNT weight percentages of 5, 7, 10 and 12. In regards to MWCNT-PC composites, the percolation threshold being around 1.8% weight CNT, we tested specimens with 4, 5, and 7 percentage weight of CNT. Figure 6.2 below shows the layout of the specimen with the locations of the electrical resistance probes.

The samples preparation takes some time but it is worthy it, because the electrical resistance measurements success highly depends on the quality of the electrodes. The specimen is first coated with silver paint and put to dry. The electrodes are then mounted on the specimen using regular tin soldering. The contact is protected against moisture and noise using conductive epoxy and Loctite glue.

Once the specimen is ready, electric current is applied to the specimen through an electrical circuit powered by a DC power source; the DC source was used for the tests for its simplicity. Nevertheless, it is worthwhile to note that in real-life practice AC source in 1 kHz is commonly used to avoid inaccuracy caused by polarization. The electrical data were then recorded using Labview software.

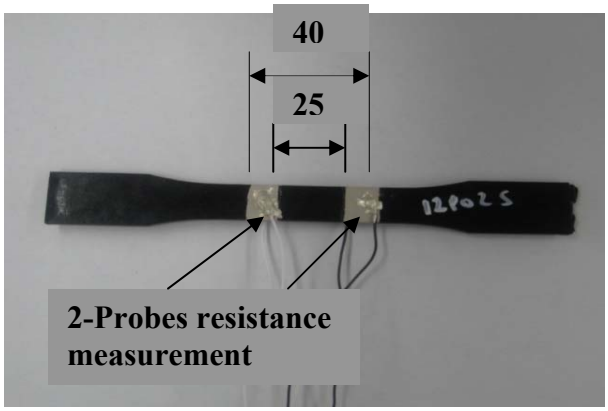

Figure 6.2: Specimen layout. All dimensions are given in mm

6.2. Experimental Results

6.2.1. Experimental Results for MWCNT-PP Composites

During the mechanical loading, the electrical resistance of the system was obtained from the 2-probe measurement as described above; at the same time, the stress-strain curves were obtain form the tensile tests data. Figure 6.3 shows the stress-strain of the three MWCNT-PP composites with 5 wt% CNT, and Figure 6.4 shows the electrical resistance change under the same tensile loading as Figure 6.3.

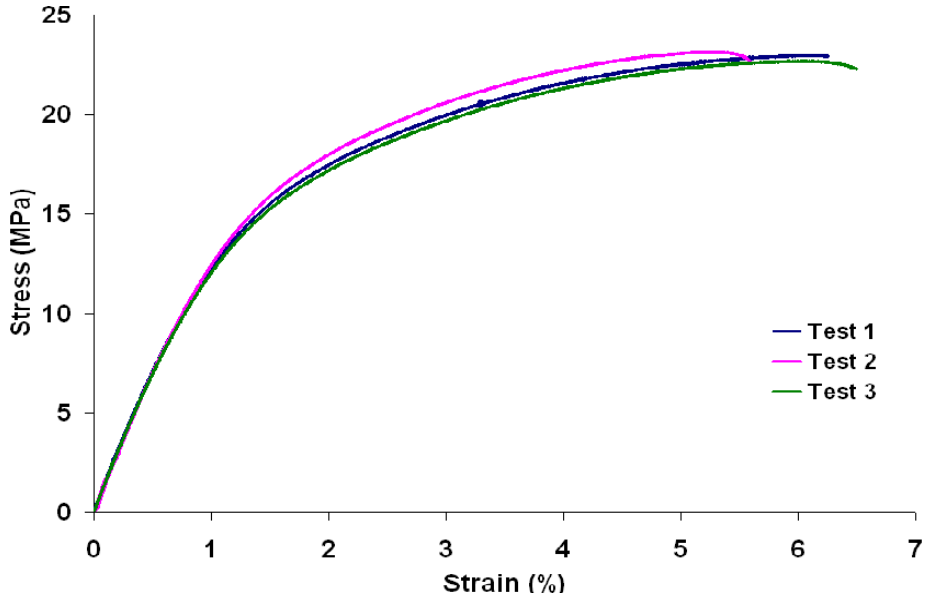

Figure 6.3: Stress-Strain curves for 5wt %MWCNT-PP composite specimens.

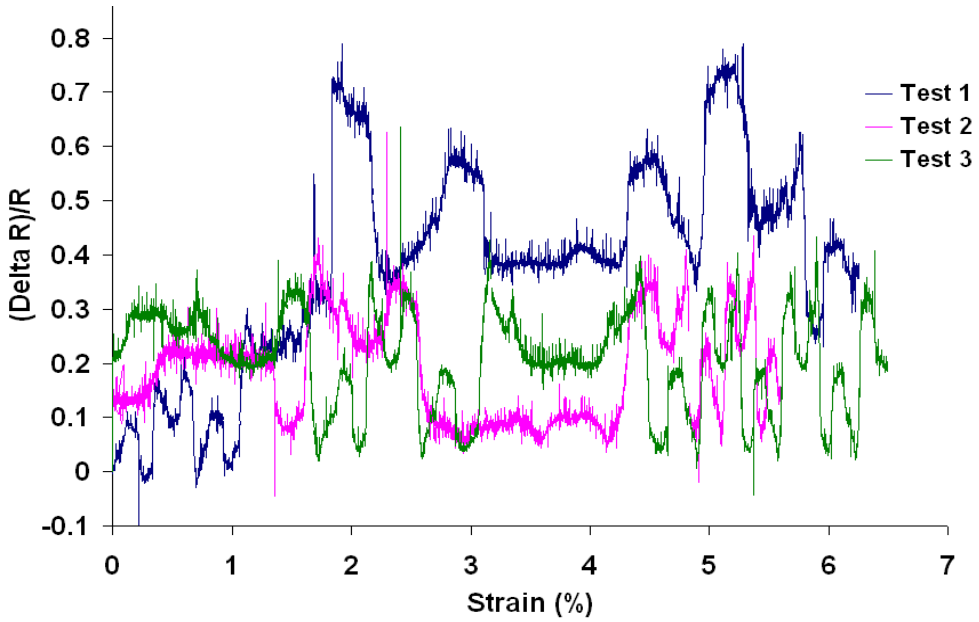

Figure 6.4: Electrical resistance change due to strain change for 5 wt% MWCNT-PP composite specimens.

The change in resistance was not clearly pronounced. This could results from the fact that with 5%CNT, which is close to the percolation threshold, the conductivity of the composite specimen is still at the lower level to highly sense the electrical resistance change. From the microstructure point of view, the connectivity of CNT network in the composite is not fully established. There is no piezoresistive effect in the composite system at low CNT content and the system behaves like its base material of polypropylene.

The same tests that were conducted on the PP-MWCNT composite specimens with 5 wt% CNT were also carried out on the composites specimens with 7% CNT. Figure 6.5 shows the stress-strain curves for the composites specimens with 7% CNT. All three tests show consistent results.

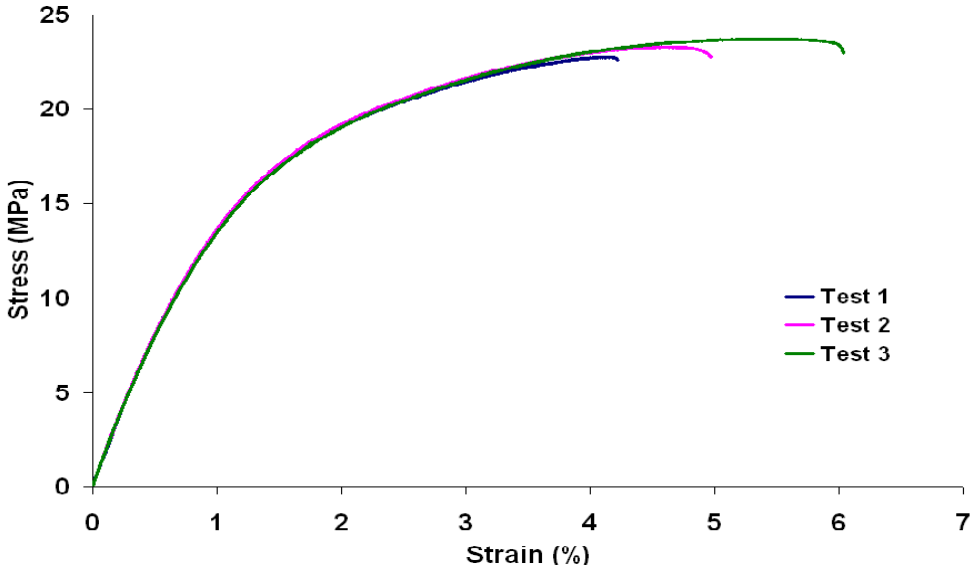

Figure 6.5: Stress-Strain curves for 7 wt% MWCNT-PP composite specimens

The electrical resistance change again did not show any repeatable patterns for piezoresistive response of the system as illustrated in Figure 6.6.

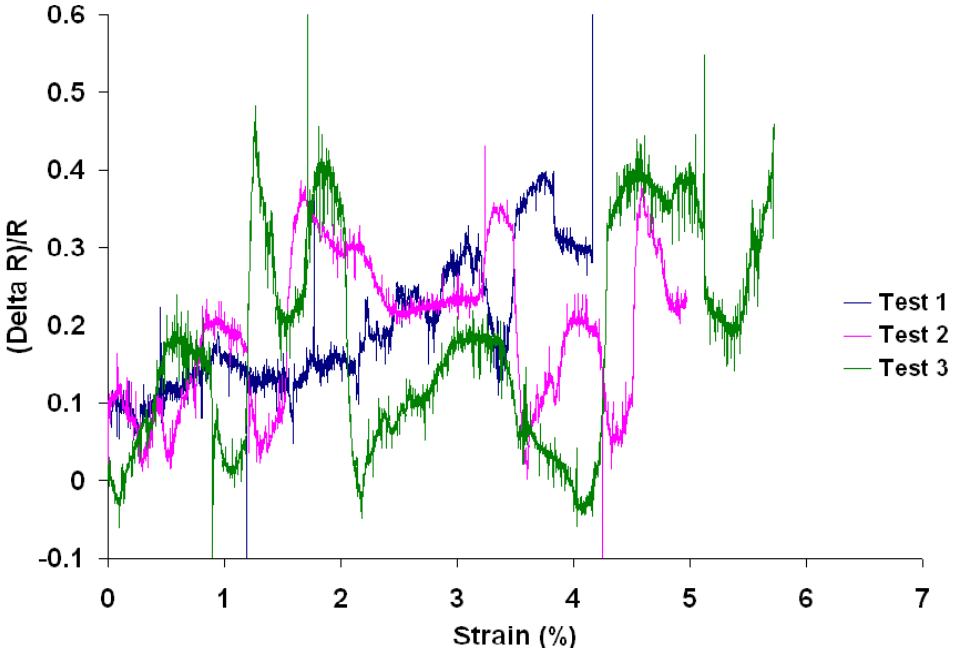

Figure 6.6: Electrical resistance change due to strain change for 7 wt% MWCNT-PP composite specimens.

For the PP nanocomposites with CNT weight percentages of 10% and 12%, the resistance change sensitivity to mechanical loading was more pronounced and clear patterns could be observed. Figures 6.7 and 6.8 show the stress-strain and resistance change curves for the composites specimens with 10% CNT respectively.

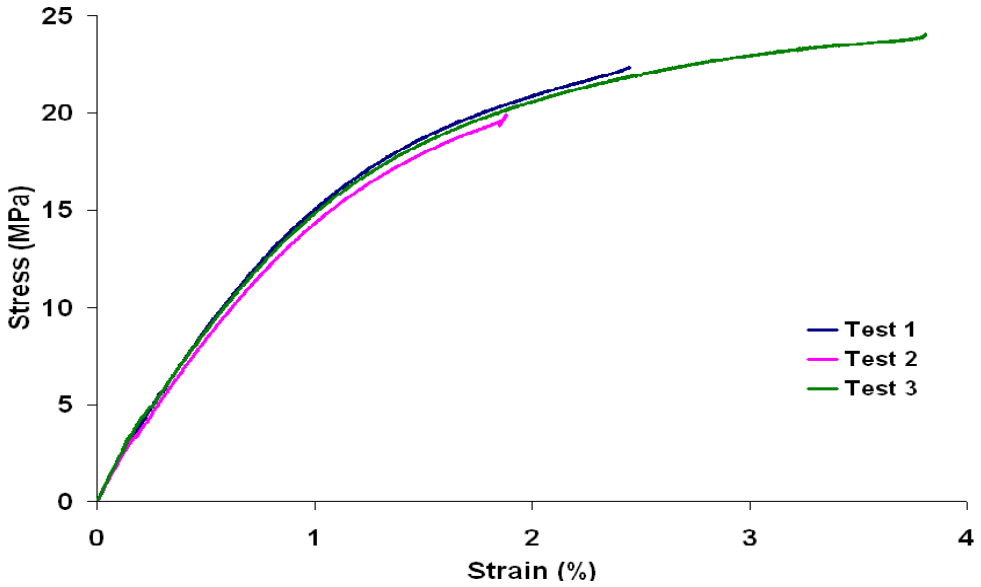

Figure 6.7: Stress-Strain curves for 10 wt% MWCNT-PP composite specimens

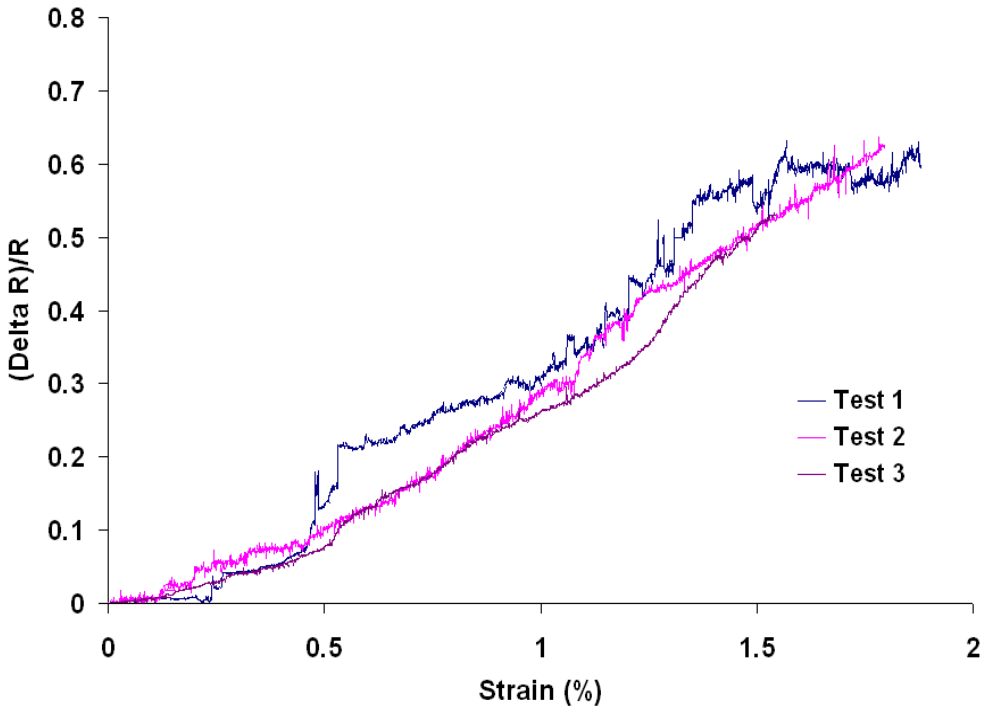

Figure 6.8: Electrical resistance change due to strain change for 10 wt% MWCNT-PP composite specimens.

Form figure 6.8 above, we can realize the increase in sensitivity to strain change by electrical resistance change measurement. It shows clear increase of resistance change when the strain increases.

The same sensitivity is also found in PP nanocomposites with 12 wt% CNT. Figure 6.9 shows stress-strain curves for the PP-MWCNT composites with 12 wt%.

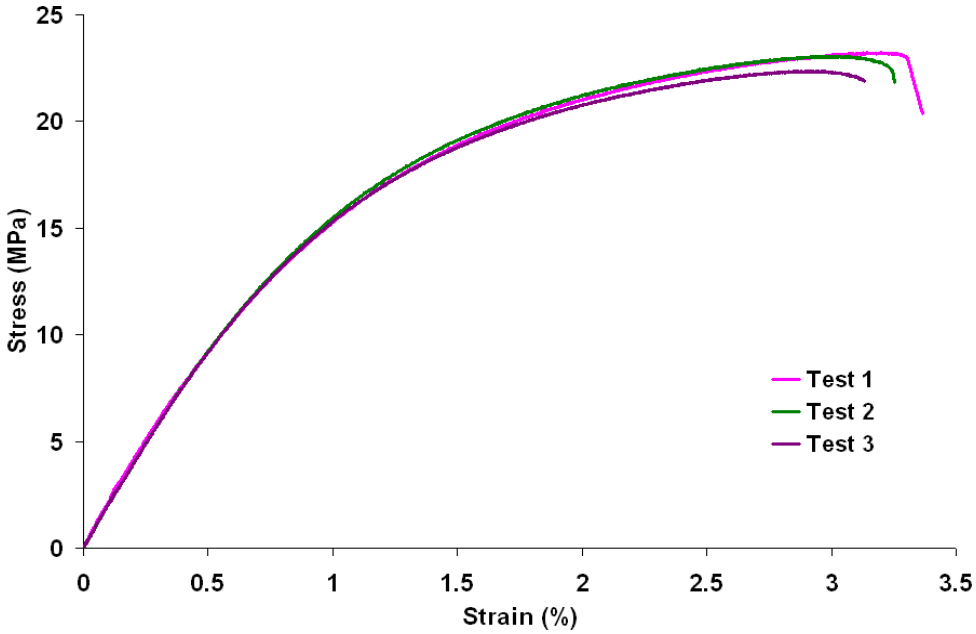

Figure 6.9: Stress-Strain curves for 12 wt% MWCNT-PP composite specimens

Figure 6.10 illustrates the resistance change sensitivity to strain change for the PP nanocomposites with 12 wt% CNT.

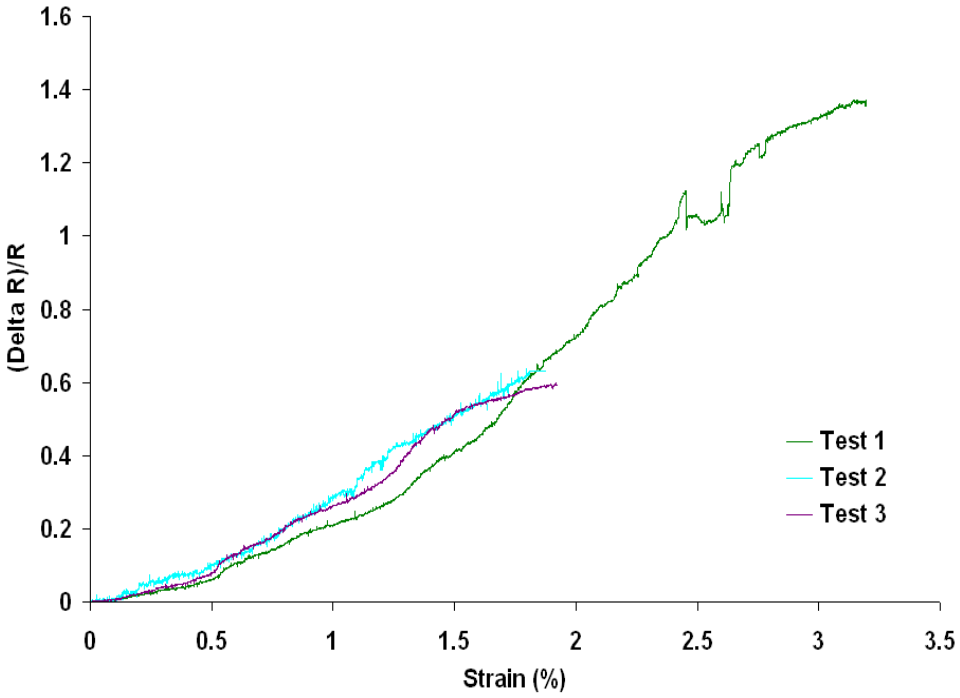

Figure 6.10: Electrical resistance change due to strain change for 12%MWCNT-PP composite specimens.

Figure 6.11 shows the comparison between the average electrical resistance change due to strain for both the MWCNT-PP composites with CNT content of 10wt% and 12wt%.

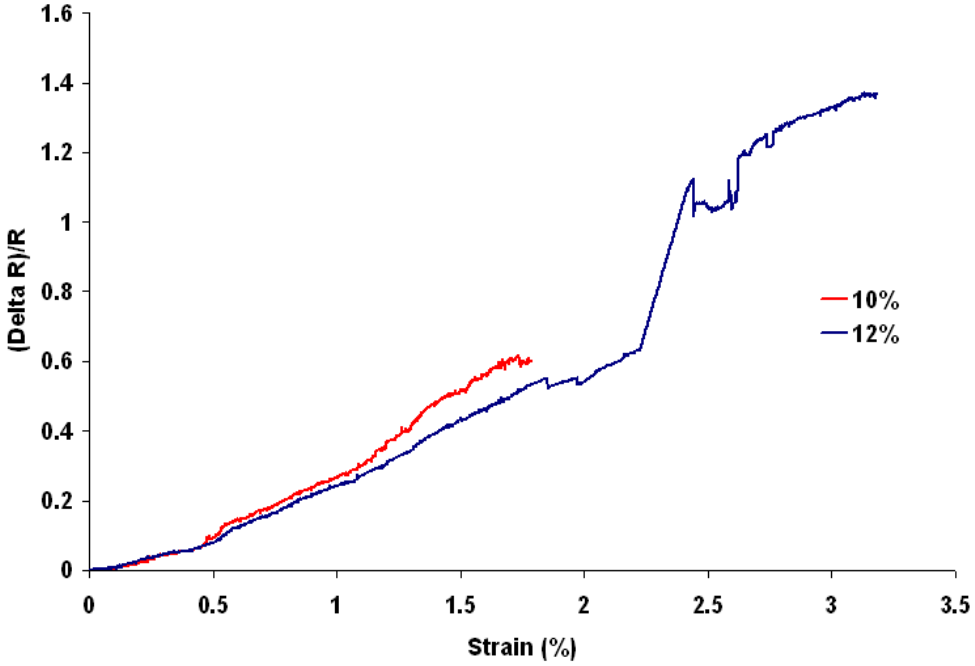

Figure 6.11: Comparison between average electrical resistance changes for MWCNT-PP composites with CNT content of 10wt% and 12wt%.

For electrical and mechanical responses comparisons, Figures 6.12 and 6.13 show the stress–strain curves overlapped with the electrical resistance change curves for MWCNT-PP composites with CNT contents of 10wt% and 12wt% respectively, to show the correspondence between the two. The trend shows a promising use of MWCNT-PP nanocomposites for sensing purposes.

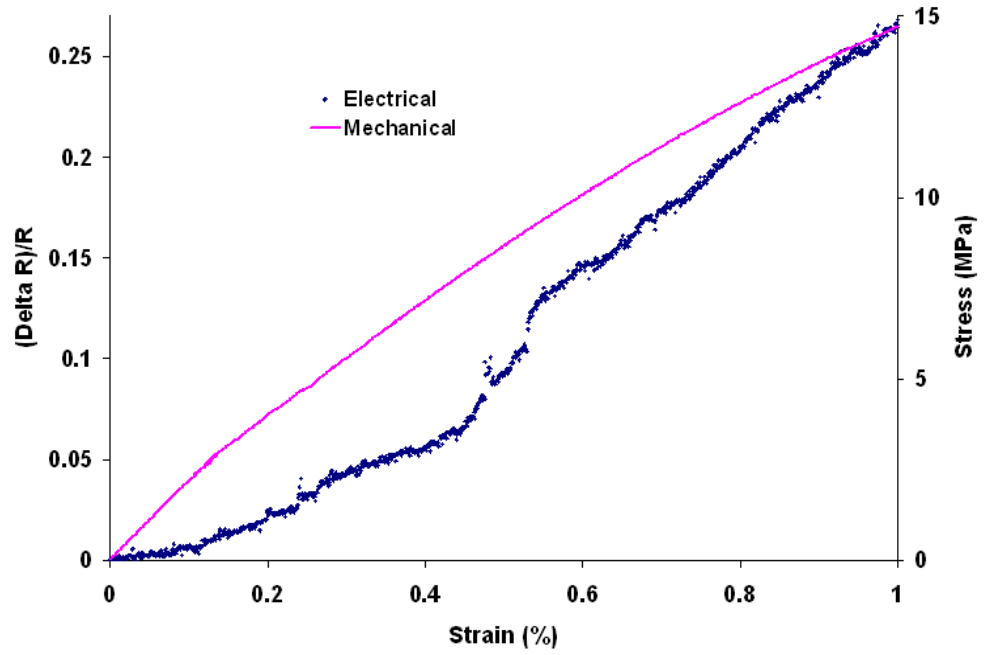

Figure 6.12: Electrical resistance and stress change due to strain change for 10 wt% MWCNT-PP composite specimens.

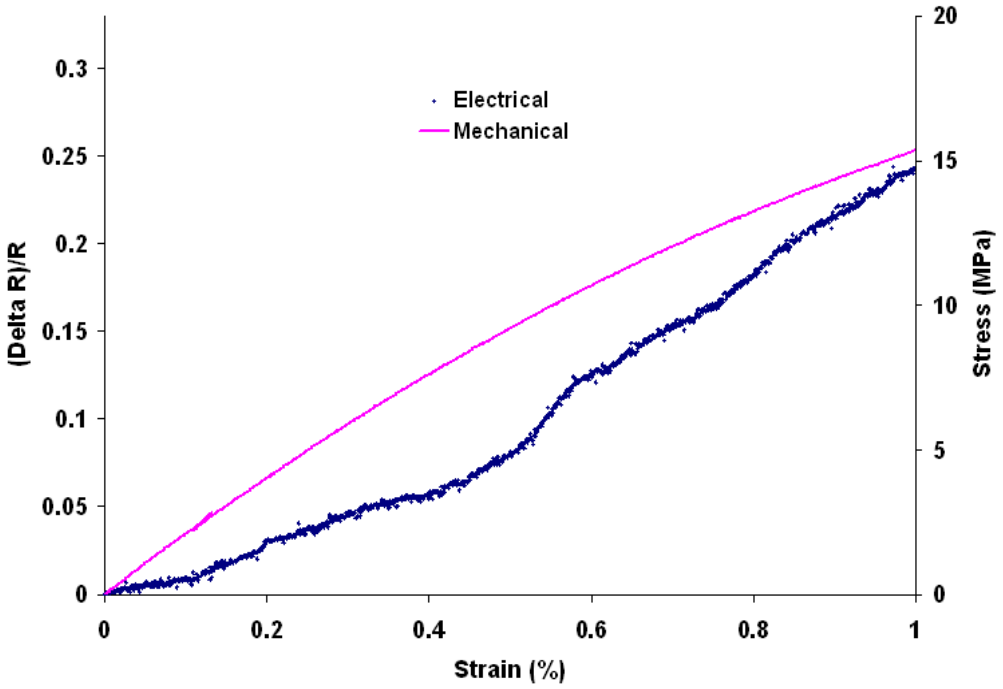

Figure 6.13: Electrical resistance and stress change due to strain change for 12 wt% MWCNT-PP composite specimens.

6.2.2. Experimental Results for MWCNT-PC Composites

In the same way we conducted the tensile tests on electromechanical behavior of MWCNT-PP composites, tests were conducted on MWCNT-PC specimens with CNT content of 4wt%, 5wt%, and 7wt% respectively. The electrical resistance of MWCNT-PC composites was obtained from the 2-probe measurement; at the same time, the stress-strain curves were obtained from the tensile tests data.

Figure 6.14 shows the stress-strain of the three MWCNT-PC composites with 4 wt% CNT.

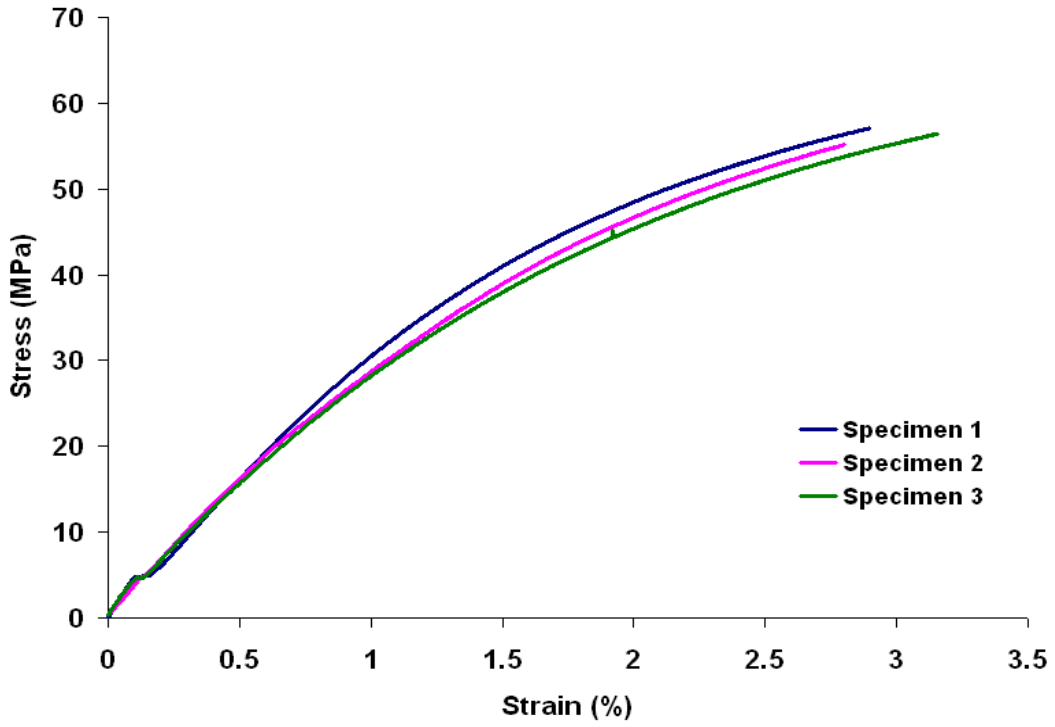

Figure 6.14: Stress-Strain curves for 4 wt% MWCNT-PC composite specimens

The change in resistance was not clearly pronounced. This could result from the fact that with 4%CNT, the conductivity of the composite specimen is still at a low level to highly sense the electrical resistance change and the composite system as a whole has

not shown piezoresistive behavior. Figure 6.15 below shows the change in electrical resistance due to the strain change.

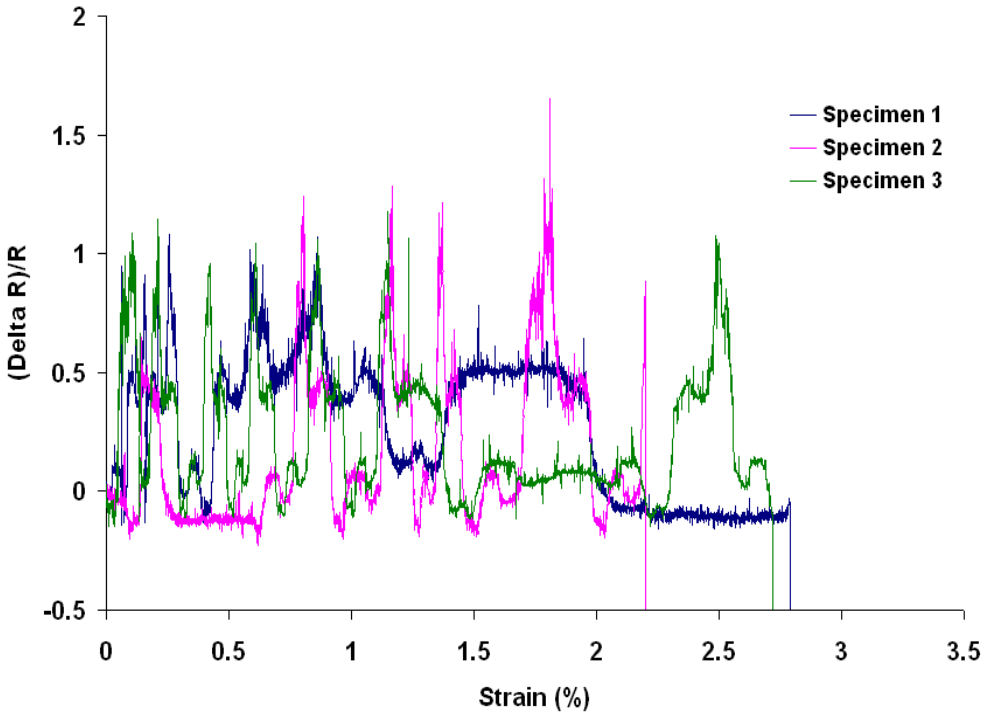

Figure 6.15: Electrical resistance change due to strain change for 4%MWCNT-PC composite specimens.

For the PC nanocomposites with CNT weight percentages of 5% and 7%, the resistance change sensitivity to mechanical loading was more pronounced and clear patterns could be observed. Figures 6.16 and 6.17 show the stress-strain and resistance change curves for the composites specimens with 5% CNT respectively. Three tests were conducted, but one of them was not successful as a result, it was disregarded.

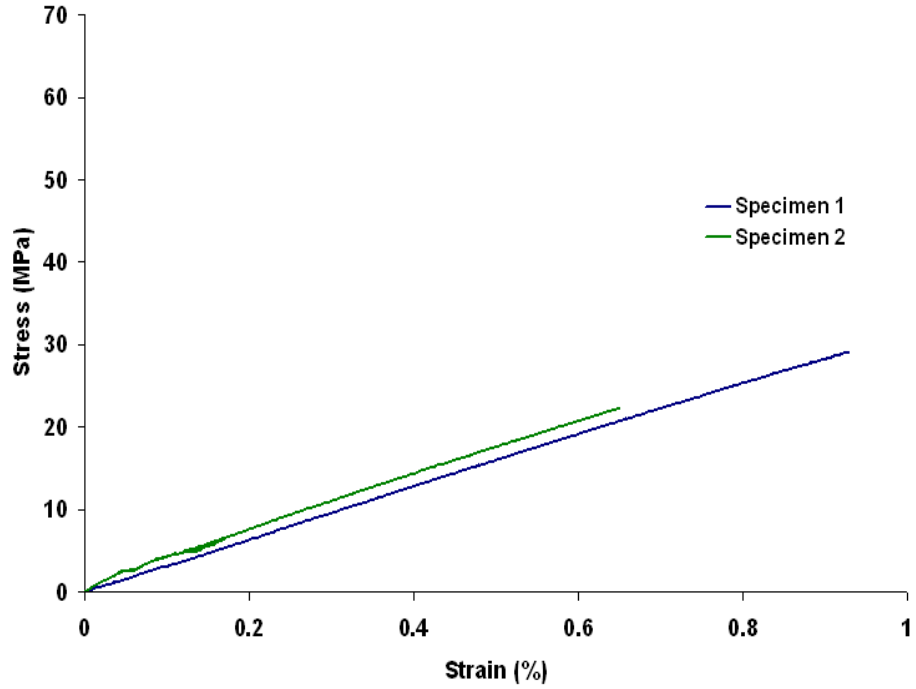

Figure 6.16: Stress-Strain curves for 5 wt% MWCNT-PC composite specimens.

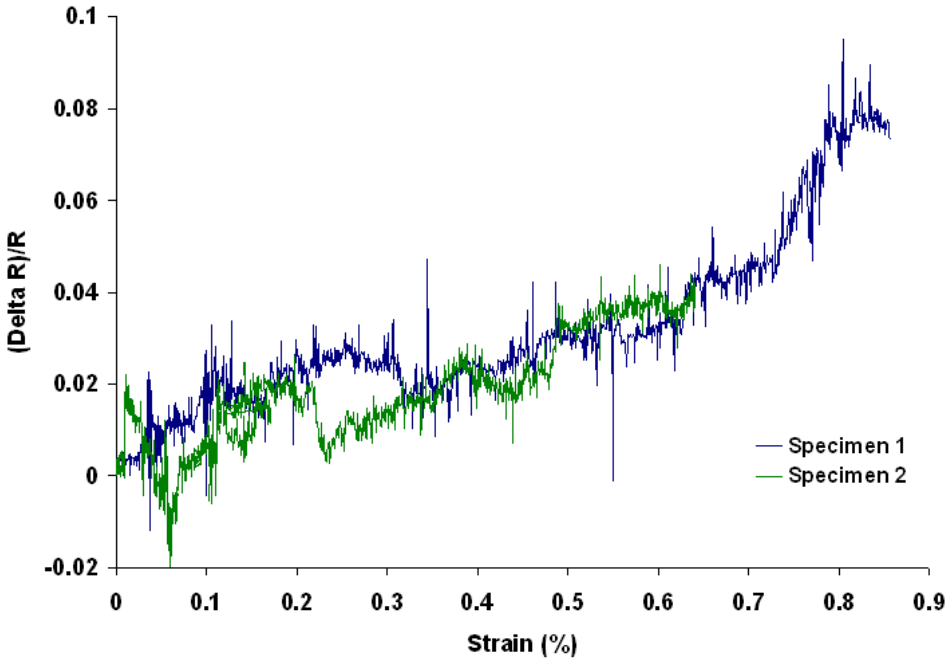

Figure 6.17: Electrical resistance change due to strain change for 5% MWCNT-PC composite specimens.

Increase in electrical resistance change sensitivity was also observed with PC nanocomposites wit 7 wt% CNT. Figures 6.18 and 6.19 show stress-strain and resistance change curves for the PC-MWCNT composites with 7 wt% respectively.

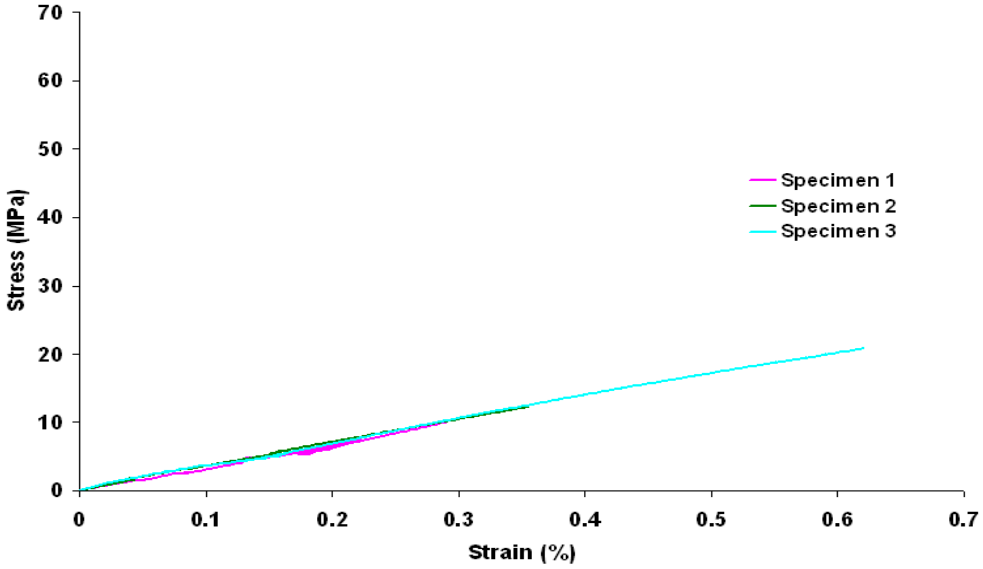

Figure 6.18: Stress-Strain curves for 7 wt% MWCNT-PC composite specimens.

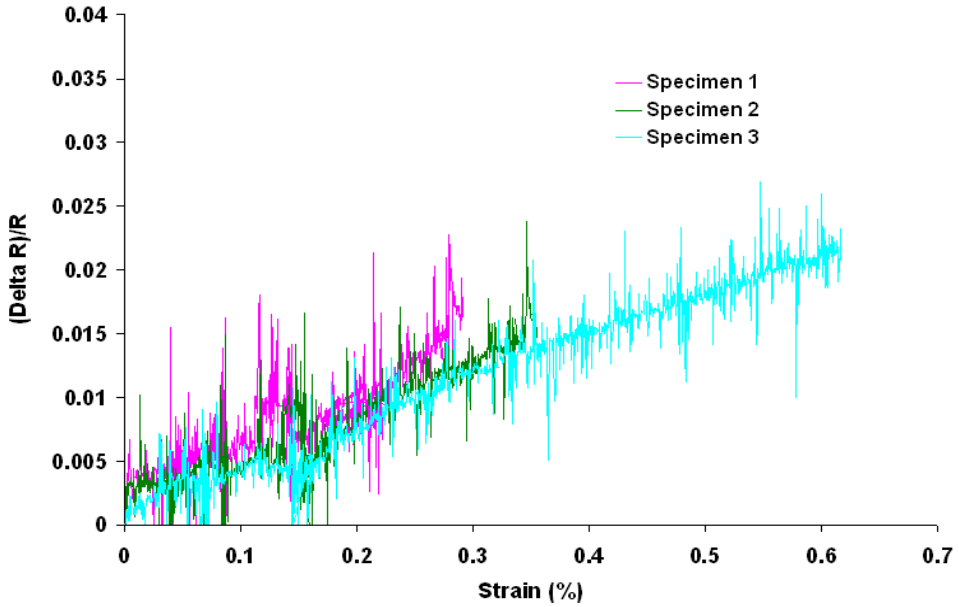

Figure 6.19: Electrical resistance change due to strain change for 7% MWCNT-PC composite specimens.

The comparison between the average electrical resistance changes for both the MWCNT-PC with 5wt% and 7wt% CNT is shown in Figure 6.20.

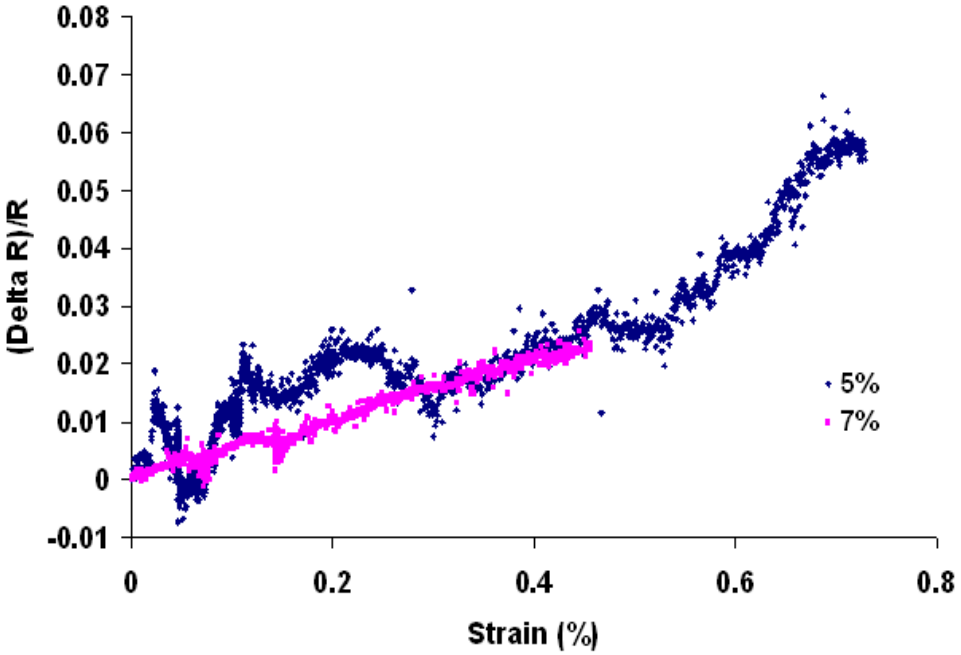

Figure 6.20: Comparison between average electrical resistance changes for MWCNT-PC composites with CNT content of 5wt% and 7wt%.

In regards to electrical and mechanical responses comparisons, Figures 6.21 and 6.22 show the stress–strain curves overlapped with the electrical resistance change curves for MWCNT-PC composites with CNT contents of 5wt% and 7wt% respectively. Both the composites show linear trends and it is an encouraging sign for future use of MWCNT-PC composites for the sensing purpose.

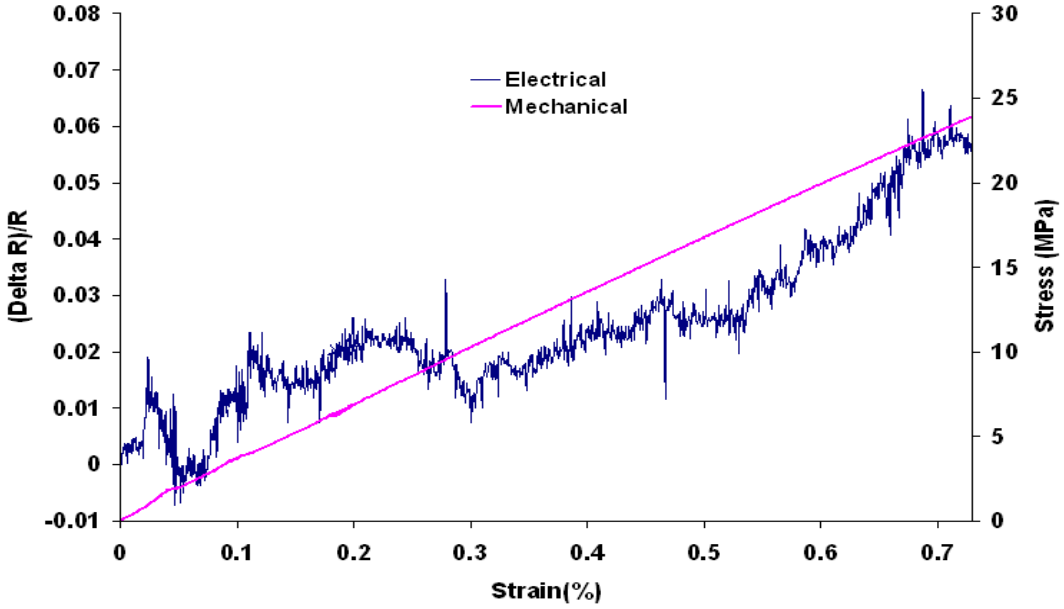

Figure 6.21: Electrical resistance and stress change due to strain change for 5 wt% MWCNT-PC composite specimens.

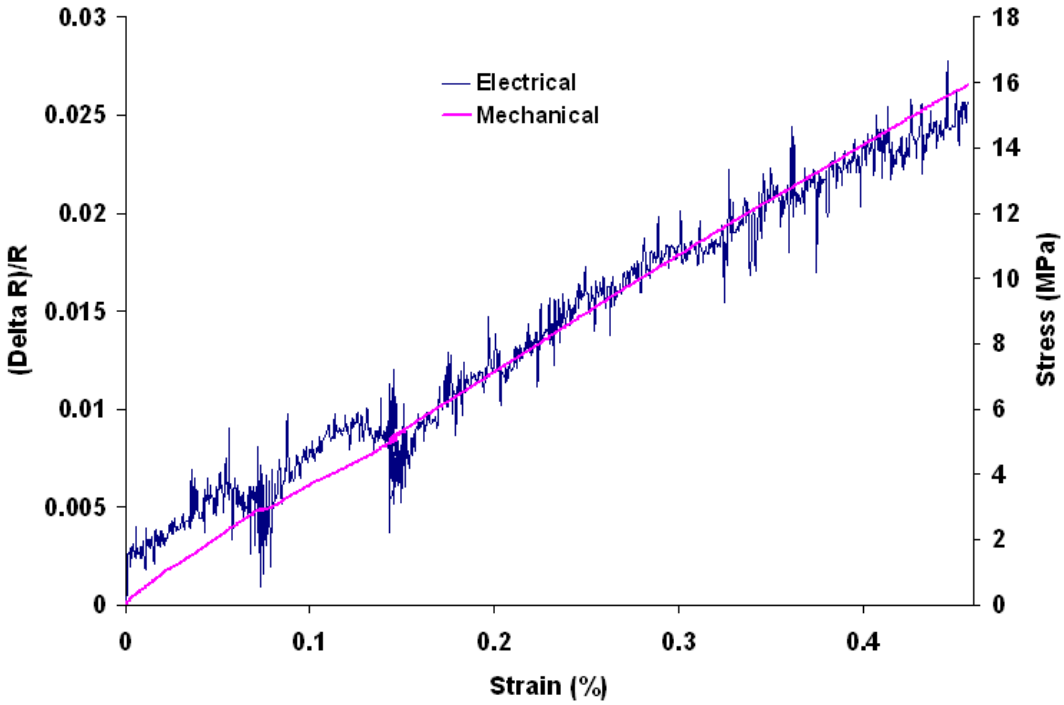

Figure 6.22: Electrical resistance and stress change due to strain change for 7 wt% MWCNT-PC composite specimens.

The MWCNT-Polymer composites specimens showed electrical resistance change sensitivity to strain change. The level of sensitivity varies with the CNT wt%; it is less pronounced in composites with weight percentages close to the percolation threshold. The sensitivity became more pronounced for nanocomposites with higher weight percentage of CNT.

The above results are a promising use of PP-MWCNT and PC-MWCNT composites for the sensing purposes. This additional property will add to the already existing advantageous range of potential applications.

PART III: THEORETICAL MODELING

7. PERCOLATION THEORIES FOR ELECTRICAL CONDUCTIVITY OF CNT-POLYMER NANOCOMPOSITES

Parallel to the experimental investigation, a percolation theory is applied to study the electrical conductivity of the nanocomposite systems in terms of content of nanotubes. In this chapter, both Kirkpatrick and McLachlan models are used to determine the transition from low conductivity to high conductivity which is designated as percolation threshold.

7.1. Kirkpatrick and McLachlan models

The concepts of percolation theory have a wide application in many disciplines of sciences. In general, percolation theory deals with the number and properties of clusters on virtual two, three or higher dimensional lattices [39].

The following relationship expressing the scaling law was proposed by Kirkpatrick [12].

$$\sigma = S|p - p_c|^q \qquad (3)$$

where σ represents a property studied, p the occupation probability, p_c the percolation threshold, S a proportional constant, and q the critical exponent. It is not possible to give an analytical form for the constant S, because of the lack of knowledge about the cluster size distributions (size and shape) in most systems. In our study, σ is the electrical conductivity, p the MWCNT weight percentage.

On the other hand, McLachlan, et al. [33] also developed a model to predict the percolation problem specifically for the electrical conductivity of the CNT-polymer nanocomposites.

The following equation represents their model:

$$(1-\phi)\left(\sigma_i^{1/s}-\sigma_m^{1/s}\right)\left(\sigma_i^{1/s}+A\,\sigma_m^{1/s}\right)+\phi\left(\sigma_c^{1/t}-\sigma_m^{1/t}\right)\left(\sigma_c^{1/t}+A\,\sigma_m^{1/t}\right)=0 \qquad (4)$$

with $A=(1-\phi_c)/\phi_c$ and ϕ_c is the percentage of CNTs, *s* and *t* as the critical exponents.

σ_m, σ_c, and σ_i represent the electrical conductivities of the composite, the CNTs, and the polymer material, respectively.

The difference between the Kirkpatrick model and the McLachlan model is that the later one takes into account the percentage ratio of the matrix and the reinforcing material making the composite as well as their respective electrical conductivities.

7.2. Comparison between the percolation models and experimental results

7.2.1. Comparison for MWCNT-PP composites

Figure 7.1 shows the comparison between the percolation modeling and experimental data of electrical conductivity for the MWCNT-PP nanocomposites in terms of the CNT weight percentage on a logarithmic scale. Both experimental data and modeling show reasonable agreement. And the percolation threshold was estimated as around 3.8wt% of CNTs.

To simulate entire range of the electrical conductivity in terms of the weight percentage of CNTs as shown in Figure 7.1, the Kirkpatrick model took the following forms according to the experimental data:

$$\sigma=\begin{cases}2.70\times10^{5}(p-p_c)^{3.8} & \text{for } p>p_c\\ 1.0\times10^{-9}(p_c-p)^{-0.9} & \text{for } p<p_c\end{cases} \qquad (5)$$

In addition to the Kirkpatrick model, the McLachlan model was also used for comparison. For this specific nanocomposite system, the McLachlan model can be further reduced as:

$$\sigma = \begin{cases} \sigma_i \left(\dfrac{\phi_c}{\phi_c - \phi} \right)^{1.8} & \text{for } \phi < \phi_c \\ \sigma_c \left(\dfrac{\phi - \phi_c}{1 - \phi} \right)^{2.8} & \text{for } \phi > \phi_c \end{cases} \qquad (6)$$

where the electrical conductivity $\sigma_i = 2.0 \times 10^{-8} S/m$ and $\sigma_c = 1.943 \times 10^{4} S/m$ for PP and MWNT, respectively.

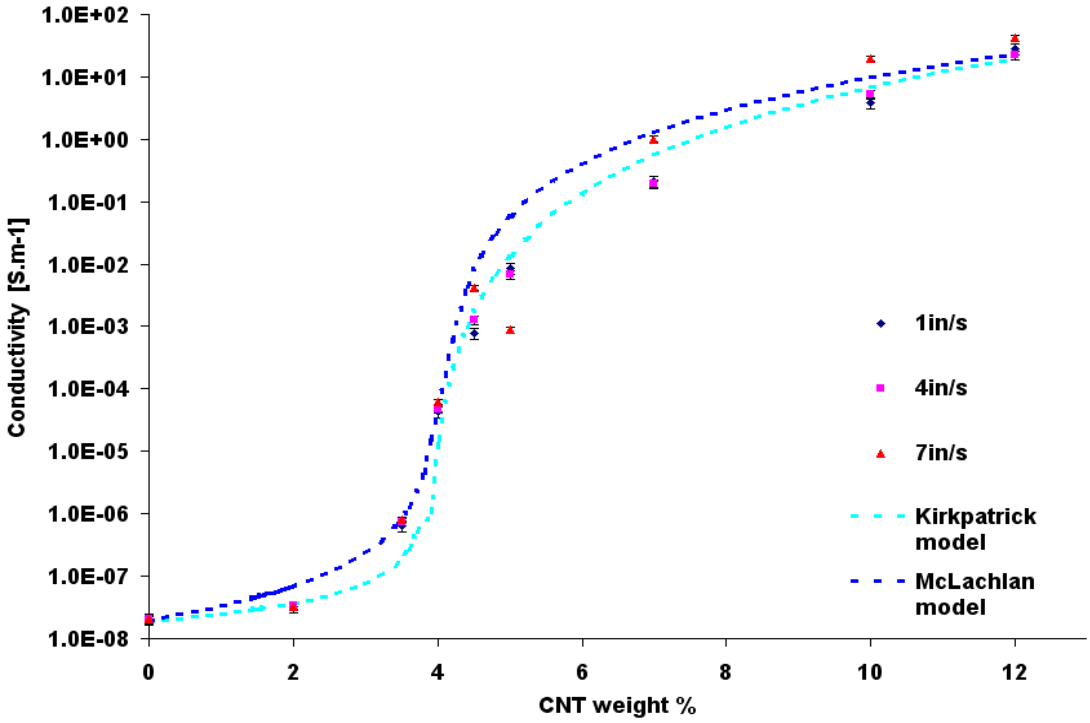

Figure 7.1: Comparison of electrical conductivity of MWNT-PP nanocomposites in terms of CNT weight percentage between modeling and experiments.

7.2.2. Comparison for MWCNT-PC composites

As far as the MWCNT-PC nanocomposites are concerned, the comparison of electrical conductivity of MWCNT-PC composites between modeling and experiments is shown in Figure 7.2. The percolation threshold was estimated at 1.8wt% of CNTs content. To simulate the electrical conductivity in terms of the weight percentage of CNTs, the Kirkpatrick model took the following forms according to the experimental data:

$$\sigma = \begin{cases} 3.67\times10^{3}(p-p_c)^{2} & \text{for } p > p_c \\ 5.0\times10^{-10}(p_c-p)^{-1.2} & \text{for } p < p_c \end{cases} \qquad (7)$$

In regards to the McLachlan model, it reduced to:

$$\sigma = \begin{cases} \sigma_i\left(\dfrac{\phi_c}{\phi_c-\phi}\right)^{1.8} & \text{for } \phi < \phi_c \\ \sigma_c\left(\dfrac{\phi-\phi_c}{1-\phi}\right)^{2.6} & \text{for } \phi > \phi_c \end{cases} \qquad (8)$$

where the electrical conductivity $\sigma_i = 4.0\times10^{-8}\,S/m$ and $\sigma_c = 1.943\times10^{4}\,S/m$ for PC and MWNT, respectively.

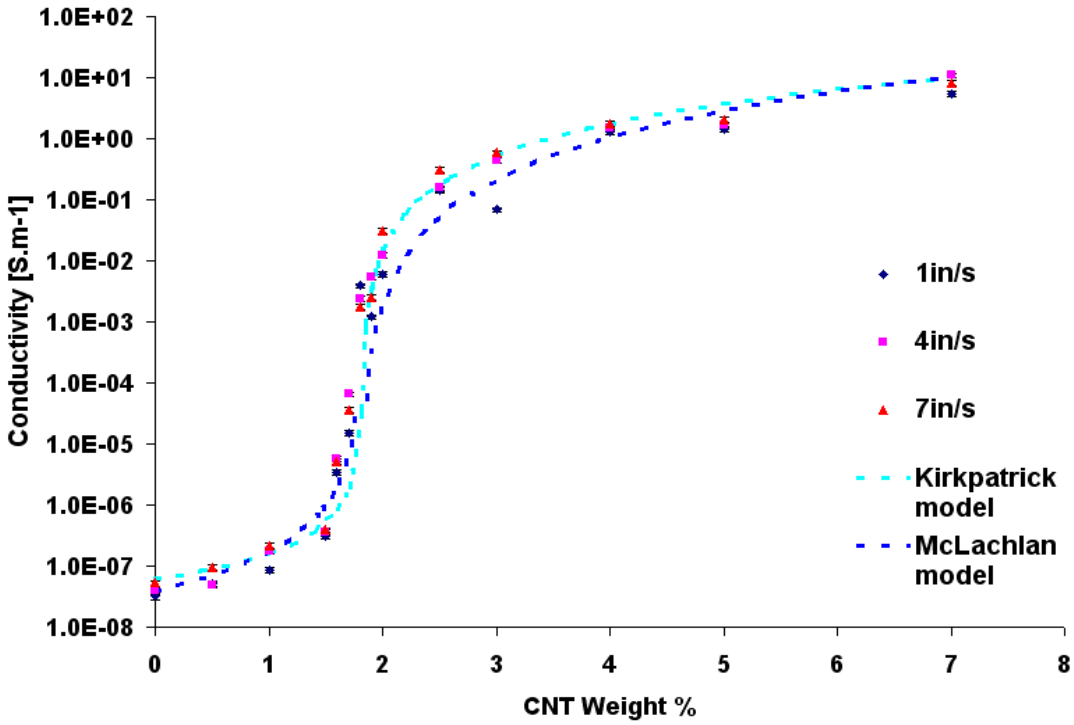

Figure 7.2: Comparison of electrical conductivity of MWNT-PC nanocomposites in terms of CNT weight percentage between modeling and experiments.

The MWCNT-PP and MWCNT-PC nanocomposites were produced by injection molding. The knowledge about the percolation value of 3.8wt% for the MWCNT-PP composites and 1.8% for the MWCNT-PC composites helps to determine when these composites change from insulators to conductors.

Two percolation models, the Kirkpatrick and McLachlan models matched well with our experimental data. In addition to that, we could realize the effect of injection speed on electrical conductivity.

8. MICROMECHANICAL MODELING OF CNT COMPOSITES

For elastic properties of two-phase composites, micromechanics theory has been proven as a powerful analytical tool. But when the micromechanics method such as Mori-Tanaka approach [40, 41] for two-phase composites applied to CNT reinforced nanocomposites, it always gives higher prediction of the elastic modulus of the system than the experimental data.

It has been suggested that the interphase zone exists between the CNT and the surrounding polymer matrix. The interphase effects on the elastic properties of composites have been studied extensively. In order to take into account of the interphase effect, Li and Shen [35] studied several different methods to target the validity range of each method. Instead of all available methods, the uniform replacement method (URM) which is the simplest one and the differential replacement method (DRM) which accounts for the inhomogeneity at the interphase were adopted here to study the effective elastic moduli of nanocomposites. The central idea of these methods is to convert a three-phase composite into a two-phase randomly oriented composite.

The above three models namely the Mori-Tanaka model for two-phase composites, the URM and the DRM will be used to model our experimental data. Thereafter, we will analyze their effectiveness toward MWCNT-PP nanocomposites.

8.1. Elastic Properties of CNT Composites

8.1.1. Effective Elastic Properties of Two-phase Composites

In Mori-Tanaka's approach, an average stress-strain method was used to derive the effective elastic moduli of two-phase composites. In general, the elastic stress-strain relation can be expressed as:

$$\sigma = L\varepsilon \qquad (9)$$

where the stress σ and strain ε are second order tensors

L a forth order tensor.

In indicial notation form, for an isotropic material, equation (9) can be expressed as:

$$\sigma_{ij} = \lambda\delta_{ij}\varepsilon_{kk} + 2\mu\varepsilon_{ij} \qquad (10)$$

where λ is the Lame's constant, μ the shear modulus.

$$\varepsilon_{kk} = \varepsilon_{11} + \varepsilon_{22} + \varepsilon_{33} \text{ and } \delta_{ij} = \begin{cases} 1, i = j \\ 0, i \neq j \end{cases}$$

In our notation, the matrix phase will be referred to as phase 0 where as the inclusion phase will be referred to as phase 1.

Let us consider a two-phase composite. Under a prescribed traction giving rise to a uniform stress $\bar{\sigma}$ in the composite, the average strain of the matrix in the real composite will differ from the individual strain in the matrix ε_0 due to the presence of the particles. Let's denote the difference in strain by $\tilde{\varepsilon}$.

Since the volume average of stresses in the matrix and inclusion, σ_0 and σ_1 respectively, should be equal to $\bar{\sigma}$,

$$\begin{aligned}\bar{\sigma} &= c_1\bar{\sigma}_1 + c_0\bar{\sigma}_0 \\ &= c_1(\bar{\sigma} + \tilde{\sigma} + \sigma^{pt}) + c_0(\bar{\sigma} + \tilde{\sigma})\end{aligned} \qquad (11)$$

where c_1 and c_0 are the volume fractions of the inclusion and matrix respectively

$(c_1+c_0=1)$

$$\tilde{\sigma} = L_0\tilde{\varepsilon}$$

σ^{pt} is the perturbation stress in the inclusion over the matrix

From equation (11):

$$\begin{aligned}\tilde{\sigma} &= -c_1\sigma^{pt} \\ L_0\tilde{\varepsilon} &= -c_1L_0(\varepsilon^{pt} - \varepsilon^*) \\ \Rightarrow \tilde{\varepsilon} &= -c_1(\varepsilon^{pt} - \varepsilon^*)\end{aligned} \qquad (12)$$

where $\tilde{\varepsilon}$ is the stress-free transformation strain

The overall average strain in the composite $\bar{\varepsilon}$ is also given by:

$$\begin{aligned}\bar{\varepsilon} &= c_0\bar{\varepsilon}_0 + c_1\bar{\varepsilon}_1 \\ &= c_0(\varepsilon_0 + \tilde{\varepsilon}) + c_1(\varepsilon_0 + \tilde{\varepsilon} + \varepsilon^{pt}) \\ &= (c_0 + c_1)(\varepsilon_0 + \tilde{\varepsilon}) + c_1\varepsilon^{pt} \\ &= \varepsilon_0 + \tilde{\varepsilon} + c_1\varepsilon^{pt}\end{aligned} \qquad (13)$$

Using the value of $\tilde{\varepsilon}$ form equation (12) in the last line of equation (13) above, we get:

$$\bar{\varepsilon} = \varepsilon_0 + c_1\varepsilon^* \qquad (14)$$

The expressions for the average hydrostatic and deviatoric stresses in the composite are given by:

$$\begin{aligned} \bar{\sigma}_{kk} &= 3\kappa \bar{\varepsilon}_{kk} \\ \bar{\sigma}'_{ij} &= 2\mu \bar{\varepsilon}'_{ij} \end{aligned} \qquad (15)$$

Using the hydrostatic component of the average stress, we get:

$$\begin{aligned} &\bar{\sigma}_{kk} = 3\kappa(\varepsilon^0_{kk} + c_1\varepsilon^*_{kk}) \\ &and \varepsilon^*_{kk} = a^* \varepsilon^0_{kk} \end{aligned} \qquad (16)$$

where $a^* = -\dfrac{\kappa_1 - \kappa_0}{[c_1(1-\alpha_0)+\alpha_0](\kappa_1 - \kappa_0) + \kappa_0}$ for spherical inclusions

Thus,

$$\begin{aligned} \bar{\sigma}_{kk} &= 3\kappa(1 + a^* c_1)\varepsilon^0{}_{kk} \\ &= 3\kappa(1 + a^* c_1)\frac{\bar{\sigma}_{kk}}{3\kappa_0} \end{aligned} \qquad (17)$$

Equation (17) will then give the Mori-Tanaka effective modulus of a two-phase composite:

$$\kappa = \kappa_0\left[1 + \frac{c_1(\kappa_1 - \kappa_0)}{c_0\alpha_0(\kappa_1 - \kappa_0) + \kappa_0}\right] \qquad (18)$$

where $\alpha_0 = \dfrac{1}{3}\dfrac{1-\upsilon_0}{1+\upsilon_0}$

υ is the Poisson's ratio

Similarly, the effective shear modulus of a two-phase composite with spherical inclusions can be obtained as:

$$\mu = \mu_0 \left[1 + \frac{c_1(\mu_1 - \mu_0)}{c_0 \beta_0 (\mu_1 - \mu_0) + \mu_0} \right] \qquad (19)$$

where $\beta_0 = \frac{2}{15} \frac{4 - 5\upsilon_0}{1 + \upsilon_0}$

Once κ and μ are known, the elastic modulus E of the composite can be obtained as:

$$E = \frac{9\kappa\mu}{3\kappa + \mu} \qquad (20)$$

8.1.2. Effective elastic properties of composites with interphase

The interphase is defined as a region between a homogeneous core and the homogeneous matrix in composites. Li and Shen [35] proposed a transformation technique shown below:

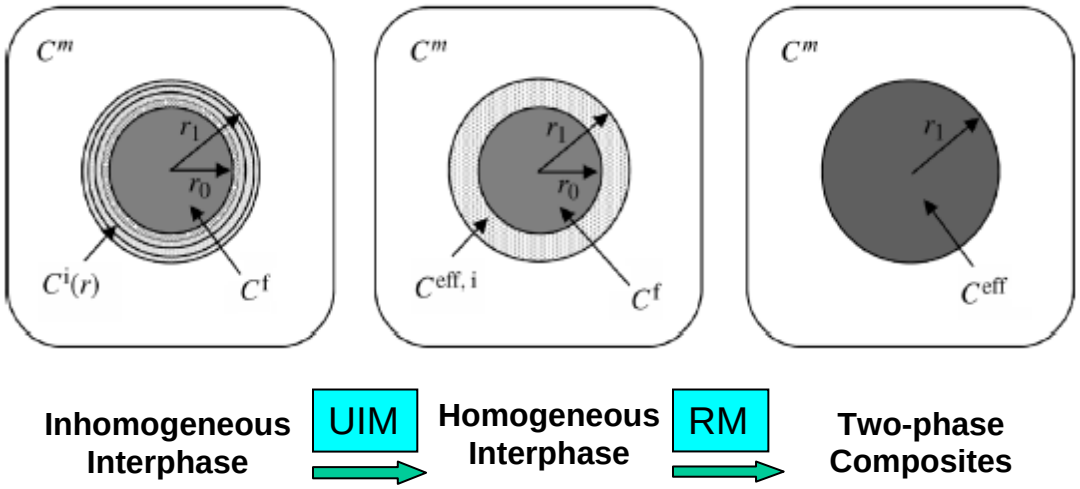

Figure 8.1: Schematic diagram to convert a three phase composite into a two phase composite.

They found the change in total strain energy of the infinite matrix subjected to far field stress is equal to:

$$\Delta f_c = -\frac{1}{2} V^f \frac{\sigma^2}{C^m} \frac{C^f - C^m}{C^m + \alpha_c^m (C^f - C^m)} \qquad (21)$$

where V^f is volume of the fiber per unit length

C^m, C^f are the elastic moduli of the matrix and fiber respectively

The simplest way to convert the inhomogeneous interphase into the homogeneous interphase is to find the elastic moduli of the effective interphase by averaging the varying interphase along the radial direction as follows:

$$C^{eff,i} = \frac{1}{r_1 - r_0} * \int_{r_o}^{r_1} C^i(r) dr \qquad (22)$$

where $C^{eff,i}$ is the effective elastic modulus of the interphase. In our modeling, we assumed a linear varying interphase.

The expression for the effective moduli of the composite using the URM method is obtained after transformations using equations (21) and (22):

$$C = C^m \left[1 + \frac{\phi_{eff}}{C^m / (C^{eff}(r) - C^m) + (1-\phi)\alpha_c^m} \right] \qquad (23)$$

with $C^{eff}(r) = C^{eff,i} + \dfrac{\phi C^{eff,i}}{C^{eff,i} / (C^f - C^{eff,i}) + (1-\phi)\alpha^{eff,i}_c}$

$$\alpha = (1+\nu)/[3(1-\nu)]$$

where C, C^m, C^f, $C^{eff,i}$ are elastic modulus of the composite, matrix, fiber and effective interphase respectively and Φ is the volume fraction

The DRM method assumes a differential approach to finding the effective modulus of the inclusion-interphase composite during the transformation. The governing differential equation is shown below.

$$\frac{dC^{eff}(r)}{dr} = -\frac{m}{r}\left\{\left[C^{eff}(r) - C^{i}(r)\right] + \frac{\alpha_C{}^{i}(r)}{C^{i}(r)}\left[C^{eff}(r) - C^{i}(r)\right]^2\right\} \qquad (24)$$

with $C^{eff}(r_0) = C^{f}$, C^{i} the interphase modulus and $\alpha_C{}^{i} = \frac{1+\upsilon}{3(1-\upsilon)}$.

8.2. Comparison between experimental data and micromechanics models

8.2.1. Comparison between experimental data and micromechanics models for MWCNT-PP composites

As expected, tensile test results showed that the elastic modulus increased with the weight percentage of MWCNTs. The Mori-Tanaka model as well as DRM, and URM methods were applied to compare with the experimental results. The DRM and URM methods incorporate the interphase effects while the Mori-Tanaka model is simply for two-phase composites. In this study, the elastic modulus of PP was supplied as 0.6GPa and the MWNTs as 1.2TPa. The interphase was assumed to have a thickness of 5 nm thickness and elastic modulus of 800 MPa. Figure 8.2 shows the comparison between the experimental data and different models for MWCNT-PP composites. The Mori-Tanaka method overestimated the elastic modulus, while URM gave the best prediction. That is an indication that there is an interphase zone between the CNTs and the matrix and the effective elastic modulus of the interphase is between the ones of the PP and the MWCNT.

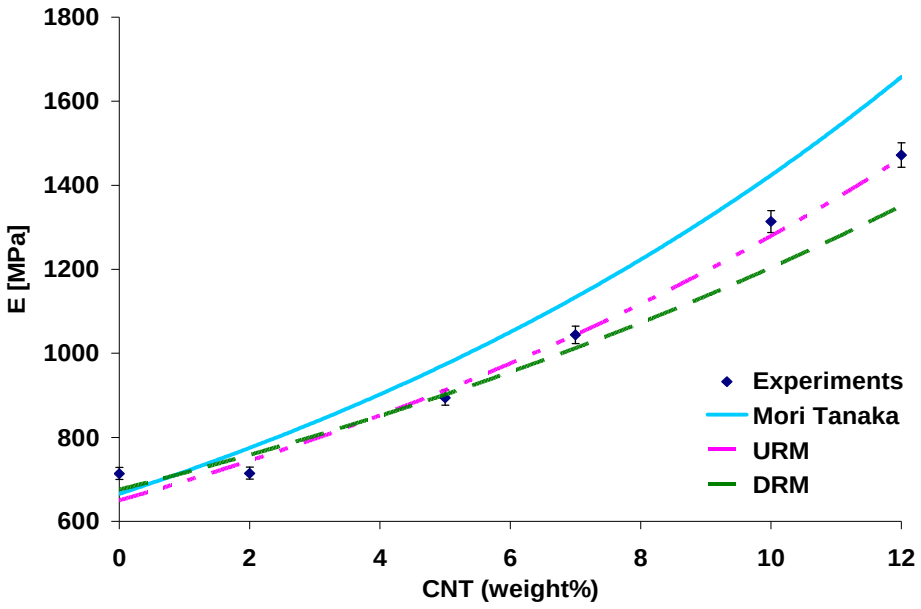

Figure 8.2: Effect of CNT weight percentage on the elastic modulus of MWCNT-PP composites.

8.2.2. Comparison between experimental data and micromechanics models for MWCNT-PC composites

Tensile test results on MWCNT-PC composites also showed that the elastic modulus increased with the weight percentage of MWCNTs. The Mori-Tanaka model as well as DRM, and URM methods were applied to compare with the experimental results. The elastic modulus of PC was supplied as 2GPa and the MWNTs as 1.2TPa. The interphase was assumed to have a thickness of 5 nm thickness and elastic modulus of 2.5 MPa. Figure 8.3 shows the comparison between the experimental data and different models in case of MWCNT-PCF composites.

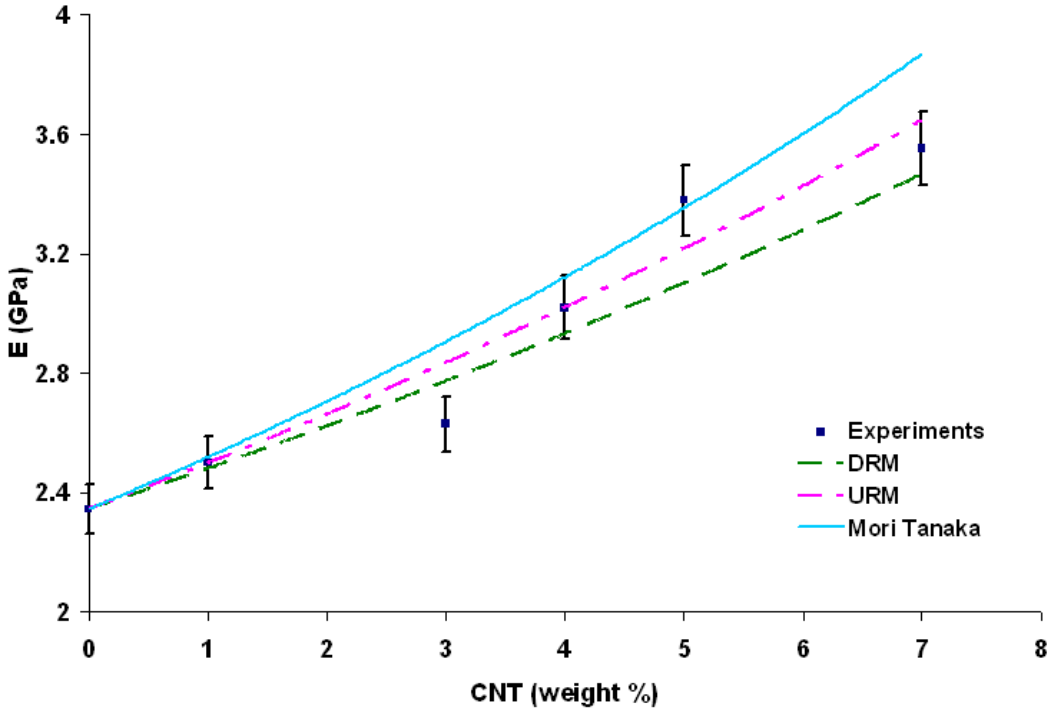

Figure 8.3: Effect of CNT weight percentage on the elastic modulus of MWCNT-PC composites.

In this chapter, the elastic modulus of the MWCNT-PP and MWCNT-PC nanocomposites were studied. The existing theoretical models such as DRM and URM predicted well comparing to our experimental results. The Mori-Tanaka model for elastic modulus of a two-phase composite overestimated the modulus of elasticity compared to our experimental data. These results show the importance of the interphase properties on the overall elastic properties of CNT composites. Both elastic moduli of the MWCNT-PP and MWCNT-PC composites showed a dramatic increase by less than 10wt% of CNT.

9. MODELING OF PIEZORESISTIVITY AND ELECTRICAL RESPONSE OF CNT COMPOSITES UNDER TENSILE LOADING

In order to use conductive composites as sensors, the cause of the electrical resistance change needs to be understood and investigated. In general, there are three major sources, which may change the electrical resistance of the composite with electrical conductive fillers under mechanical loading: straining, fiber breakage and/or delamination, and percolation.

First, if there is no damage and/or percolation, the change of resistance is linearly proportional to strain due to piezoresistivity of the conductive fillers. Then, due to the excessive damage of the fibers and/or large straining, the resistance change can increase dramatically with increase of the strain. It has been observed [56-60] that the relation between the resistance change and tensile strain follows an exponential or power law.

9.1. Weibull distribution model

In order to model the resistance change of the MWCNT-Polymer composites, the Weibull distribution function will be used due to the random nature of the CNT contacts. Due to the probabilistic nature of the event, the best solution is to apply statistics theory using the Weibull distribution function [61]:

$$P(s) = \frac{K}{\lambda}\left(\frac{S}{\lambda}\right)^{k-1} e^{-\left(\frac{S}{\lambda}\right)^{k}} \qquad (25)$$

where P is the probability density function, S the applied stress, k >0 the shape parameter, and $\lambda > 0$ the scale parameter.

Using the probability density function, the electrical conductivity can be obtained as

$$\frac{\sigma}{\sigma_0} = 1 - aP \qquad (26)$$

where a is a constant.

The relative resistance change $\Delta R/R_0$ can be derived as

$$\frac{\Delta R}{R_0} = \frac{1+\varepsilon}{\frac{\sigma}{\sigma_0}} - 1 \qquad (27)$$

where ε is the tensile strain, σ is the conductivity and σ_0 the initial conductivity without loading.

Using the exponential or power law to describe the relationship between changes in conductivity versus the applied stress, we obtain:

$$\frac{\sigma}{\sigma_0} = b(S - S_0)^t \text{ (Power law) } or \ \frac{\sigma}{\sigma_0} = ce^{-(S-S_0)t} \text{ (exponential law)} \qquad (28)$$

where S_0 is the reference stress, b and c are constants.

Using the power law for modeling, the relative resistance change can be obtained

$$\frac{\Delta R}{R_0} = \frac{1+\varepsilon}{b(S - S_0)^t} \text{-1} \qquad (29)$$

9.2. Comparison between Experimental Data and Power Law Model

For modeling the experimental data, we used the power law to describe the relationship between changes in conductivity versus the applied stress.

9.2.1. Comparison between experimental data and model for MWCNT-PP composites

The combination of the Weibull distribution and the power law was used to capture the effect of straining on electrical resistance change. As shown in figure 9.1, the power law model matched well with the experimental data for the MWCNT-PP composites at 10 and 12 weight percentage of CNT.

The model is given by:

$$\frac{\Delta R}{R_0} = \frac{1+\varepsilon}{0.01S^{0.22}} - 1 \qquad \text{with S>0} \qquad (30)$$

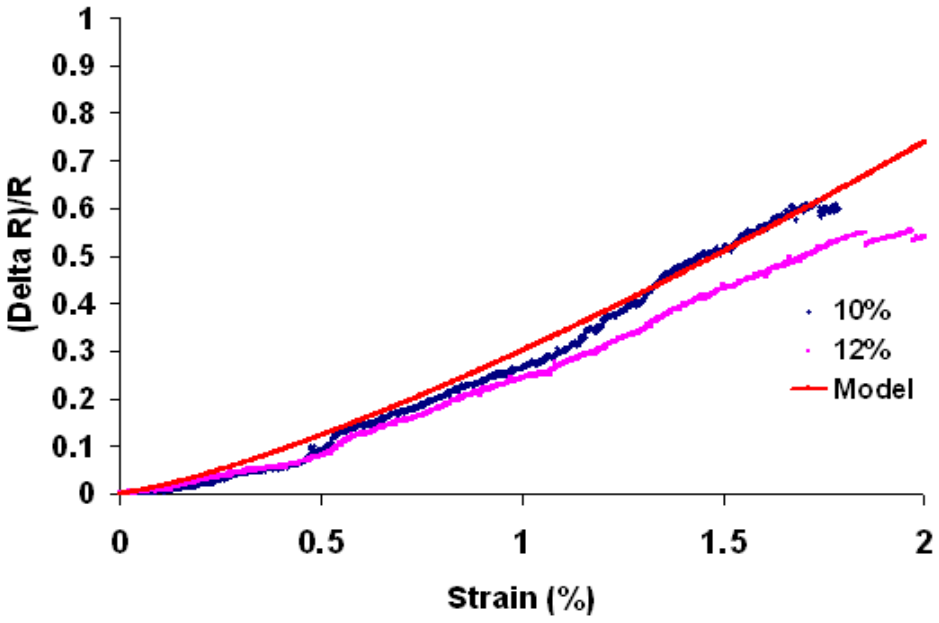

Figure 9.1: Comparison of relative resistance versus strain between the statistic model and average experimental data for MWCNT-PP with 10% and 12% weight CNT.

9.2.2. Comparison between experimental data and model for MWCNT-PC composites

The Weibull model was also used to model the experimental data for MWCNT-PC composites. In case of MWCNT-PC composite specimens, the relative resistance showed a more linear change versus the strain. Figure 9.2 below shows the relationship between the relative resistance versus strain between the statistic model and average experimental data for both MWCNT-PC with 5% and 7% weight CNT. The power law model matched very well with the experimental data and was given by the following relationship:

$$\frac{\Delta R}{R_0} = \frac{1+\varepsilon}{0.0015S} - 1 \qquad \text{with S>0} \qquad (31)$$

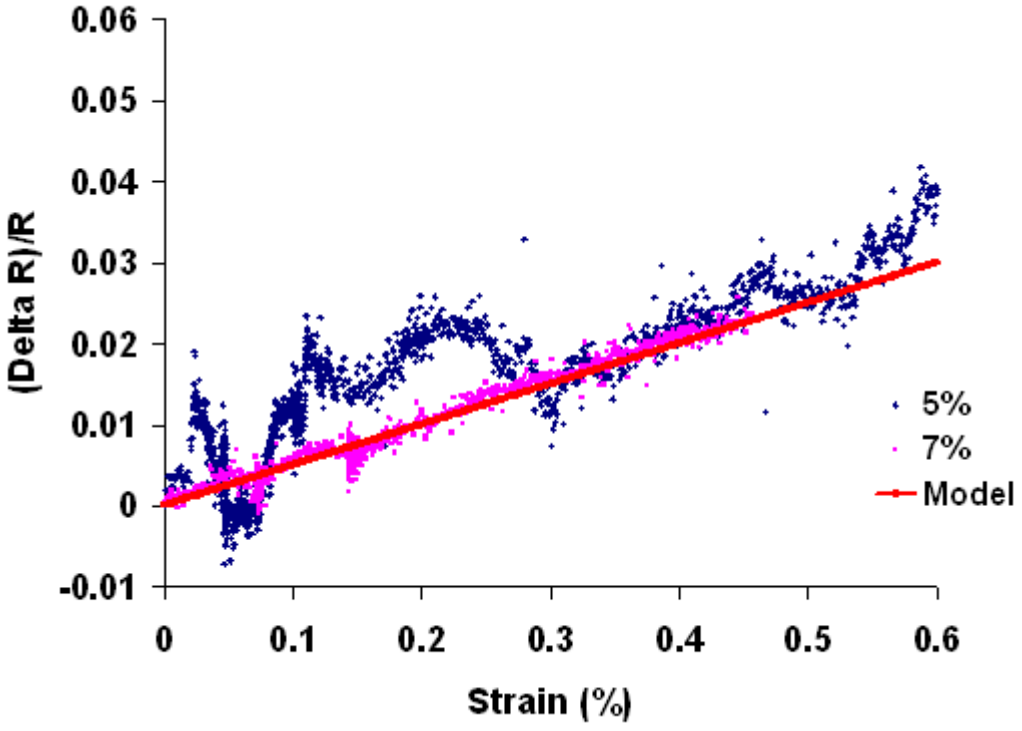

Figure 9.2: Comparison of relative resistance versus strain between the statistic model and average experimental data for MWCNT-PC with 5% and 7% weight CNT.

The composites specimens showed electrical resistance change sensitivity to strain change. The level of sensitivity varies with the CNT wt%; it is less pronounced in composites with weight percentage close to the threshold value of conductivity. The sensitivity became more pronounced for nanocomposites with higher CNT weight percentages.

The above results are promising use MWCNT-Polymer composites for the sensing purposes. This additional property will add to the already existing advantageous range of potential applications.

10. CONCLUSIONS AND FUTURE WORK

Mechanical properties of carbon nanotubes, and in particular their predicted high strengths (around 60GPa) and moduli (about 1TPa), make them attractive candidates as a reinforcement filler material in polymer based structural composites. In addition, their outstanding electrical and thermal properties show that carbon nanotubes incorporated into polymers can significantly enhance these properties as well. Electrical conductivity and mechanical tensile tests were carried out on MWCNT-Polymer composites (MWCNT-PP and MWCNT-PC), produced by injection molding.

In general, most polymers are insulators, but with the inclusion of a small amount of CNT, they become highly conductive. The conductivity can be changed up to the order of 10^8 magnitude difference with less than 10% weight CNT filler. Here, 2-probe measurement was used to determine the electrical conductivity of the nanocomposite systems. The percolation threshold value for the tested composites was obtained. The knowledge about the percolation value of 3.8wt% for the MWCNT-PP composites and 1.8% for the MWCNT-PC composites helps to determine when these composites change from insulators to conductors.

Two percolation models, the Kirkpatrick and McLachlan models were also used to model the change of conductivity in terms of CNT contents. The results matched well with our experimental data. In addition to that, the effect of our main production parameter, the injection velocity, on electrical conductivity of MWCNT-Polymer composites was analyzed. We could realize the effect of injection speed on electrical conductivity i.e. the conductivity is higher for nanocomposites produced at a higher injection velocity. This was mainly due to the fact carbon nanotubes tends to align

themselves within the polymer matrice as the injection speed increases. TEM images also reinforced the above conclusion.

In regards to mechanical properties, tensile tests were conducted. The elastic modulus and stress-strain relations of the MWCNT-PP and MWCNT-PC nanocomposites were obtained. The elastic moduli for both MWCNT-PP and MWCNT-PC composites showed a dramatic increase by less than 10wt% of CNT.

However, modeling the effective properties of a nanotube-reinforced polymer is made difficult because of complexities related to the structure and properties of the nanotubes, the orientation and dispersion of the nanotubes within the polymer, and the characteristics of the interface between the CNTs and the polymer. Three micromechanics based models– Mori Tanaka, Differential Replacement Model (DRM) and Uniform Replacement Model (URM) - were adopted to study the effective elastic modulus of CNT composite system in terms of CNT content. The Mori-Tanaka model which is a two-phase composite model overestimated the modulus of elasticity compared to our experimental data, while the DRM and URM methods developed by Shen and Li for composites with inhomogeneous interphase gave better predictions and the results obtained from these two models agreed well with the experimental results. These analyses show the importance of the interphase properties on the overall elastic properties of CNT composites. Advanced models of how these factors influence the effective properties of the nanotube-reinforced polymer will be necessary in order to optimize the fabrication and effective properties of nanotube polymer composites.

As for the effect of the injection velocity on mechanical behaviors of MWCNT-Polymer composites, the experimental results did not indicate significant change on elastic modulus and stress-strain relations of composites.

In addition to injection velocity, strain-rate sensitivity to mechanical properties was studied for the MWCNT-PC composites with three strain-rate considerations: 0.1/min, 0.01/min, and 0.001/min. For MWCNT-PP composites, only two strain-rates loadings of 0.1/min and 0.01/min were conducted due to the limited availability of the specimens. It was surprising to see that the stress-strain curves of MWCNT-PP did not show significant strain-rate effect. The tensile stress flow of MWCNT-PC composites increases with increasing strain-rate.

Based on the findings about the improved mechanical and electrical properties of polymer based CNT composites, it has attracted attention for multifunctional applications of CNT-polymer composites. To that perspective, the electrical resistance change of CNT composites was measured under tensile loading. The correlation of piezoresistance and tensile strain was studied. When the CNT content is close to the percolation threshold, no piezoresistive behavior of the system can be observed. When the CNT content is higher (10wt% or higher for MWCNT-PP, 5wt% or higher for MWCNT-PC), the electrical resistance change increases with increase of strain. At small strain range, both MWCNT-PP and MWCNT-PC show linear resistance change in terms of strain. This can be calibrated with stress-strain curve for strain sensing application. At a large strain, the resistance change of CNT-PP increases exponentially. This may be due to the damage of the sample, and have potential for damage self-sensing.

In conclusions, electrical and mechanical behaviors of MWCNT-PP and MWCNT-PC nanocomposites have been studied in terms of CNT contents and injection velocity. Percolation theories have been applied to study the electrical conductivity of the composites. The percolation thresholds have been determined. Three micromechanics based models have been applied to study the effective elastic modulus of the nanocomposites. These models will be able to give some guidance for processing of the nanocomposites. Finally, the piezoresistance of the composites have been investigated under tensile loading. The results show promising potential applications of the produced nanocomposites for strain sensing and damage self-sensing ability.

CONTRIBUTION OF THIS RESEARCH WORK

In this research, a comprehensive study on electrical and mechanical properties of CNT-polymer composites was conducted. The percolation thresholds for electrical conductivity of our polymer composites were found. In addition to the percolation threshold, the influence of production parameter, the injection velocity, was analyzed and showed significant influence.

Mechanical properties were also analyzed as well as the influence of production parameters on modulus of elasticity. Strain-rate loadings showed an impact on elastic modulus.

To the author knowledge, the use of our research CNT-polymer systems for sensing purposes has not been studied. Thus, the knowledge about the application range in regards not only to the percolation threshold but also the CNT weight contents will help for further research and applications.

All the above analysis can have applications ranging from EMI/RFI shielding, conductive ducts, electrostatic dissipation (ESD), radar-absorbing materials for low-observable ("stealth") to sensors.

FUTURE WORK

i. Viscoelastic Behavior of CNT-polymer Composites

Since both PP and PC are thermoplastic materials, they show viscoelastic behavior under mechanical loadings. In order to model the entire range of the stress-strain relations of the CNT composites under tensile loading, a micromechanics based viscoelasticity theory should be adopted in the future work.

ii. Size Effect on Electrical Sensitivity of CNT-polymer Composites

Our research study on the electrical resistance response to mechanical tensile loading was conducted on standard tensile test bar specimens. Since the electrical conductivity varies with material dimensions, further research on different samples sizes ranging from regular tensile bar specimens to microfilm sheets should be analyzed for sensitivity purposes. Samples with different dimensions will be subjected to mechanical tensile loadings and the electrical conductivity response will be analyzed and compared.

References:

[1] Ijima, S. Helical microtubules of graphitic carbon. *Nature* **354**, 56 (1991).

[2] Ebbesen, T.W. and Ajayan, P.M.. Large-scale synthesis of carbon nanotubes. *Nature* **358**, 220 (1992).

[3] Ijima, S. , Brabec, C., Maiti, A. and Bernholc, J. Structural flexibility of carbon nanotubes. *J. Chem. Phys*. **104**, 2089 (1996).

[4] Wagner, H.D., Lourie, O., Feldman, Y. and Tenne, R. Stress-induced fragmentation of multiwall carbon nanotubes in a polymer matrix. *Applied Physics Letter* **72**, 188 (1998).

[5] Yu, M.F., Lourie, O., Dyer, M.J., Moloni, K., Kelly, T.F. and Rouff, R.S.. Strength and breaking mechanism of multiwalled carbon nanotubes under tensile load. *Science* **287**, 637 (2000).

[6] Ramanathan, T., Liu, H., and Brinson, L. C. Functionalized SWNT/Polymer Nanocomposites for Dramatic Property Improvement. *Journal of Polymer Science B* **43**(2005).

[7] Jia, Z., Wang, Z., Xu , C., Liang, J., Wei, B., Wu, D., and Zhu, S. Study on Poly (methyl methacrylate)/Carbon Nanotube Composites. *Materials Science and Engineering A,* **271**, 395–400 (1999).

[8] Thostenson, E. T. and Chou, T.W. On the Elastic Properties of Carbon Nanotube-based Composites: Modeling and Characterization. *Journal of Physics D: Appl. Phys*., **36,** 573–582 (2003).

[9] Seidel, G. D., and Lagoudas, D. C. Micromechanical analysis of the effective elastic properties of carbon nanotube reinforced composites. *Mechanics of Materials* **38**, 884-907 (2006).

[10] Cho, J.W. and Paul, D.R. Nylon 6 nanocomposites by melt compounding. *Polymer*, **42**(3), 1083-1094 (2001).

[11] Dennis, H.R., Hunter, D.L., Chang, D., Kim, S., White, J.L., Cho, J.W., and Paul, D.R. Effect of melt processing conditions on the extent of exfoliation in organoclay-based nanocomposites. *Polymer*, 42(23), 9513-9522 (2001).

[12] Anderson, P. G. Twin screw extrusion guidelines for compounding nanocomposites. *Proceedings of Annual Technical Conference of the Society of Plastics Engineers*, **48**, 1-5 (2002).

[13] Dolgovskij, M.K., Fasulo, P.D., Lortie, F., Macosko, C.W., Ottaviani, R.A., and Rodgers, W.R. Effect of mixer type on exfoliation of polypropylene nanocomposites. *Proceedings of Annual Technical Conference of the Society of Plastics Engineers*, **49**, 2255-2259 (2003).

[14] Fasulo, P.D., Rodgers, W.R., Ottaviani, R.A., and Hunter, D.L. Extrusion Processing of TPO nanocomposites. *Polymer Engineering and Science*, **44**, 1036-1045 (2004).

[15] Lertwimolnun, W. and Vergnes, B. Influence of compatibilizer and processing conditions on the dispersion of nanoclay in a polypropylene matrix. *Polymer*, **46**(10), 3462-3471 (2005).

[16] Dalton, A.B., Blau, W.J., Chambers, G., Coleman, J.N., Henderson, K., Lefrant, S., McCarthy, B., Stephan, C., and Byrne, H.J. A functional conjugated polymer to process,

purify and selectively interact with single wall carbon nanotubes. *Synthetic Metals* **121**, 1217-1218 (2001).

[17] Ramanathan, T., Fisher, F., T., Ruoff, R. S. and Brinson. L. C. Amino-Functionalized Carbon Nanotubes for Binding to Polymers and Biological Systems. *Chem. Mater.* **17***,* 1290-1295 (2004).

[18] Shaffer, M. S. P., Fan, X. and Windle, A. H. . Dispersion and Packing of Carbon Nanotubes. *Carbon* **36** (11), 1603–1612 (1998).

[19] Gong, X., Liu, J., Baskaran, S., Voise, R. D. and Young, J. S. Surfactant-Assisted Processing of Carbon Nanotube/ Polymer Composites. *Chem. Mater.* **12***,* 1049-1052 (2000).

[20] Stephan , C., Nguyen , T.P., Lamy de la Chapelle , M., Lefrant , S., Journet , C., and Bernier, P. Characterization of Single Walled Carbon Nanotubes-PMMA Composites. *Synthetic Metals* **108**, 139–149 (2000).

[21] Shaffer, M. S. P. and Windle, A. H. Fabrication and Characterization of Carbon Nanotube/Poly (vinyl alcohol) Composites. *Advanced Materials* **11**, 937-941 (1999).

[22] Chang, T.E., Kisliuk, A., Rhodes, S.M., Brittain, W.J. and Sokolov, A.P. Conductivity and Mechanical Properties of Well-dispersed Single-wall Carbon Nanotube/Polystyrene Composite. *Polymer*, doi:10.1016/j.polymer.2006.09.013

[23] Ahmad, K., Pan, W. and Shi, S.L. Electrical Conductivity and Dielectric Properties of Multiwalled Carbon Nanotube and Alumina Composites. *Applied Physics Letters* **89**, 133122 (2006).

[24] Liang, G.D., Bao, S.P., Tjong, S.C. Microstructure and Properties of Polypropylene Composites filled with Silver and Carbon Nanotube Nanoparticles Prepared by Melt-compounding. *Materials Science and Engineering B* **142**, 55–61 (2007).

[25] So, H. H., Cho, J.W. and Sahoo, N.G. Effect of Carbon Nanotubes on Mechanical and Electrical Properties of Polyimide/Carbon Nanotubes Nanocomposites. *European Polymer Journal* **43**, 3750–3756 (2007).

[26] Collins, P.G. and Avouris, P. Nanotubes for Electronics. *Scientific American* **283(6)**, 62 (2000).

[27] Thostenson, E.T., Ren, Z. and Chou, T.W. Advances in the science and technology of carbon nanotubes and their composites: a review. *Composites Science and Technology*, **61**, 1899 (2001).

[28] Haggenmuller, R., Gonmas, H.H., Rinzler, A.G., Fischer, J.E., Winey. K.I. Chem. Phys. Letter 330(3/4), 219-225 (2000).

[29] Jin, J.X., Pramoda, K.P., Xu, G.Q. Material Resistance Bulletin 37, 271-278 (2000).

[30] Jia, Z.J., Wang, Z.Y., Xu, C.L., Liang, J., Wei, B.Q., Wu, D.H., and Zhu, S.W. Materials Science and Engineering A 271, 395-400 (1999).

[31] Li Chen, Xiu-Jiang Pang, Zuo-Long Yu. Study on polycarbonate/multi-walled carbon nanotubes composite produced by melt processing. *Materials Science and Engineering* A **457**, 287-291 (2007).

[32] Scott Kirkpatrick. Percolation and Conduction. *Review of Modern Physics* ***45***, 574-588 (1973).

[33] McLachlan, D. S. et al. AC and DC percolative conductivity of single wall carbon nanotube polymer composites. *Journal of Polymer Science B,* ***43***: 3273-3287 (2005).

[34] Odegard, G., Gates, T. Constitutive modeling of nanotube/polymer composites with various nanotube orientations. SEM Annual Conference on Experimental and Applied Mechanics, June 10-12 June, 2002, Milwaukee, WI.SEM, Milwaukee, WI.

[35] Shen, L. and Li, J. Homogenization of a fiber/sphere with an inhomogeneous interphase for the effective elastic moduli of composites. *Proceedings of the Royal Society* A **461**, 1475-1504 (2005).

[36] Liao, K. and Li, S. Interfacial characteristics of a carbon nanotube-polystyrene composite system. *Applied Physics Letters*., **79**, 4225-4227 (2003).

[37] Wagner, H.D. Nanotube–polymer adhesion: a mechanics approach. *Chem. Phys. Lett*., 361, 57-61 (2002).

[38] Fisher, F.T., Bradshaw, R.D. and Brinson, L.C.. Viscoelasticity and physical aging of carbon nanotube-reinforced polymers. *SEM 2002 Annual Conference proceedings*.

[39] Ngabonziza, Y., Li, J. and Barry, C. Electrical Conductivity and Elastic Properties of MWCNT-PP Nanocomposites. *Proc. of American Society of Mechanical Engineers International Mechanical Engineering Congress and Exposition,* (2008).

[40] Mori, T. and Tanaka, K.. Average stress in matrix and average elastic energy of materials with misfitting inclusions. *Acta Metallurgica **21(5)**, 571-574*(1973).

[41] Weng, G.J. The theoretical connection between Mori–Tanaka's theory and the Hashin – Shtrikman – Walpole bounds. *Int. J. Eng. Sci*. **28**, 1111–1120 (1990).

[42] Kim, D., Lee, J. S., Barry, C. F., and Mead, J. L. Evaluation and prediction of the effects of melt processing conditions on the degree of mixing in alumina / poly (ethylene terephthalate) nanocomposites. *Journal of Applied Polymer Science*, **109**(5), 2924-2934 (2008).

[43] Manas-Zloczower, I., Nir, A., and Tadmor, Z., 1082. *Rubber Chem. Tech*. 55:1250-1285.

[44] Manas-Zloczower, I., Nir, A., and Tadmor, Z. *Polymer Composites*, **6**(4):222 – 231 (1985).

[45] Gong, X., Liu, J., Baskaran, S., Voise, R., and Young, J. Surfactant-assisted processing of carbon nanotube/polymer composites. *Chemistry of Materials **12**, 1049-1052* (2000).

[46] Zhu, J., Kim, J., Peng, H., Margrave, J., Khabashesku, V., and Barrera, E. Improving the dispersion and integration of single-walled carbon nanotubes in epoxy composites through functionalization. *Nano Letters **3(8)**, 1107-1113* (2003).

[47] Malloy, R. A. Plastics Part Design for Injection Molding, Hanser/Gardner Publications, Cincinnati, OH (1994).

[48] J. Ingram, Y. Zhou, S. Jeelani, T. Lacy, M.F. Horstemeyer. Effect of strain rate on tensile behavior of polypropylene and carbon nanofiber filled polypropylene. *Material Science and Engineering A,* **489**, 99-106 (2008).

[49] Li, J. and Weng, G.J. Strain-rate sensitivity, relaxation behavior, and complex moduli of a class of isotropic viscoelastic composites. *Journal of Engineering Materials and Technology* **116**, 495-504 (1994).

[50] Li, J., and Weng, G.J. Anisotropic stress-strain relations and complex moduli of a viscoelastic composite with aligned spheroidal inclusions. *Composites Engineering*, **4(11)**, 1073-1097 (1994).

[51] Dalton, A. B., Stephan, C., Coleman, J. N., McCarthy, B., Ajayan, P. M., Lefrant, S.,

Bernier, P., Blau, W. J. and Byrne, H. J. Selective Interaction of a Semiconjugated Organic Polymer with Single-Wall Nanotubes. *J. Phys. Chem. B* **104***,* 10012-10016 (2000).

[52] Chung, D.D.L. and Wang, S. Self-monitoring of Damage and Strain in Carbon Fiber Polymer-Matrix Structural Composites by Electrical Resistance Measurement. *Polymers and Polymer Composites*, **11**(7): 515-525 (2003).

[53] Todoroki, A., Tanaka, M. and Shimamura, Y. Electrical Resistance Change Method for Monitoring Delamination of CFRP laminates: Effect of Spacing between Electrodes. *Composites Science and Technology*, **65**:37-46 (2005).

[54] Shen, L., Li, J., Liaw, B.M., Delale, F. and Chung, J.H. Modeling and Analysis of the Electrical Resistance Measurement of Carbon Fiber Polymer-Matrix Composites. *Composites Science and Technology,* **67**: 2513-2520 (2007).

[55] Pham,G. T., Park ,Y., Liang, Z., Zhang, C., Wang, B. Processing and modeling of conductive thermoplastic/carbon nanotube films for strain sensing. *Composites: Part B,* **39**: 209–216 (2008).

[56] Ueda, N., Taya, M. Prediction of the Electrical Conductivity of Two-dimensionally Misoriented Short Fiber Composites by a Percolation Model. *Journal of Applied Physics*, **60**:459 (1986).

[57] Carmona, D., Canet, R., Delhaes, P. Piezoresistivity of Heterogeneous Solid. *Journal of Applied Physics,* **61**:2550 (1987).

[58] Taya, M. Micromechanics Modeling of Smart Composites. *Composites A*, **30**:531 (1999).

[59] Park, J.M., Okabe, T., Song, D.Y, Takeda, N., Kitano A. Proceedings of SPIE, 4328:323 (2001).

[60] Okuhara, Y., Jang, B.K., Matsubara, H., Sugita. M. Proceedings of SPIE, 5057:54 (2003).

[61] Weibull, W.A. A Statistical Distribution Function of Wide Applicability. *Journal of Applied Mechanics*, ASME, **18**:293–7 (1951).

[62] Pan, Z. W., S. S. Xie, L. Lu, B. H. Chang, L. F. Sun, W. Y. Zhou, G. Wang , Zhang , D. L. Tensile tests of ropes of very long aligned multiwalled carbon nanotubes. *Applied Physics Letters*, **74**(21): 3152-3154 (1999).

[63] Qian, D., Dickey, E. C., Andrews, R., Rantell, T. Load transfer and deformation mechanisms in carbon nanotube-polystyrene composites. *Applied Physics Letters*, **76**(20): 2868-2870 (2000).

[64] Thess, A., R. Lee, P. Nikolaev, H. Dia, P. Petit, J. Robert, C. Xu, Y. H. Lee, S. G. Kim, A. G. Rinzler, D. T. Colbert, G. E. Scuseria, D. Tománek, J. E. Fischer and R. E. Smalley. Crystalline ropes of metallic carbon nanotubes. *Science*, **273**: 483-487 (1996).

[65] López, M. J., A . Rubio, J. A. Alonso, L.-C. Qin and S. Iijima. Novel polygonized single-wall carbon nanotube bundles. *Physical Review Letters*, **86**(14): 3056 (2001).

[66] Sandler, J., M. S. P. Shaffer, T. Prasse, W. Bauhofer, K. Schulte and A. H. Windle. Development of a dispersion process for carbon nanotubes in an epoxy matrix and the resulting electrical properties. *Polymer*, **40**(21): 5967-5971 (1999).

[67] Andrews, R., D. Jacques, M. Minot and T. Rantell . Fabrication of carbon

multiwalled nanotube/polymer composites by shear mixing. *Macromolecular Materials and Engineering*, **287**(6): 395-403 (2002).

[68] Gao, G., T. Çagin and W. A. Goddard III. Energetics, structure, mechanical and vibrational properties of single-walled carbon nanotubes. *Nanotechnology*, **9**:184-191 (1998).

[69] Hernández, E., C. Goze, P. Bernier and A. Rubio. Elastic properties of C and $B_xC_yN_z$ composite nanotubes. *Physical Review Letters*, **80**(20): 4502-4505 (1998).

[70] Che, J., T. Çagin and W. Goddard III . Generalized extended empirical bondorder dependent force fields including nonbond interactions. *Theoretical Chemistry Accounts*, **102**: 346-354 (1999).

[71] Sánchez-Portal, S., E. Artacho, J. M. Soler, A. Rubio and P. Ordejón . *Abinitio* Structural, Elastic, and Vibrational Properties of Carbon Nanotubes. *Physical Review B*, **59**(19): 12678-12688 (1999).

[72] Lu, J. P. Elastic Properties of Carbon Nanotubes and Nanoropes. *Physical Review Letters*, **79**(7): 1297-1300 (1997).

[73] Pujari, S., Ramanathan, T., Kasimatis, K., Masuda, J., Andrews, R., Torkelson, J. M, Brinson, L. C., Burghardt, W., R. Preparation and Characterization of Multiwalled Carbon Nanotube Dispersions in Polypropylene: Melt Mixing Versus Solid-State Shear Pulverization. *Journal of Polymer Science: Part B: Polymer Physics*, **47**:1426-1436 (2009).

[74] Ceysson, O., Salvia, M. and Vincent, L. Damage Mechanisms Characterization of Carbon Fiber/Epoxy Composite Laminates by Both Electrical Resistance Measurements and Acoustic Emission Analysis. *Scripta Materialia*, **34**(8): 1273-1280 (1996).

[75] Todoroki, A. The Effect of Number of Electrodes and Diagnostic Tool for Monitoring the Delamination of CFRP Laminates by Changes in Electrical Resistance. *Composites Science and Technology*. **61**:1871-1880 (2001).

[76] Wang, S., Mei, Z. and Chung, D.D.L. Interlaminar Damage in Carbon Fiber Polymer- Matrix Composites, Studied by Electrical Resistance Measurement. *International Journal of Adhesion and Adhesives*, **21**:465-471 (2001).

[77] Li, N., Huang, Y., Du, F., He, X. B., Lin, X., Gao, H. J. Electromagnetic interference (EMI) shielding of single-walled carbon nanotube epoxy composites. *Nano Letter* **6**(6):1141-5 (2006).

[78] Huang, Y., Li, N., Ma, Y., Du, F., Li, F., He X. The influence of single-walled carbon nanotube structure on the electromagnetic interference shielding efficiency of its epoxy composites. *Carbon*. **45**(8):1614-21 (2007).

[79] Jou, W.S., Cheng, H.Z., Hsu, C.F. The electromagnetic shielding effectiveness of carbon nanotubes polymer composites. *Journal of Alloys Compound* : 434-435(SPEC. ISS.): 641-5 (2007).

[80] Liu, Z.F., Bai, G., Huang, Y., Ma, Y.F., Du, F., Li, F.F. Reflection and absorption contributions to the electromagnetic interference shielding of single-walled carbon nanotube/polyurethane composites. *Carbon*. **45**(4):821-7 (2007).

[81] Yang, Y., Gupta, M.C., Dudley, K.L. Studies on electromagnetic interference shielding characteristics of metal nanoparticle- and carbon nanostructure-filled polymer composites in the Ku-band frequency. *Micro and Nano Letters*. **2**(4):85-9 (2007).

[82] Yang, Y.L., Gupta, M.C., Dudley, K.L., Lawrence, R.W. Electromagnetic interference shielding characteristics of carbons nanofiber-polymer composites. *Journal of Nanoscience Nanotechnology*. **7**(2):549-54 (2007).

[83] Zhang, C.S., Ni, Q.Q., Fu, S.Y., Kurashiki, K. Electromagnetic interference shielding effect of nanocomposites with carbon nanotube and shape memory polymer. *Composites Science and Technology*. **67**(14):2973-80 (2007).

[84] Das, N.C., Maiti, S. Electromagnetic interference shielding of carbon nanotube/ethylene vinyl acetate composites. *Journal of Material Science*. **43**(6):1920-5 (2008).

[85] Yuen, S.M., Ma, C.C.M., Chuang, C.Y., Yu, K.C., Wu, S.Y., Yang, C.C. Effect of processing method on the shielding effectiveness of electromagnetic interference of MWCNT/PMMA composites. *Composites Science and Technology*. **68**(3-4):963-8 (2008).

[86] Yang, Y.L., Gupta, M.C. Novel carbon nanotube-polystyrene foam composites for electromagnetic interference shielding. *Nano Letters*. **5**(11):2131-4 (2005).

[87] Yang, Y.L., Gupta, M.C., Dudley, K.L., Lawrence, R.W. A comparative study of EMI shielding properties of carbon nanofiber and multi-walled carbon nanotube filled polymer composites. *Journal of Nanoscience Nanotechnology*. **5**(6):927-31 (2005).

[88] Donohoe, J.P., Xu, J., Pittman, C.U. Variability of dual TEM cell shielding effectiveness measurements for vapor grown carbon nanofiber/vinyl ester composites. *Electromagnetic Compatibility International Symposium.*190-4 (2005).

[89] Kim, H.M., Kim, K., Lee, C.Y., Joo, J., Cho, S.J., Yoon, H.S. Electrical conductivity and electromagnetic interference shielding of multiwalled carbon nanotube composites containing Fe catalyst. *Applied Physics Letters*. **84**(4):589-91 (2004).

[90] Li, Y., Chen, C., Zhang, S., Ni, Y., Huang, J. Electrical conductivity and electromagnetic interference shielding characteristics of multiwalled carbon nanotube filled polyacrylate composite films. *Applied Surf Science*. **254**(18):5766-71 (2008).

[91] Hornbostel, B., Leute, U., Pötschke, P., Kotz, J., Kornfeld, D., Chiu, P-W. Attenuation of electromagnetic waves by carbon nanotube composites. *Physica E: Low-dimensional Systems and Nanostructures.* **40**(7):2425-9 (2008).

[92] Al-Saleh, M.H., Sundararaj, U. Electromagnetic interference shielding mechanisms of CNT/polymer composites. **Carbon**. doi:10.1016/j.carbon.2009.02.030 (2009)

[93] Frogley, M.D., Zhao, Q., Wagner, H.D. Direction-Sensitive strain-mapping with carbon nanotube sensors. *Composite Science and Technology*. **62**(1): 147-150 (2002).

[94] Park, J.M., Kim, D.S., Lee, J.R., Kim, T.W. Nondestructive damage sensitivity and reinforcing effect of carbon nanotube/epoxy composites using electro-micromechanical technique. *Material Science Engineering C*. **23**:971–5 (2003).

[95] Pham, G.T., Park, Y.B. , Liang, Z., Zhang, C., Wang, B. Processing and modeling of conductive thermoplastic/carbon nanotube films for strain sensing. *Composites Part B*. **39**: 209–216 (2008).